

**UDC 621
CODEN: MINSC5
ISSN 1857 – 5293**

**MECHANICAL SCIENTIFIC
ENGINEERING JOURNAL**

**МАШИНСКО НАУЧНО
ИНЖЕНЕРСТВО СПИСАНИЕ**

**Volume 31
Number 1–2**

Skopje, 2013

<i>Mech. Eng. Sci. J.</i>	Vol.	No.	pp.	Skopje
	31	1–2	1–112	2013
<i>Маш. инж. науч. спис.</i>	Год.	Број	стр.	Скопје

**MECHANICAL ENGINEERING – SCIENTIFIC JOURNAL
МАШИНСКО ИНЖЕНЕРСТВО – НАУЧНО СПИСАНИЕ**

Published by
Faculty of Mechanical Engineering, Ss. Cyril and Methodius University in Skopje, R. Macedonia
Издава

Машински факултет, Универзитет „Св. Кирил и Методиј“ во Скопје, Република Македонија

Published twice yearly – Излегува два пати годишно

INTERNATIONAL EDITORIAL BOARD – МЕЃУНАРОДЕН УРЕДУВАЧКИ ОДБОР

Slave Armenski (Faculty of Mechanical Engineering, Ss. Cyril and Methodius University in Skopje, Skopje, R. Macedonia), **Aleksandar Gajić** (Faculty of Mechanical Engineering, University of Belgrade, Belgrade, Serbia), **Čedomir Duboka** (Faculty of Mechanical Engineering, University of Belgrade, Belgrade, Serbia), **Maslina Daruš** (Faculty of Science and Technology, University Kebangsaan Malaysia, Bangi, Malaysia), **Robert Minovski** (Faculty of Mechanical Engineering, Ss. Cyril and Methodius University in Skopje, Skopje, R. Macedonia), **Wilfried Sihn** (Institute of Management Science, Vienna University of Technology, Vienna, Austria), **Ivan Juraga** (Faculty of Mechanical Engineering and Naval Architecture, University of Zagreb, Zagreb, Croatia), **Janez Kramberger** (Faculty of Mechanical Engineering, University of Maribor, Maribor, Slovenia), **Karl Kuzman** (Faculty of Mechanical Engineering, University of Ljubljana, Ljubljana, Slovenia), **Clarisse Molad** (University of Phoenix, Phoenix, Arizona, USA), **Todor Neshkov** (Faculty of Mechanical Engineering, Technical University of Sofia, Sofia, Bulgaria), **Zlatko Petreski** (Faculty of Mechanical Engineering, Ss. Cyril and Methodius University in Skopje, Skopje, R. Macedonia), **Miroslav Plančak** (Faculty of Technical Sciences, University of Novi Sad, Novi Sad, Serbia), **Remon Pop-Iliev** (Faculty of Engineering and Applied Science, University of Ontario Institute of Technology, Oshawa, Ontario, Canada), **Predrag Popovski** (Faculty of Mechanical Engineering, Ss. Cyril and Methodius University in Skopje, Skopje, R. Macedonia), **Dobre Runčev** (Faculty of Mechanical Engineering, Ss. Cyril and Methodius University in Skopje, Skopje, R. Macedonia), **Aleksandar Sedmak** (Faculty of Mechanical Engineering, University of Belgrade, Belgrade, Serbia), **Ilija Ćosić** (Faculty of Technical Sciences, University of Novi Sad, Novi Sad, Serbia), **Rolf Steinhilper** (Faculty of Engineering Science, University of Bayreuth, Bayreuth, Germany)

Editor in Chief Одговорен уредник
Assoc. Prof. Igor Đurkov, Ph.D **Вон. проф. д-р. Игор Ѓурков**

Co-editor in Chief Заменик одговорен уредник
Assoc. Prof. Darko Danev, Ph.D **вон. проф. д-р. Дарко Данев**

Ass. Prof. Dame Dimitrovski, Ph.D., secretary **Доц. д-р Даме Димитровски, секретар**

Technical editor managing Технички уредник
Blagoja Bogatinoski **Благоја Богатиноски**

Lectors Лектура
Georgi Georgievski (Macedonian) **Георги Георгиевски (македонски)**

Proof-reader Коректор
Alena Georgievska **Алена Георгиевска**

UDC: "St. Kliment Ohridski" Library – Skopje УДК: НУБ „Св. Климент Охридски“ – Скопје

Copies: 300 Тираж: 300

Price: 520 denars Цена: 520 денари

Address Адреса
Faculty of Mechanical Engineering **Машински факултет**
(Mechanical Engineering – Scientific Journal) (Машинско инженерство – научно списание)

Editor in Chief Одговорен уредник

P.O.Box 464 пошт. факс 464

МК-1001 Skopje, Republic of Macedonia МК-1001 Скопје, Република Македонија

Mech. Eng. Sci. J. is indexed/abstracted in INIS (International Nuclear Information System)
www.mf.ukim.edu.mk

<i>Mech. Eng. Sci. J.</i>	Vol.	No.	pp.	Skopje
	31	1–2	1–112	2013
<i>Маш. инж. науч. спис.</i>	Год.	Број	стр.	Скопје

TABLE OF CONTENTS (СОДРЖИНА)

434 – Zoran Bogatinoski, Bojana Trajanoska, Gabriela Arsova-Miloševska Rigid and semi-rigid steel beam-column connections (Крути и полукрути челични врски на столб носач)	3–12
435 – Filip Zdraveski, Dimitri Kozinakov Analysis of stability of point-supported-glass wall systems under wind load (Анализа на стабилноста на стаклени фасади со потпирање во точка под дејството на силите од ветер).....	13–18
436 – Jelena Micevska Research trends in the field of industrial design engineering (Актуелни истражувања во областа на инженерскиот индустриски дизајн).....	19–24
437 – Simona Taševska, Sofija Sidorenko Engineering analyses of bionics structures of composable modules (Инженерски анализи на бионички структури од составливи модули)	25–32
438 – Tashko Rizov, Risto Tashevski Geo-based systems in augmented reality (Системи базирани на географско позиционирање во аугментната реалност)	33–40
439 – Ile Mirčeski, Tatjana Kandikjan, Sofija Sidorenko, Petar Simonovski Comfort analysis of driver's seat for passenger car through simulation of the sitting process (Анализа на удобноста на возачкото седиште за патнички автомобил со симулација на процесот на седење).....	41–51
440 – Viktor Iliev, Predrag Popovski, Zoran Markov Water hammer analysis using characteristics method and numerical simulation (Анализа на хидрауличен удар со примена на методот на карактеристики и нумеричка симулација)	53–62
441 – Igor Šešo, Done Taševski Developing simulation application using graphical programming language for optimization of solar collector position (Развој на симулационена програма за оптимизација на поставеноста на сончев колектор со користење на графички програмски јазик).....	63–75

442 – Gordana Popsimonova, Biljana Ristovska, Dame Dimitrovski, Goce Georgievski Greenhouse production in Macedonia – challenges and opportunities (Стакларничко производство во Македонија – предизвици и можности)	77–84
443 – Vase Jordanoska, Radmil Polenaković Franchising as a form for starting a small business – presence and opportunities for development in Republic of Macedonia (Франшизата како облик за започнување мал бизнис – застапеност и можности за развој во Република Македонија).....	85–89
444 – Bojan Prangoski A review of some recent results about Laplace transform and convolution of ultradistributions (Преглед на некои неодамнешни резултати за Лапласовата трансформација и конволуција на ултрадистрибуции).....	91–97
445 – Marjan Džidrov, Viktor Gavriloski, Jovana Jovanova Vibration based fault detection techniques for mechanical structures (Техники на детекција на грешки во механичките структури базирани на анализа на вибрациите)	99–105
446 – Nikola Avramov, Petar Simonovski Finite element analysis of an accident severity according to the european standard EN1317 (Анализа на големината на сообраќајната несреќа според стандардот EN1317 со помош на метод на конечни елементи)	107–110
Instructions for authors	111–112

RIGID AND SEMI-RIGID STEEL BEAM-COLUMN CONNECTIONS

Zoran Bogatinoski¹, Bojana Trajanoska¹, Gabriela Arsova-Miloševska²

¹Faculty of Mechanical Engineering, "SS. Cyril and Methodius" University in Skopje,
P.O. Box 464, MK-1001 Skopje, Republic of Macedonia

²Tenzor, Skopje, Republic of Macedonia
zoran.bogatinoski@mf.edu.mk

Abstract: In this paper a theoretical and experimental research of the steel beam-column connections is presented. Eight types of specimens were being researched, composed of rigid and semi-rigid connections from which 4 connections are with IPE-profile and 4 connections with tube's section for the beam. From the numerical analysis of the researched models, and especially from the experimental research in the Laboratory for Structures in the Faculty of Mechanical Engineering – Skopje, specific conclusions were received that are ought to have theoretical and practical usage for researchers in this area of interest.

Key words: rigid and semi-rigid connections; beam-column connections; design (structural design); bending moment; rotation; plastic hinge; collapse

КРУТИ И ПОЛУКРУТИ ЧЕЛИЧНИ ВРСКИ НА СТОЛБ НОСАЧ

Апстракт: Во овој труд е претставено теоретско и експериментално истражување на челични врски на столб носач. Испитувани се осум различни модели, составени од крути и полукрути врски, од кои четири се изведени со IPE-профили за носачот, а другите четири профили со цевкаст пресек. Од нумеричката анализа на испитуваните модели и од експерименталните тестирања извршени во лабораторијата за конструкции на Машинскиот факултет во Скопје, изведени се специфични заклучоци кои имаат теоретско и практично значење за истражувачите во ова подрачје.

Клучни зборови: крути и полукрути врски; врски на столб носач; дизајн; момент на свиткување; ротација; пластичен зглоб; колапс на структурата

1. INTRODUCTION

With the beginning of the third Millennium as the traffic and population increased, so did the need for buildings and motorway structures. The building land in the centers of the big towns became tight and its price increased. In the same time the "highest buildings" became an aspiration and prestige of the structural designers. Consequently the use of multi-storey composite structures (steel columns, steel beams, and reinforced concrete slabs) became a necessity. The multi-storey composite structure is used for different types of build-

ings such as office buildings, bank buildings, industrial buildings, public buildings, high-rise parking buildings, etc. These kinds of buildings are built all around the world, mainly in the highly developed countries depicting their financial and technical power.

The safety and function expressed through the control of the mass, stiffness, strength, and ductility at the structural design of the multi-storey composite structures, and mostly of the connections of the elements exposed under cyclic-horizontal loading (such is earthquake, wind loading) recognize in

combination with other loadings is of highest priority for this kind of structures (buildings).

See Figs. 1–3: Multi-storey structures (administrative and residential buildings).



Fig. 1. High-rise parking building (under construction)



Fig. 2. Skyscrapers in Chicago, USA

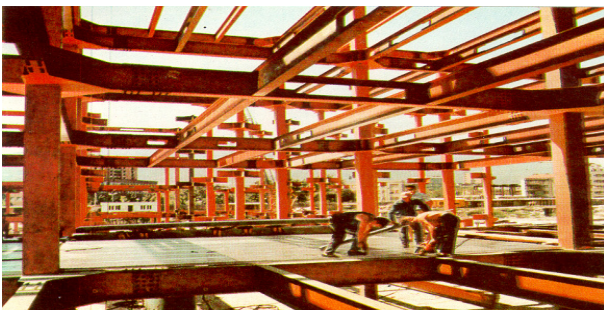


Fig. 3. "GTC" in center of Skopje (under construction)

The behavior of the beam-column connections in the multi-storey frame structures (MSFS) is viewed as a whole and it's in the direct correla-

tion and dependence with the behavior of their main constructive fundamental elements (steel beams, columns and the elements for their connection). In other words, the way the beams, the columns and their elements of connection behave, that way the MSFS behaves, i.e. the connection between the steel beams with the steel column [2].

The behavior of the beam-column connection in the MSFS depends mostly from their constructive solution. However, dominant in this paper is the research of new or modified constructive solutions of the connections, and all with the purpose of improvement their loading in the conditions in real external loadings. Some constructive solutions can be controlled by the dissipation of energy, meaning, can be controlled by the stress and deformational distribution in the sections of the elements of the MSFS, i.e. the constructive solution in the connection directly influences the appearance of the plastic hinges in some of the sections of the elements, when their loading is exhausted.[3]

2. DESIGN CRITERIA FOR CONTROLLED DAMAGES AND COLLAPSE FOR BEAM-COLUMN CONNECTIONS

In the numerical modeling of the beam-column connection the demands of the new codes [1] are incorporated, which is the well-known concept of the seismic resistant structures that proposes development of plastic hinges in the beams, and rarely in the part of the columns. Consequently, the size of the statically influence that dictates the order of the plastic hinge appearance should be taken under consideration, i.e. column bending strength should be larger then beam bending strength. As a result, for each beam-column connection the following equation should be satisfied [2]:

$$\sum M_{R,c} > \sum M_{R,b} \quad (1)$$

where $\sum M_{R,c}$ is a sum of existent bending moments in the column, and $\sum M_{R,b}$ is a sum of existent bending moments of the beams in the connection point.

With the alternative of the mechanism of collapse (the order of the element's plastification) and generally the mechanism of energy dissipation, two different approaching exist:

– The first approach is based on the contribution of the panel-zone in the energy dissipation with the purpose of its reduction and also accepting

a part of the plastic deformations, without excluding the contribution of the columns and the beams.

– The second approach excludes the panel zone into the energy dissipation. As a result, in this case, the end parts of the beam should accept the plastic deformations. Accordingly, the beam-column connection should be specified in detail.

Design of beam-column connection without the contribution of the panel-zone into the energy dissipation

Supposing that the shearing stress is equally distributed in the panel-zone (part of the web of the column between the two beams) shearing stress developed in the panel-zone is presented as follows:

$$\tau_p = \frac{V_p}{(d_c - 2 \cdot t_{cf}) \cdot t_p}, \quad (2)$$

where V_p is a shearing force into the panel-zone at the steel beam-column connection.

$$V_p = \frac{\sum M_b}{(d_b - t_{bf})} - V_c \quad (3)$$

In the beam-column composite connection V_p is a shearing force in the columns designed through the assumption that the zero-moment is located into the middle part of the column section.

$$V_p = \frac{M_b^+}{(d_b - t_{bf})} + \frac{M_b^-}{d_b} - V_c, \quad (4)$$

Consequently, taking into consideration the balance of $\sum M_b = \sum M_c$, the result is as follows:

$$V_p = \frac{\sum M_b}{(d_b - t_{bf})} \cdot \left(1 - \frac{d_b - t_{bf}}{H - d_b}\right), \quad (5)$$

the middle stress of shearing in the panel-zone is as follows:

$$\tau_p = \frac{\sum M_b}{t_p \cdot (d_c - 2 \cdot t_{cf}) \cdot (d_b - t_{bf})} \cdot \left(1 - \frac{d_b - t_{bf}}{H - d_b}\right). \quad (6)$$

3. TYPES OF RESEARCHED MODELS – NUMERICAL DESIGN

For numerical design of the nonlinear answer of the 8 types of models (SP1, SP2, SP3, SP4, SP5, SP6, SP7 and SP8) were used nonlinear programs DRAIN-2DX and ANSYS Workbench [5].

SP1 MODEL (Fig. 4) is a modification of the standard and most commonly used rigid beam-column connection with end-plate welded with fillet welds at the end of the beam. The modification used consists of additional triangular webs at the end of the beam that are welded to its upper and lower level with the end-plate, so that the stiffness in the end of the beam is enhanced, as the loads of the welded beam-column connection of the plate [2, 3]. This is the hot rotated beam (according to DIN1025) IPE200 [4], with height $h = 200$ mm, width of the level $b = 100$ mm, thickness of the web $t_r = s = 5.6$ mm, and thickness of the levels $t_p = t = 8.5$ mm. The material of the beam is S275. JO + M according to EN10025-2/2004 with the following mechanical characteristics:

$$f_y = \sigma_T = ReH = 338 \text{ MPa},$$

$$f_u = \sigma_m = Rm = 464 \text{ MPa}, A = 33.1\% [5].$$

The connection between the steel beams (designed by the valid standards MKS (JUS) U.E7.140 correlated with EC3) was realized by the modified beam-column connection using end-plate connection that was welded to the end of the beam. At the end-plate 2 holes were made ($d = 17$ mm), deployed in 4 rows, total 8 holes in one plate, i.e. on one beam-column connection. For connecting the beams through the end-plates with the columns, high valued bolts M16 class 10.9 were used, pre-tensioned with the right moment ($M_u = 253$ Nm).

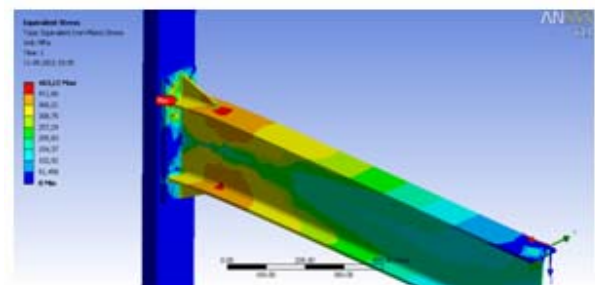


Fig. 4. The stress distribution in SP1 model

In Figure 4 the stress distribution is shown and it is clearly visible that the influence of the welded triangular webs is big, i.e. the maximal stress is moved from the end-plate through the middle of the beam i.e. from the end of the beam to the top of the triangular webs. In the place where the maximal stress is in the pressed layer is expected the appearance of the plastic hinge because of the stability problem of lateral buckling [MKS (JUS) U.E7.101 – for calculating the lateral buckling in the beam]; or the appearance of the stability

problem of the buckling in the pressed part of the web of the beam (MKS (JUS) U.E7.121– for calculating the buckling of plates) [1].

SP2 MODEL (Fig. 5) is a designed rigid beam-column connection with end-plate welded with angular welds to the end of the beam. Same as the previous, in this connection 2 triangular webs are used at the end of the beam that are welded to the upper and the lower part of the tubular beam with the end-plate, so that the stiffness of the end of the beam is enhanced, as the loading of the welded beam-column connection in the plate. The beam in the SP2 model is a hot shaped hollow profile with rectangular cross-section (according to DIN59411, JUS C.B5.213) [1] 200.100.5, with height $h = 200$ mm, width of the level $b = 100$ mm, thickness of the walls in the section $t = s = 5$ mm. The material of the beam is S355J2H according to EN10219-1/2006/EN10021 with the following mechanical characteristics: $f_y = \sigma_T = ReH = 437$ MPa, $f_u = \sigma_m = Rm = 554$ MPa, $A = 24.8$ %.

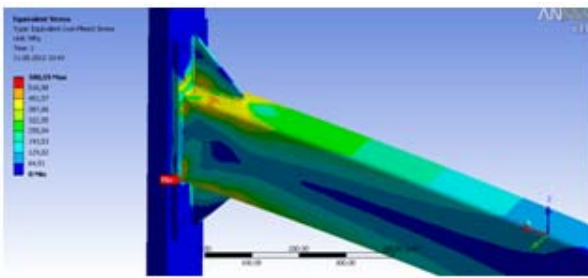


Fig. 5. The stress distribution in SP2 model

Our valid standards MKS (JUS) U.E7.140 (in correlation with EC3) were used for the design of the beam, adapted for the shape of the beam. Here, same as the previous model, end-plate connection is used with an end-plate that has a bigger height than the one of the SP1 model, as a result to the specific shape of the beam (rectangular cross-section), also welded to the end of the beam. At the beginning, on the plate were made 2 holes ($d = 17$ mm), deployed in 4 rows. That is total 8 holes on one plate i.e. on one beam-column connection for connecting the beams through the end-plates with the columns (on the column levels were made holes with the same schedule and number as the end-plates), with bolts M16 class 10.9.

In Figure 6 the stress distribution is shown and the influence of the welded triangular webs. The maximal stress is moved from the end-plate to the middle of the beam, i.e. at the end of the beam to the top of the lower triangular web [1].

SP3 MODEL (Fig. 6) is a designed rigid beam-column connection with an ending joint that is welded to the dismantling connection on the beam with the column. The joint is made by welding 3 separate plates under an angel of 90° to the background end-plate, where holes are made for the connection with the beam and the connection with the column. The design of the joint is made so that its loading is bigger than the loading at the end of the beam so that the reallocating of the eventual plastic hinge will be on a bigger distance from the column, different from the previous 2 analyzed models. The loading of the joint depends from: W_x – section modulus receiving the bending moment, A_r – surface of the web receiving the cutting (shearing) and the mechanical characteristics of the adopted material.

Holes are made on the beam IPE200, i.e. 2 in the levels and 3 on the web, total 7 bolts for the connections on the beam with the joint. For bigger beams, the number of bolts in the levels and webs can increase. Important for the design of this model is the loading of the bolts in the levels which are different from the ones for the connection of the joint with the column and are mainly undertake cutting. Depending from their projected loading in correlation with the loading of the joint and the loading of the beam, the schedule of the collapse of elements that are contained in the connection can be directed, i.e. can be predicted the mechanism of collapse. With the model SP3 is needed precision during the construction of the joint and making holes for the bolts on the joint and the end of the beam, same as the setting schedule of the bolts during the construction of the beam.

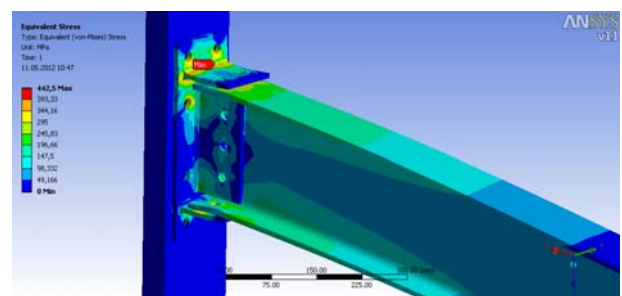


Fig. 6. The stress distribution in SP3 model

In this model the maximal stress, appears in the horizontal angular welds of the joint, but these, same as the elements of the joint, are designed with bigger static sizes at the end of the beam, so that they are not a danger for connection collapse. Relatively smaller are the stresses, but still big

enough in the place of the connection in the levels of the beam, with the joint, same as the connection between the web and the vertical web in the joint. The forces from the bending moment in the end of the beam are expected to cause stretching in the tensioned level and an eventual buckling in the pressed level, if appeasement does not occur in the leveled screws that are exposed to cutting (shearing). The further development can go into a direction of defining the exact correlations of the geometrical and static characteristics at the end of the beam, the number and the diameter of the means of connection (bolts) and the dimensions of the joint, everything in manner of getting a controlled collapse mechanism of the connection [1].

SP4 MODEL (Fig. 7) is a designed rigid beam-column connection. The connection of the beam (IPE200) with the column is made only by the levels of the beam, through before made joints, one for each one of the levels of the beam. The joints can be made from hot rolled or welded L-profiles depending from the needed thickness, with welded triangular web in the middle of its strengthening. The connection of the joint with the level of the beam is made with 4 bolts, or total of 8 bolts on the two of the levels of the beam. The joints are design so that their loading is bigger than the loading in the end of the beam and the eventual collapse would be made in the assets for the connection of the joints with the beams. The connection in each of the joints with the column is made with 4 high valued bolts class 10.9, strained at the desirable moment. These bolts are designed so that they mustn't release during the most extreme loadings in the connections, i.e. the collapse of the connection would take place in the end of the beam, in the joint, in the assets for the connection between the beam and the joint, but not in the following elements.

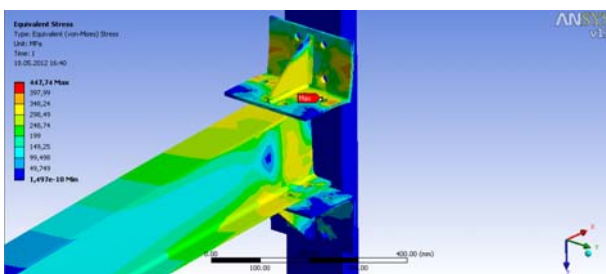


Fig. 7. The stress distribution in SP4 model

In the SP4 model the maximal stress appears in the vertical angular welds on the joint and in the levels in the beam in the place of the connection with the joint. Because the joint (same as in the

SP3 model and the rest of the models where a joint is used) is designed with big static sizes in the end of the beam, the maximal stress don't represent a danger for collapse of the connection. The forces from the bending moment in the end of the beam is expected to cause stretching in the tightened level and an eventual buckling in the pressed level, if before didn't come to appeasement in the leveled screws that are exposed to cutting (shearing). In this model, different from the previous SP3 model, this influence is emphasized as a result to the connection that was made only through the levels of the beam, and not through the web that was the case in the SP3 model [1].

SP5 MODEL (Fig. 8) is a designed rigid beam-column connection. The connection between the beam (200.100.5) and the column is realized through 2 already prepared and welded horizontal plates to the end of the upper and the lower part of the beam that are additionally strengthened with 2 vertical webs. On the plates are made holes together with the holes on the already made joints. The dimensions of the joints are same as the ones in the SP4 model, however in this model are used exterior (the furthest) holes on the joints for the connection with the horizontal plates at the end of the beams; the joints can be made from hot rolled or welded L-profiles depending on the needed thickness, with a welded triangular web in the middle of its strengthening. The connection between the joint and the plates that are in the end of the beam is made with 4 bolts, or total of the 8 bolts for one beam. The joints are designed so that their loading is bigger than the loading of the beam and the eventual collapse would happen in the assets for the connection between the joints and the beams after some plastic deformations in the end of the beams. The connection between every joint and column is made with 4 high valued bolts class 10.9, strained at the desirable moment. These bolts are designed so that they mustn't release during the most extreme loadings in the connections i.e. the collapse of the connection would take place in the end of the beam, in the joint.

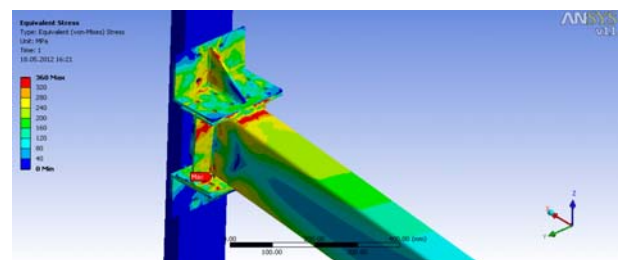


Fig. 8. The stress distribution in SP5 model

The forces from the bending moment in the end of the beam is expected to cause stretching in the tightened level and an eventual buckling in the pressed level, if before didn't come to appeasement in the leveled bolts that are exposed to cutting (shearing). In this model this influence is emphasized as a result to the connection that was made only through the levels of the beam, and not through the web that was the case in the SP3 model [1].

SP6 MODEL (Fig. 9) is a designed semi-rigid beam-column connection. The connection between the beam and the column is made only through the web in the beam (3 bolts) and the final welded joint. The welded T-joint is dismantling connected with the column with total of 4 high valued bolts 10.9. The joint is made by welding the 2 plates under an angle of 90° , where already were made holes for the connection with the web of the beam and the connection with the column. The design of the joint is made so that its loading is big enough so that the eventual collapse would appear in the end of the beam, i.e. the beam-column connection. On the beam IPE200 are made 3 holes on the web for the T-joint. For bigger beams, the number of bolts on the web can increase.

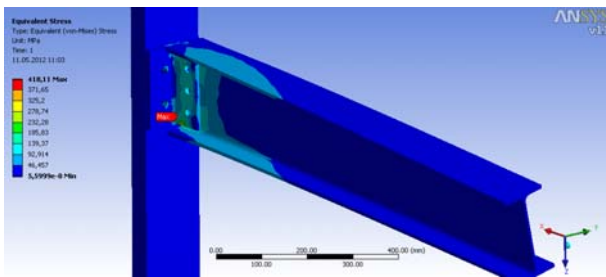


Fig. 9. The stress distribution in SP6 model

In the SP6 model the maximal stress, appears in the web of the beam to the final (upper and lower) screws and accordingly to the vertical welded plate of the joint. Because of this, the joint and its vertical plate which binds the beam, is designed with bigger static characteristics. The collapse of the connection is expected in the web of the beam as the result of the stretching and cutting the part of the web next to the hole in the upper bolts or as a result to the cutting of one of the external (upper or lower) bolts [1].

SP7 MODEL (Fig. 10) is a designed semi-rigid beam-column connection. The connection between the beam and the column is made through

the temporary end of the beam and the final welded T-joint with the help of total 3 bolts. The welded T-joint is dismantling connected to the column with a total of 4 high valued bolts class 10.9. The joint is made by welding the 2 plates under an angle of 90° , where already were made holes for the connection in the web of the beam and the connection with the column. The design of the joint is made so that its loading is big enough that the eventual collapse would appear at the end of the beam, i.e. the beam-column connection. On the beam ([] 200) a steel plate is welded with transverse web on which are made 3 holes for the connection with the T-joint. For bigger beams, the number of bolts on the web can increase.

This design of the connection would be an answer to the previous model (SP6) in case where for the beams a rectangular hollow section would be used instead of an open I-section. This is a quashing connection because it takes a specific bending moment followed by movements. The eventual collapse would appear firstly in some of the ending bolts that are the most loaded and where a superimposition of the cutting forces emerges from the transversal shearing force and the forces from the receiving bending moment.

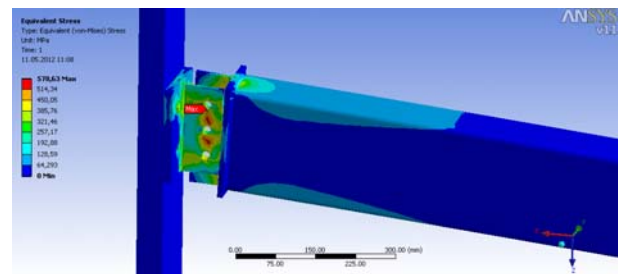


Fig. 10. The stress distribution in SP7 model

In the model, the maximal stress appears in the web of the beam, next to the holes for the screws and accordingly to the vertical welded plate of the joint. Also, big stress appears in the welds from the joint same as in the end of the beam and it's upper and lower part next to the welded plate. Because the joint, and by this its upper vertical plate by which the beam is tied, is designed with bigger static characteristics from the prepared end of the beam. The collapse of the connection is expected in the part of the beam as a result of the stretching and cutting of the vertical part of the plate next to the hole in the upper screw or as a result to the cutting of one of the external (upper or lower) bolts [1].

SP8 MODEL (Fig. 11) is a designed semi-rigid beam-column connection. The connection between the beam and the column is realized with 3 long bolts between the end of the beam and the final welded U-joint. The welded U-joint is dismantling connected to the column with the total of 4 high valued bolts class 10.9. The joint is made by welding the 3 plates under an angle of 90° , where already were made holes for the connection with the web of the beam and the connection with the column. The design of the joint is made so that its loading is big enough that the eventual collapse would appear in the end of the beam, i.e. the beam-column connection. Three holes are made on the beam ([] 200) for the connection with the U-joint. For bigger beams, the number of bolts on the web can increase.

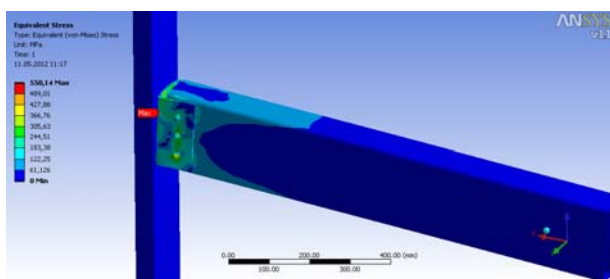


Fig. 11. The stress distribution in SP8 model

In the model the maximal stress is in the welds from the U-joint for the connection between the beam and the column (reactivity wall), but the same are designed so that a danger of collapse does not exist. Also, the bigger stress appears in the holes for the longer bolts, same as in the bolts itself. Because the joint is designed with bigger static characteristics in the end of the beam, the collapse of the connection is expected in the part of the beam as a result of the cutting of vertical part of the beam next to the hole in the upper bolt or as result of the cutting of one of the external bolt [1].

4. EXPERIMENTAL RESEARCH

The experimental research of the 8 designed models is completely done in the Laboratory for structures in the Institute for welding and welded structures in the Faculty of Mechanical engineering in Skopje. As a final the result from the experimental research are the characteristic diagrams: F- Δ L (force-displacement) and M- Φ (bending moment-rotation in the end of the beam) (Fig. 12) [1].

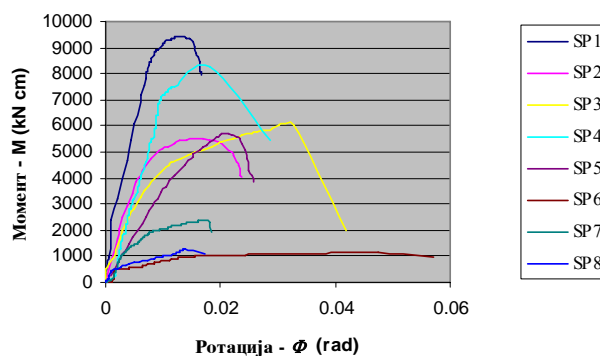


Fig. 12. M- Φ diagram for all of the 8 models (experimental analysis)

The equipment for adding and transferring the force contains one axial press (piston) that is placed vertical on the steel frame in the experimental desk and the same through the force sensor presses the end of the consul omission, causing negative bending moment and shearing in the connection in the end of the beam (Fig. 14).

For every model (SP1, SP2, SP3, SP4, SP5, SP6, SP7 and SP8), a loading diagram was previously made, through adding the displacements. The process was made by adding the displacements, and not adding force, because in nonlinear conditions, when it comes to reducing the force, leading an experiment by adding force is practically uncontrolled and it may come to sudden collapse of the model. Adding the increased displacement in the end of the console overhang of the beam through the piston of the researched device was made gradually only in one direction until was used the total capacity from each of the models and their demolition. The research is presented in the following images (Figs. 13–20) for each of the models in some of the fazes of research:



Fig. 13. SP1 model: Appearance of the plastic hinge (stability problem of lateral buckling)



Fig. 14. SP2 model: Appearance of plastic hinge (stability problem of buckling in the lower pressed part of the beam)



Fig. 16. SP4 model: Appearance of plastic hinge (stability problem of lateral buckling of the lower pressed part of the beam)



Fig. 15. SP3 model: Connection collapsing due to cutting of the second row bolts in the connection of the upper part of the beam



Fig. 17. SP5 model: Appearance of the plastic hinge (stability problem of buckling in the lower pressed part of the beam)



Fig. 18. SP6 model: Connection collapsing due to cutting of lower bolt in the connection of the rib of the beam



Fig. 20. SP8 model: Collapse of the connection due to plastic deformations of cutting at the end of the beam in the upper long bolt



Fig.19. SP7 model: Connection collapsing due to cutting of the upper bolt of the connecting ribs

5. CONCLUSION

During the design and analyzing of the beam-column connections under the influence of the horizontal loading (seismic loading, loading under strong winds), very important is the control of the weight, stiffness, strength and the ductility of the material of the elements by what directly depends the behavior of the elements in the connections, and by that the behavior of these structures; it is proved that many demolitions of the structures that had happened were as a result to the no rigid materials [2].

From the comparative experimental analysis of all of the 8 researched models can be concluded that the capacity of the carrying of the bending moment of the models with rigid connection (SP1, SP2, SP3, SP4 and SP5) is significantly bigger than the one with the semi-rigid connections (SP6, SP7 and SP8), what was already expected; if the rigid connections are separately analyzed (SP1, SP2, SP3, SP4 and SP5), the SP1 model has the biggest capacity to carry the banding moment over the others, but in the other hand the smallest rotating capability (plastic deformability) over the other 4, i.e. the 7 models counting the models with the

semi rigid connections (SP6, SP7 and SP8); the SP3 model has the biggest rotating capability over the other 4 models with the rigid connections (SP1, SP2, SP4 and SP5); the deformation (rotation) capability in the researched models is inversely proportional to the capacity of carrying of the beam, i.e. the semi-rigid connections have bigger plastic deformability and possibility for bigger rotation during the use of their total capacity to carry, but they have smaller capacity to carry comparing to the ones with rigid connection (Fig. 12).

The main idea and direction for further researches is obtaining one "*ideal*" beam-column connection that in the same time will have relatively high strength and deformational characteristics, i.e. capacity to carry bigger bending moments with bigger rotating capability in the same time.

5. REFERENCE

- [1] G. Arsova-Miloševska: *Design of new solutions of rigid and semi-rigid connections*, Doctoral dissertation, 2012.
- [2] Z. Bogatinoski: *Numerical modeling and experimental analysis of composite steel frames under cyclic loading*, Doctoral dissertation, 2000.
- [3] B. Trajanoska: *Numerical modelling of welded steel connections*, Master thesis, 2011.
- [4] DIN V ENV 1993-1-1, Stahlbau, Stahlhochbau, 1994, Beuth.
- [5] EUROCODE 1, EUROCODE 3, EUROCODE 8
- [6] ANSYS Workbench / Powell, G. H., Prakash, V., "DRAIN-2DX" and "DRAIN-3DX", University of California, Berkeley, California, 1993–94.

ANALYSIS OF STABILITY OF POINT-SUPPORTED-GLASS WALL SYSTEMS UNDER WIND LOAD

Filip Zdraveski, Dimitri Kozinakov

*Institute of Welding and Welded Structures, Faculty of Mechanical Engineering,
"SS. Cyril and Methodius" University in Skopje,
P.O. Box 464, MK-1001 Skopje, Republic of Macedonia
dimitri.kozinakov@mf.edu.mk*

Abstract: Pre-tensioned point supported glass walls are widely used in modern architecture today. This paper deals with the stability of glass support structure to predict the collapse behavior of the same. All windows in their corners are connected to spider arm and thus transferring the wind force on the bowstring structure. The results of the analysis provide load-displacement relationship and the impact of the pretension magnitude forces on the stability of support structure.

Key words: FEM analysis; point supported glass walls; stability; pre-tension system

АНАЛИЗА НА СТАБИЛНОСТА НА СТАКЛЕНИ ФАСАДИ СО ПОТПИРАЊЕ ВО ТОЧКА ПОД ДЕЈСТВОТО НА СИЛИТЕ ОД ВЕТЕРОТ

Апстракт: Предзатегнатите стаклени фасади се користат широко во модерната архитектура. Овој труд се занимава со стабилноста на стаклените фасади, сидови и со предвидување на услови во кои ќе настане нејзино губење т.е. колапс. Сите панели во нивните јазли се поврзани со крак на елемент „spider“ преку кој се пренесува силата од ветерот на потпорната структура во вид на лак и стрела. Резултатите од анализата обезбедуваат врска меѓу силата и деформацијата и влијанието на предзатегањето врз стабилноста на структурата.

Клучни зборови: анализа со МКЕ; стаклена фасада; потпирање во точки; стабилност; предзатегање

1. INTRODUCTION

For this analysis the system shown on Fig. 1 is selected. This system is consisted of the following elements:

- TR-F (B) – Tension Rod-Front (Back)
- SP – Strut Pipe
- VR – Vertical Rod
- HR – Horizontal Rod

Elements TR-F and TR-B form “front” and “back” arch of the so called “bow and arrow” system. The crossed bows are hold strained with the elements marked as SP on Fig.1 which plays the role of “arrow” in the system. Elements TR-F and TR-B can only transfers tension force, while SP can be exposed to compression forces.

Two arches crossed set receive the pressure difference which exists between the outside and inside of the window panels. The force from the windows is transferred through the “arrows” to one of the arches, front or back one.

VR or DLR – Dead Load Rod (element for taking dead load) is set vertically and close to the window panels. The reason why VR is set near the window panels is to eliminate the bending moment caused by the dead load and the distance from the panels to the support points.

The elements on Fig. 1 designated as HR are used to give stability of support structure in A-A plane. They do the role of “stabilizers” of the support structure in the horizontal plane.

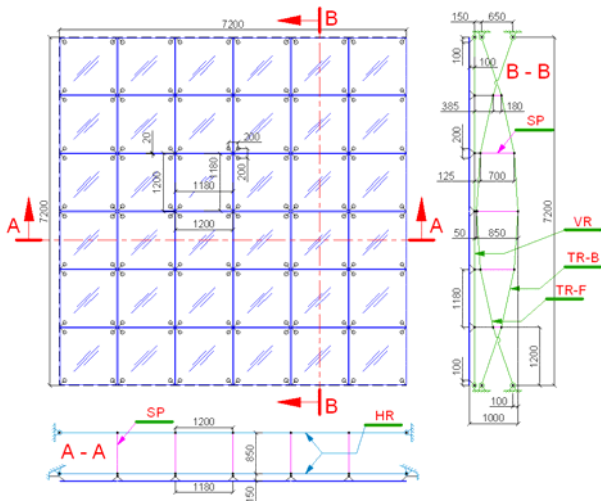


Fig. 1. System used for the analysis

On Fig. 2 are shown the functions that support structure should perform:

- Receives transversal forces, F1, F2
- Transfers axial forces, G
- Resists with bending stiffness, M_{B-B}
- Resists with torsion stiffness, HC_{A-A}

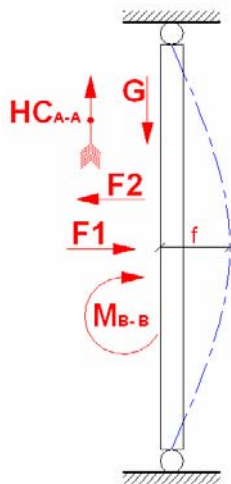


Fig. 2. Functions of the support structure

Generally speaking, glass support system should perform the same way as simple beam with two point support providing transversal, axial, bending and torsion stiffness.

2. MODELING THE SYSTEM

In order to perform the FEM analysis first we need to select the material properties of the elements constituting the support structure. These properties are shown in Table 1.

Table 1

Selected material and physical properties

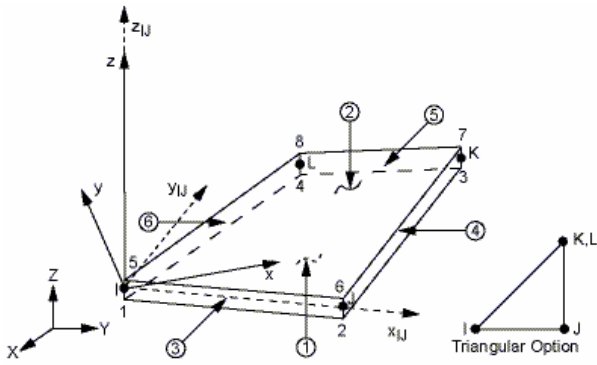
Window Panel	$E_{\text{glass}} = 72\,000\text{ N/mm}^2$
	$\mu = 0.3; \alpha_T = 0.6 \cdot 10^{-5}/^\circ\text{C}$
	$\delta = 12\text{ mm}$
	$\rho = 2.52 \cdot 10^{-6}\text{ kg/mm}^3$
Strut Pipe	$m = 50\text{ kg/panel}$
	$R_{p0.2} = R_m = 80\text{ N/mm}^2$
	$E_{\text{steel}} = 200\,000\text{ N/mm}^2$
	$\mu = 0.3; \alpha_T = 1.8 \cdot 10^{-5}/^\circ\text{C}$
Tension Rod	$\text{Ø} = 20\text{ mm} \rightarrow A = 314\text{ mm}^2$
	$I_{zz} = 7853.98\text{ mm}^4$
	$\rho = 7.83 \cdot 10^{-6}\text{ kg/mm}^3$
	$m = 0.0025\text{ kg/mm}$
Vertical Rod	$R_{p0.2} \approx 300\text{ N/mm}^2$
	$E_{\text{steel}} = 200\,000\text{ N/mm}^2$
	$\mu = 0.3; \alpha_T = 1.8 \cdot 10^{-5}/^\circ\text{C}$
	$\text{Ø} = 13\text{ mm} \rightarrow A = 133\text{ mm}^2$
Horizontal Rod	$\rho = 7.83 \cdot 10^{-6}\text{ kg/mm}^3$
	$m = 0.001\text{ kg/mm}; R_{p0.2} \approx 300\text{ N/mm}^2$
	$\sigma_{\text{pre-stress}} = 10\text{ N/mm}^2; \varepsilon = 0.00005$
	$E_{\text{steel}} = 200\,000\text{ N/mm}^2$
Horizontal Rod	$\mu = 0.3; \alpha_T = 1.8 \cdot 10^{-5}/^\circ\text{C}$
	$\text{Ø} = 10\text{ mm} \rightarrow A = 78.5\text{ mm}^2$
	$\rho = 7.83 \cdot 10^{-6}\text{ kg/mm}^3$
	$m = 0.0006\text{ kg/mm}; R_{p0.2} \approx 300\text{ N/mm}^2$
Horizontal Rod	$\sigma_{\text{pre-stress}} = 10\text{ N/mm}^2; \varepsilon = 0.00005$
	$E_{\text{steel}} = 200\,000\text{ N/mm}^2$
	$\mu = 0.3; \alpha_T = 1.8 \cdot 10^{-5}/^\circ\text{C}$
	$\text{Ø} = 6\text{ mm} \rightarrow A = 28\text{ mm}^2$
Horizontal Rod	$\rho = 7.83 \cdot 10^{-6}\text{ kg/mm}^3$
	$m = 0.00022\text{ kg/mm}; R_{p0.2} \approx 300\text{ N/mm}^2$
	$\sigma_{\text{pre-stress}} = 10\text{ N/mm}^2; \varepsilon = 0.00005$
	$E_{\text{steel}} = 200\,000\text{ N/mm}^2$

Next important step is defining type of finite elements that will be used for building the model. This is very important because it will affect structure behavior.

Glass support structure is modeled in Ansys. Following elements are selected:

- SHELL63 – this element simulates glass panel behavior (Fig. 3). Acts as membranes which can transfer bending. This element has six degrees of freedom at each node.
- BEAM188 – it is suitable for analysis of slender to thin beam structures. This is linear element with two nodes (Fig. 4) and it has six degrees of freedom at each node. It is used for modeling the spider and the arrow of the support structure.
- LINK10 – this element can perform only tension or compression (Fig. 5). It is used for modeling the arches, front and back, as well as the horizontal stabilizers.

After selecting material and physical properties and also defining the finite elements, support structure of the glass curtain wall is prepared for analysis (Fig. 6).



x_{IJ} = Element x-axis if ESYS is not supplied.

x = Element x-axis if ESYS is supplied.

Fig. 3. SHELL63 element

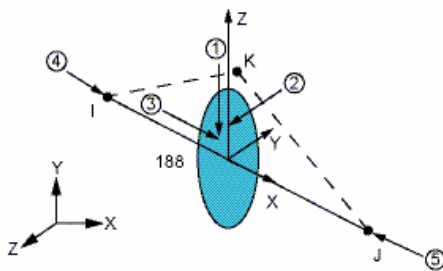


Fig. 4. BEAM188 element

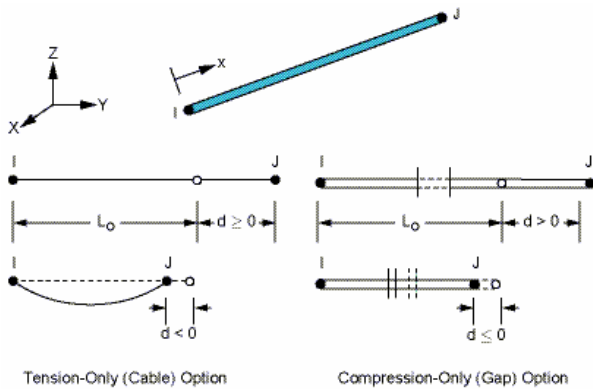


Fig. 5. LINK10 element

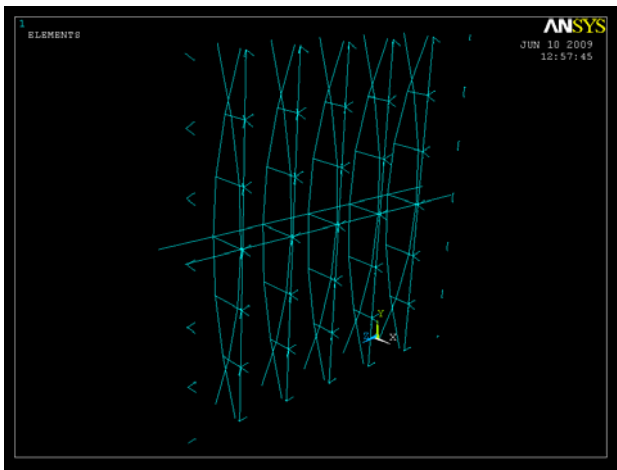


Fig. 6. Completed FEM model

3. ANALYSIS OF THE SYSTEM UNDER EXTERNAL FORCE

First we define the goal of the analysis: determination of the capacity of the support structure with pre-tension of 10 MPa to receive lateral load (Fig. 7), or to put it different what is the maximal load that each “arrow” can receive without causing loss of stability of the system.

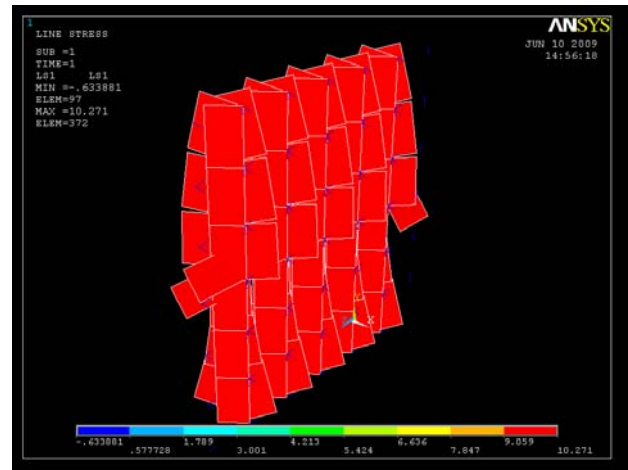


Fig. 7. Fully pre-tensioned support structure with 10 MPa

At the beginning each arrow is loaded with force of 100 N. The force is increased step by step considering the condition $\sigma < R_{p0.2}$ until the system is stable.

Figs. 7 and 8 and 9 show that increasing the load from 100 N till 330 N causes TR-B to become additionally stressed, while TR-F is relaxing. When the force at each arrow reaches 350 or 360 N the system is losing stability and this state is rigid body motion. The undefined motion of the support structure is shown on Fig. 10.

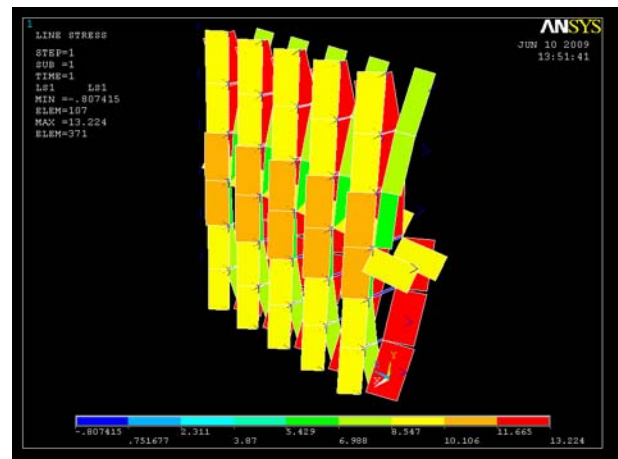


Fig. 8. System with 100 N load at each arrow – normal stress

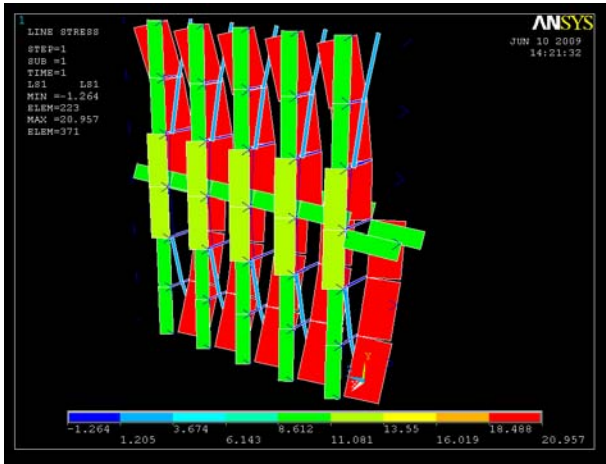


Fig. 9. System with 330 N load at each arrow – normal stress

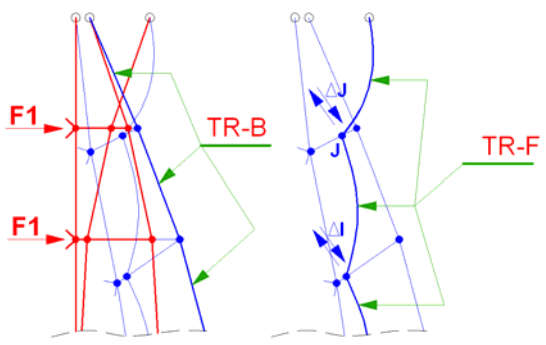


Fig. 10. Support structure losing stability

Glass support structure (Fig. 10) is losing stability when the nodes I and J become free to move. In this case, TR-F is completely relaxed from tension and practically doesn't participate in the support of the glass wall.

4. ANALYSIS OF THE SYSTEM WITH MODIFICATIONS

The system on Figs. 6 and 7 is modified in order to receive wind load of 100 kg/m^2 . This force is bigger than the one prescribed with the standard. One window panel has area of 1.2 m^2 . The force that one arrow will receive is approx. equal to

$$100 \text{ kg/m}^2 \times 1.2 \text{ m}^2 = 144 \text{ kg} \text{ or } 1440 \text{ N.}$$

Considering that we are doing linear analysis of the support system, we can calculate the necessary pre-tension of the arches TR-F and TR-B, knowing that 350 N is the boundary force which can be applied before system losses stability. Therefore, $1440/350 \approx 4$ meaning 4 times larger pre-tension than the one for the primary system

with 10 MPa. The first adopted modification is pre-tension of the arches equal to 40 MPa.

Each VR receives the dead load of five panels (1 panel = 50 kg). Summary force that each VR receives from dead load is $5 \cdot 50 \text{ kg} \cdot 10 \text{ m/s}^2 = 2500 \text{ N}$. According to Tab. 1 for VR cross section is equal to 78.5 mm^2 . The force of 2500 N reduced to cross section of VR is equal to normal stress of 40 MPa. For safety reasons (earthquake and anti-lock) this value is increased for 10 MPa. Second adopted modification is 50 MPa pre-tension of VR elements.

It is assumed that horizontal stabilizers (HR) are pre-tensioned with the force that can eventually show up in the plane of the façade. According to Tab. 1 the cross section of HR is 28 mm^2 . It is supposed that the force in A-A plane cannot be larger than 50 kg. In order to maintain front HR to stay stressed, it is adopted that pre-tension of HR will be 20 MPa.

These changes to the original proposed system are shown on Figs. 11 and 12. Fig. 11 shows only the support system without the panels attached. Figs. 12 and 13 show the general system under dead load with and without panels shown.

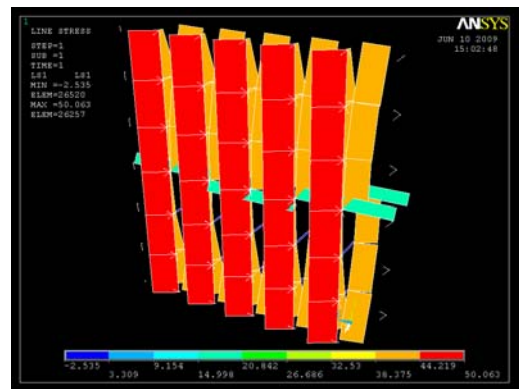


Fig. 11. TR = 40 MPa, VR = 50 MPa and HR = 20 MPa

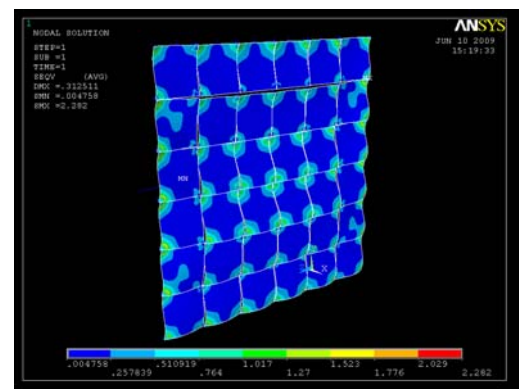


Fig. 12. Glass panels Von Mises stresses from dead load

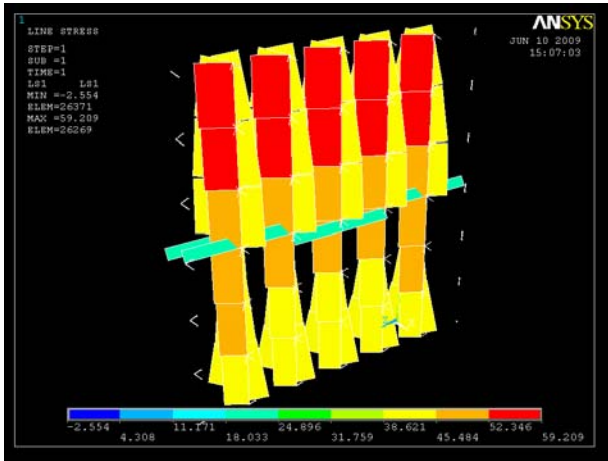


Fig. 13. Normal stresses on support structure from dead load

It can be noticed from Fig. 13 that the most loaded VR elements are the one on the top of the structure – 59 MPa. The lowest are less stressed. They should always carry minimum tension in order to maintain the stability of the system.

When the system glass supported structure is subject to wind load of 100 kg/m^2 and dead load of all elements the results shown on Fig. 14 are obtained. Support system is on border to become unstable, but it is still stable. The tension stress in the front arches TR-F maintains value from 3 to 13.5 MPa.

The stress distribution of the wind panels is shown on Fig. 15. Maximal value of the stress appears around the connection point with the spider arm with value of 17.4 MPa, while the average value is between 6 to 10 MPa.

The thickness of the window panel is acceptable but can be subject for further optimization.

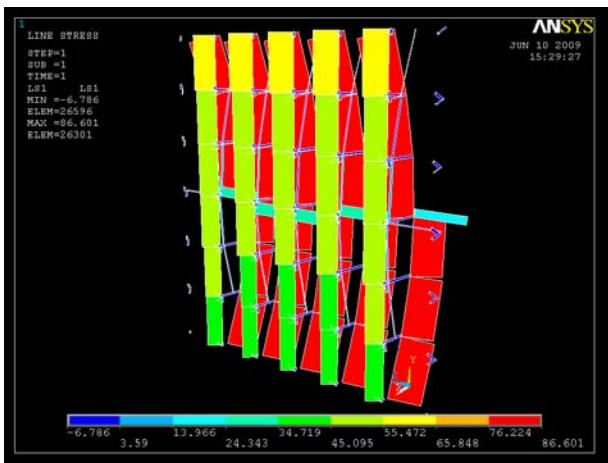


Fig. 14. Support structure stress distribution under wind load of 100 kg/m^2

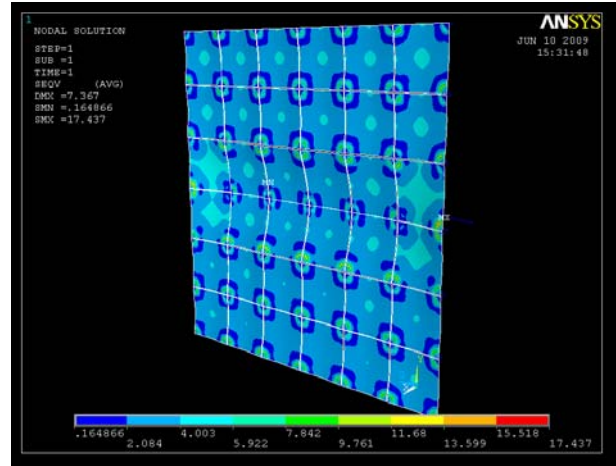


Fig. 15. Panels stress distribution under wind load of 100 kg/m^2

On Fig. 16 is shown total displacement of the glass curtain system. Maximal total displacement is on the middle of the system and it is equal to 7 mm. The deflection of each panel is different and it is in the range of 3 to 4 mm (we can calculate deflection as difference between absolute displacements).

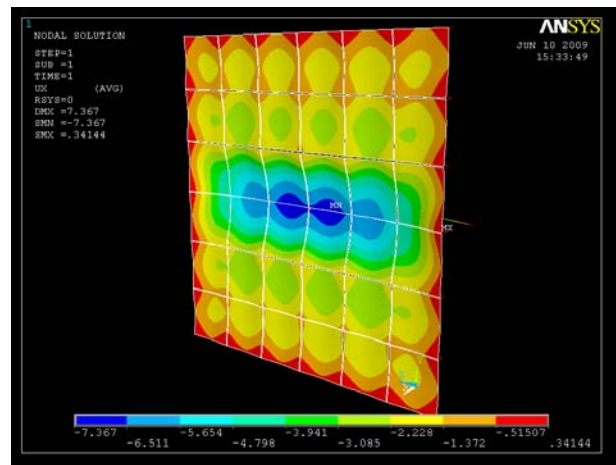


Fig. 16. Total displacement in wind direction

Here should be noticed that above analyzed structure is usable only for pre-defined referent temperature. Considering materials used for the glass curtain wall (Tab. 1), the referent temperature at which properties are normally defined is equal of 23 to 25°C. The system can be also considered as stable at this temperature.

The last modification of the system is changing the sections of the arches from $\varnothing = 13 \text{ mm}$ to $\varnothing = 20 \text{ mm}$ ($A = 314 \text{ mm}^2$). The results under wind load of 100 kg/m^2 are shown on Fig. 17. The normal stress in TR-B is decreased from 86.6 MPa to

value of 59.4 MPa and the stress in TR-F is increased to value of 21.6 MPa from value of 13.5 MPa. This means that support structure is generally stiffer and displacements are smaller. Last modification shows that small change in the dimensions significantly can affect the stability of the system.

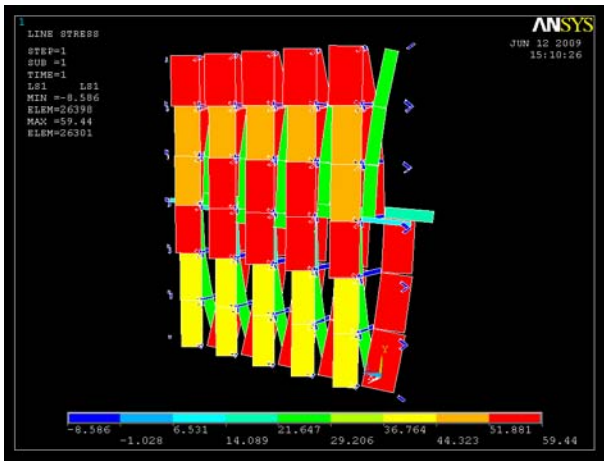


Fig. 17. Support structure with increased arches cross section

CONCLUSION

Conclusions from the conducted analysis can be summarized in the following statements:

- TR-F and TR-B form arches which receives the wind force or the pressure difference between the outside and inside of the building.

- HR elements work as horizontal stabilizations of the support structure or they receive the lateral load which is in plane with the glass curtain wall.

- VR or DLR takes dead load from the window panels and they should be set near the window in order to avoid the effect of bending.

- All stresses in the support structure should be lower than the value $1/1.5$ from the Yield Stress $R_{p0.2}$ in order to be on the safe side.

- There should be minimum pre-tension in the relaxed elements (i.e. arches) in order to prevent losing stability.

- The level of minimum pre-tension at full load should be subject for optimization.

REFERENCES

- [1] Mick Eekhout: *Product Development in Glass Structures*, [EEK90], 010 Publishers, Rotterdam, The Netherlands (1990).
- [2] Mick Eekhout: *Stressed Glass, Zappi or Product Development for the Nai*, [EEK96a], Nai Publishers, Rotterdam, The Netherlands (1996),.
- [3] [Mick Eekhout: *Tubular Structures in Architecture*, EEK96b], Cidect, Zurich, Switzerland (1996),.
- [4] Mick Eekhout: *Frameless Glazing*, [EEK98], 010 Publishers, Rotterdam, The Netherlands (1998).
- [5] *Intelligent Glass Facades : Material, Practice*, Design by Andrea Compagno. Zurich: Artemis, C1995.
- [6] Koffel, W. E., Memari, A. M., Rittenhouse, T., Dawson, H. and Ettouney, M.: *Curtainwalls in Modern Buildings*, Structure Magazine, January 2005, pp 32–35.
- [7] mstock, J. S.: *Handbook of Glass in Construction*, McGraw-Hill, New York, (1997).
- [8] Button, D. and Pye, B.: *Glass in Building: Guide to Modern Architectural Glass Performance*, Butterworth Architecture, Oxford (1993).
- [9] Schittich, C., Staib, G.: *Glass Construction Manual*, Birkhauser-Publishers for Architecture, Basel (1999),.
- [10] Eurocode EN 1991-1-4 WIND ACTIONS.

RESEARCH TRENDS IN THE FIELD OF INDUSTRIAL DESIGN ENGINEERING

Jelena Micevska

*Institute of Engineering Design, Mechanization and Vehicle, Faculty of Mechanical Engineering,
"SS. Cyril and Methodius" University in Skopje,
P.O. Box 464, MK-1001 Skopje, Republic of Macedonia
jelena.micevska@mf.edu.mk*

Abstract: Industrial Design Engineering (IDE) is relatively new discipline which aims to combine both Industrial Design and Engineering Design. It is believed that all spheres of the design are mostly practical disciplines and that there is no room for scientific research. But we, the researchers, want to believe that this statement is not true. There are lots of aspects in the design and the related disciplines that need to be analyzed improved or changed. This alterations and modifications are only possible with research. Having in mind that researcher may be subjective on this matter, vast analysis was conducted. The aim of the analysis was to give more objective answer to the question, wheatear or not there is need for research in the field of design, or more precisely IDE. Additionally, an effort was made to determine which areas of the IDE are most challenging for the researchers.

Key words: industrial design engineering; user-centered design; emotional design

АКТУЕЛНИ ИСТРАЖУВАЊА ВО ОБЛАСТА НА ИНЖЕНЕРСКИОТ ИНДУСТРИСКИ ДИЗАЈН

Апстракт. Инженерскиот индустриски дизајн (ИИД) е релативно нова научна дисциплина која претставува комбинација на индустрискиот дизајн и конструирањето. Во пошироката јавност се верува дека сите подобласти на дизајнот се главно практични дисциплини и дека тука не постои простор за истражување. Истражувачите веруваат дека тоа не е така. Постојат многу аспекти во овие области кои треба да се анализираат, подобрат или изменат. Подобрувањата и измените се можни само со истражување. Имајќи го предвид фактот дека истражувачите можат да бидат субјективни во однос на оваа тема, спроведена е детална анализа. Целта на истражувањето е да се даде објективен одговор на прашањето дали е потребно истражувањето во областа на дизајнот, или поточно во областа на ИИД. Направен е и обид да се одредат области на ИИД кои се интересни и претставуваат предизвик за истражувачите.

Клучни зборови: инженерски индустриски дизајн; дизајн насочен кон корисникот; емоционален дизајн

1. INTRODUCTION

It is very important at the beginning to define the main terms used in this paper. Those are industrial design, design engineering and industrial design engineering.

In order to give more thoroughly explanation, we should start by defining the most basic term. That is the term DESIGN which is consistent in all the other terms mentioned before. Design is a creative activity whose aim is to establish the multifaceted qualities of objects, processes, services and

their systems in whole life-cycles. Therefore, design is the central factor of innovative humanization of technologies and the crucial factor of cultural and economic exchange [1]. With this definition, it is only confirmed what is commonly known, and that is, that the term design has very wide meaning (Fig. 1). This is why in order to have more precise meaning, it is necessary to accompany the word design with words that have specific meanings and will define specific areas like graphic, fashion, automotive, product, industrial, engineering, etc.

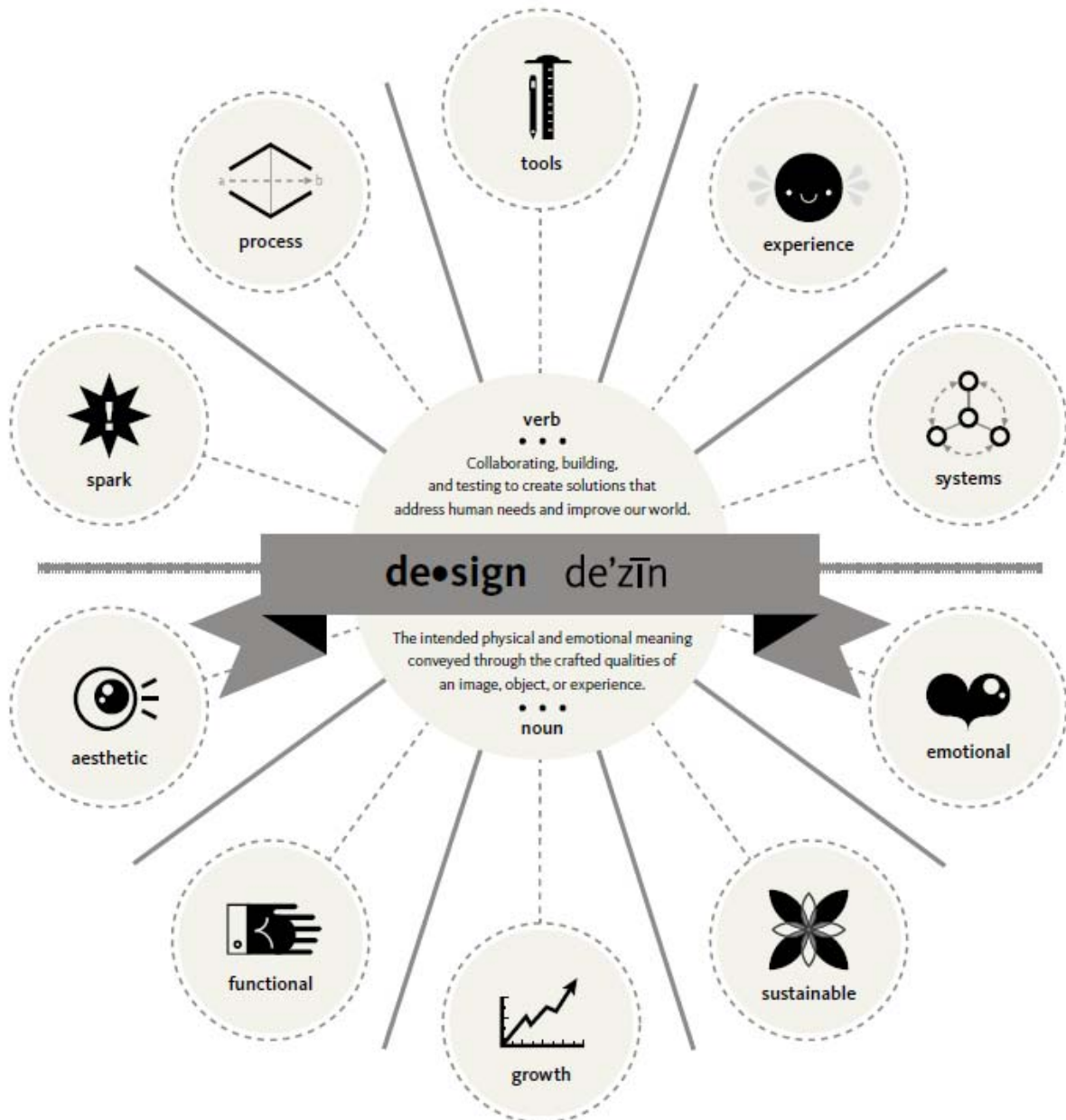


Fig. 1. Elements of design (Ten essential of good design) [4]

According to the Industrial Designers Society of America [2], **industrial design (ID)** is the professional service of creating and developing concepts and specifications that optimize the function, value and appearance of products and systems for the mutual benefit of both user and manufacturer.

Design engineering (DE) is an interdisciplinary discipline, same as industrial design. Design activities carried out by design engineers have mainly a functional purpose. They are aimed to achieve purposes related with the function in the creation of new systems and principles that usually are embodied within artifacts. Thus, their knowl-

edge and skills are suitable for designing the functional part of products, but they are not so well equipped to design the experiences of the products they make function [3].

Industrial design engineering (IDE) is a discipline which is aimed to be the link between the industrial design and the design engineering.

According to Cross [5] the industrial design engineer with its knowledge and skills from both engineering design and industrial design is the only solution for overcoming the frequent conflict between industrial designers and engineers.

The following text is dedicated to the industrial design engineers. The possible use of the terms designer or industrial designer in this context is referring to the term industrial design engineer.

Hypothesis 1

The field of the industrial design engineering had become more interesting for the researchers in the recent years.

Hypothesis 2

The main focus of the researchers in the field of IDE is the end user.

METHOD

The aim of this research is determination of the research trends in the field of industrial design engineering. The method that is used in order to complete this aim is extensive descriptive analysis. For this reason an overview of the work done by researchers in this field in the period of the last 15 years was conducted. In the process numerous papers, articles and PhD thesis from various sources were taken in consideration.

RESULTS

After the conducted analysis, there is no doubt in the accuracy of the statement of the Hypothesis 1. The number of over 9 conferences a year worldwide, with over 1000 papers is enough to confirm that. We can add to that the PhD research programs in 7 universities in Europe alone, truth to be told Europe has the highest number of PhD programs in the field of IDE.

Sleeswijk Visser [6] in his PhD thesis also endorses this statement that the interest of researches in the design has been growing rapidly from year to year.

As a result, of the conducted analysis it can be concluded that most of the researches are evolving around people / end users. This fact is not surprising since the products are designed and produced for the people and the producers' only concern is if they are willing to buy this product. We can easily say that the success of a new product is closely related to the willingness of consumers to buy the product. The consumer is most likely to buy a product which fulfills the wishes and demands he

imposes on the product. These wishes and demands are fulfilled by means of the attributes of the product [7]. This is confirmed and revised by many researchers and authors over the years. González & Palacios [8] go even further by saying that, firms that do not attend to their customer's needs in today's highly competitive environment, will not survive. McDonagh *et al.* [9] explain that in this environment many products are developed by different brands with similar functionality, but different in usability and appearance. Bloch *et al.* [10] gives accent to the design by saying that superior design is what distinguishes products from competitors and helps them to gain recognition in a crowded marketplace. The fact that the economy benefits from it, it is most likely for design, to be an interesting field for researchers from different areas.

The research area in the design dealing with users is called User-Centered Design. Usability Professionals Association [11] defines **user-centered design** as an approach to design that grounds the process in information about the people who will use the product. Having users as a main concern, new more specific disciplines started emerging, such as **Ergonomics** and **Human Factors**, which are focused on the fit of the technology and human performance. The concern for the user's needs emerged with the **Participatory Design** which was rising in the 1970s [6], which aim was to involve the stakeholders in the development process of a new product incorporating the user needs in the design.

Nowadays, the number of disciplines and subareas in the field of IDE is vast and there is no precise framework for each one of them, such as people-centered design [12], user-centered design [13], customer-centered design [14], [15], human-centered design [16], and very often some of them overlap in their interests.

In the recent years it has been reached even deeper into the design philosophy and suddenly new areas of interest emerged, **User Experience Design (UX)**.

"... witnessed by the many books and conferences [9], the experience of products is steadily gaining ground as a topic in design research. Notwithstanding, 'experience' may well be the most elusive concept to catch in scientific discourse, prone to misinterpretation and in danger of being divorced from those who do the experiencing..." Van Rompay [17].

The increased need for this approach is caused by the overcrowded market with products; people can now choose from dozens of very similar products. So why will someone choose to buy one product out of dozen similar ones? It is the emotional responses that one has with the product [18]; which is kind of an added value. Consumers nowadays along with the product buy value in a form of entertainment, experience and identity [19].

Surprising enough is the fact given by Van Kesteren [20] that for most of the people the design and the exterior of a product is determining factor for buying it and not the innovative technology in it. Users prefer products to be functional and easy to use, but additionally, they want to be in some way emotionally touched by the product [20].

The user experience itself cannot be controlled, predicted or designed. 'The user experience' does not exist, since experiencing is a constructive activity, belonging to individual people [6]. Designers cannot control the effects of their designs, but they can have an awareness of the complexity of how people experience things, and use this awareness as a starting point for designing products. While designers cannot control the subjective user experience (internal states, mood, idiosyncratic associations), they can have influences (intended or not intended) on a part of the user experience with the functional and expressive qualities of the products, which are interpreted through various filters of personal, social and cultural meaning [21]. Designers can design for experience by a sensitive and skilled way of understanding the users [6].

This approach or philosophy also spread in the business environment, coining expressions like "experience economy" or "dream society" [22]. They explain that advanced technology, extra functionality, reliability and performance are not enough to satisfy customers anymore. To get an edge over their competitors, companies need something more than well-functioning products and offer designs that their users can enjoy beyond pure utility [23].

In the last few years User Experience (UX) Design became one on the most popular design areas. Consequently, it can be concluded that Hypothesis 2 is true; then again it needs a light redefining. Since the main interest here are the end users, however not for their needs and requirements lone, but more for their experiences. Therefore it

can be said that the main focuss of today's researches in the field of IDE is the user experience.

DISCUSSION

User experience is very closely connected to the user's emotions, therefore very often the term Emotional Design is used with the similar meaning as user experience design. It can be said that the emotional design is considered to be subarea of the UX design.

Don Norman, one of the leading researchers on this topic, has his own definition of the emotional design (Fig. 2). In his book, Emotional design, Norman [24] shows that design of most objects are perceived on three levels (dimensions). Therefore a good design should follow all three levels:

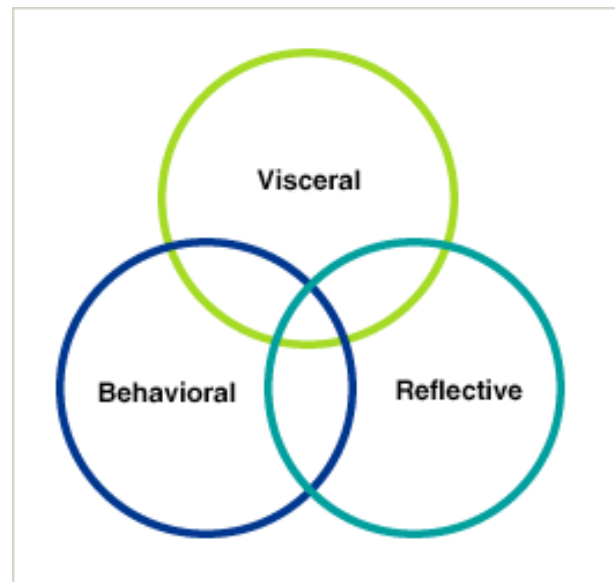


Fig. 2. Emotional design defined by D. Norman [24]

The **Visceral** level is obtained through intuition rather than from reasoning or observation. This level is influenced significantly by appearance, texture and sound of objects.

The **Behavioral** level refers to the actions or reactions of a person, usually in relation to the environment, to an object or person. Behavior can be conscious or unconscious, overt or covert and voluntary or involuntary. This level is all about functionality and it is influenced by pleasure and effectiveness of use (accessibility and usability).

The **Reflective** level refers to the capability of quiet thought or contemplation. This level is influenced strongly by self-image, satisfaction, memory

and the meaning of things. This level becomes more important as products mature.

Emotional design is widespread research area, and as a result, of that, numerous conferences are held worldwide. The Delft University of Technology is one of the leading academic institutions dedicated to researches in this area.

One of the first Ph.D. researches in the field of emotional design was the Desmet's Pd.D. thesis [25]. As a part of his research, he was analyzing people's emotions, their facial expressions and their connections to different products. As a result to his research new model was purposed, called PrEmo. PrEmo is a non-verbal, self-report instrument that measures 14 emotions which are often elicited by product design. He states that the sudden interest in emotional responses is evoked by the increased competitiveness on every market [25].

Demir [26] gives nice example of companies that embraced this way of designing. It is one of the world's most famous design agencies, Frog design, that took the motto 'form follows emotion' as the basis for their designs. The founder of the company, Hartmut Esslinger, stated "... even if a design is elegant and functional, it will not have a place in our lives unless it can appeal at a deeper level, to our emotions ..." [19].

Although some interesting and promising studies have been reported, this research field is still short of conceptual clarity, and therefore lacks consensus on what the actual object of study should be. In fact, the concept of emotion has been somewhat vague and has been used as a collective noun for all kinds of affective phenomena [25].

Design literature tends to refer to 'emotions' when studying anything that is thought of intangible, non-functional, non-rational or, for that matter, non-cognitive. Some of the reported studies involve 'experiential needs' [27], 'affective responses' [28], 'customer delight' [29], 'pleasure' [30], 'emotional behavior' [31], and 'affective computing' [32].

CONCLUSION

The expansion of the Emotional Design started with the first Design & Emotion Conference organized at the Technical University in Delft, Netherlands, in the 1999, event with 41 participants. The 2010 Design & Emotion Conference in Chicago had over 250 participants. Confirming

once more, how much has the interest in this topic increased. Another similar event is the Designing Pleasurable Product & Interfaces dated back from the 2003 in Pittsburgh [23].

The rise of the Emotional Design may be considered as the next rational step toward user satisfaction. After exploring and improving the design methods, perfecting the technology, all there is left unknown and uncertain are the users. This is why number of studies evolving round the user is increased. Feedback from studies and researches is beneficial for both parties the users and the produces. After all that is the final goal.

In addition, it is more than obvious that nowadays people's emotions are still the main research point in the field of design. It all started around 15 years ago and since then the number of researchers in this field is continuously growing. Consequently the number of published papers, articles and books increases and yet there is still so much to be done. This is not the result of researchers' failure, but evidence how complex this matter is. In order to provide some general truths regarding people's emotions a lot of work and dedication is needed. This complex and challenging field needs a lot of researchers' attention. In fact, there is room for every researcher willing to devote some of their time and work.

REFERENCES

- [1] ICSID International Council of Societies of Industrial Design: *Defintion of Design*, www.icsid.org/about/about/articles31.htm (2013).
- [2] Industrial Designer Society of America: *What is Industrial Design?*, www.idsa.org/what-is-industrial-design (2010).
- [3] J. L. Casamayor: *Industrial design, industrial design engineering and design engineering: Different perspectives of a PhD in design*, Proceedings of CEPHAD 2010 Conference, The borderland between philosophy and design research, Copenhagen, Denmark, vol. 1, pp. 3–7 (2010).
- [4] Autodesk: *Imagine design create*, New York, NY (2011).
- [5] N. Cross: *Engineering design methods: strategies for product design*, 4th edition, John Wiley & Sons, Chichester, UK (2008).
- [6] F. Sleeswijk Visser: *Bringing everyday life into design*, Ph.D. thesis (in English), Delft University of Technology, Netherlands (2009).
- [7] K. J. Lancaster: *Consumer demand: A new approach*. Columbia University Press, New York (1971).
- [8] F. J. M. González, T. M. B. Palacios: The effect of new product development techniques on new product success in Spanish firms. *Industrial Marketing Management*, vol. 31, pp. 261–271 (2002).
- [9] D. McDonagh, A. Bruseberg, C. Haslam: *Visual product evaluation: exploring users' emotional relationships with products*. *Applied Ergonomics*, vol. 33 (3), pp. 231–40 (2002).
- [10] P. H. Bloch, F. F. Brunel, T. J. Arnold: Individual differences in the centrality of visual product aesthetics: concept and measure-

- ment. *Journal of Consumer Research*, vol. **29**, pp. 551–565 (2003).
- [11] Usability Professionals Association: *What is User-Centered Design?*, http://www.upassoc.org/usability_resources/about_usability/what_is_ucd.html (2013).
- [12] N. Wakeford (2004): Innovation through people-centred design—lessons from the USA. DTI global watch mission report, in F. Sleeswijk Visser (2009).
- [13] K. Vredenburg, S. Isensee, C. Righi (2002): *User-centered design: an integrated approach*, Prentice-Hall, New Jersey, in F. Sleeswijk Visser (2009).
- [14] K. Chandler, K. Hyatt: *Customer-centred design: a new approach to usability*, Prentice Hall, New Jersey, in F. Sleeswijk Visser (2009).
- [15] H. Beyer, K. Holtzblatt: *Contextual Design: Defining Customer-centred Systems*, Morgan Kaufmann, San Francisco in F. Sleeswijk Visser (1998)
- [16] ISO 13407: *Human-centred design process for interactive systems*, International Standard EN/ISO 13407:1999, in F. Sleeswijk Visser (2009).
- [17] T. J. L. Van Rompay: *Expressions: Embodiment in the experience of design*, Ph.D. thesis (in English), Delft University of Technology, Netherlands (2005).
- [18] M. E. H. Creusen: *Product appearance and consumer choice*, Ph.D. thesis (in English), Delft University of Technology, Netherlands (1998).
- [19] H. Esslinger in F. Sweet: *Frog: Form Follows Emotion*, Thames and Hudson, London, in P. M. A. Desmet (2002).
- [20] I. E. H. Van Kesteren. *Selecting materials in product design*, Ph.D. thesis (in English), Delft University of Technology, Netherlands (2008).
- [21] J. Fulton Suri: *Empathic Design: Informed and inspired by other people's experience*. It press in F. Sleeswijk Visser (2009).
- [22] R. Jensen: *The Dream Society*, McGraw-Hill, New York (1999).
- [23] G. Laurans: *On the moment-to-moment measurement of emotion during person-product interaction*, Ph.D. thesis (in English), Delft University of Technology, Netherlands (2011).
- [24] D. Norman: *Emotional Design: Why we love (or hate) everyday things*, Basic Books (2004).
- [25] P. M. A. Desmet: *Designing Emotions*, Ph.D. thesis (in English), Delft University of Technology, Netherlands (2002).
- [26] E. Demir: *Understanding and Designing for emotions*, Ph.D. thesis (in English), Delft University of Technology, Netherlands (2010).
- [27] M. B. Holbrook (1985): Emotion in the consumption experience: Toward a new model of the human consumer. In: R. A. Peterson, W. O. Hoyer, & W. R. Wilson (Eds.), *The role of affect in consumer behavior: Emerging theories and applications* (pp. 17–52). Lexington, M. A.: Heath in P. M. A. Desmet (2002).
- [28] C. M. Derbaix, M. T. Pham: Affective reactions to consumption situations: A pilot investigation. *Journal of Economic Psychology*, vol. **12**, pp. 325–355, in P. M. A. Desmet (2002).
- [29] A. Burns, R. Barrett, P. Evans: *Delighting customers through emphatic design*, Manuscript submitted for publication in P. M. A. Desmet (2002).
- [30] P. W. Jordan, M. Servaes: *Pleasure in product use: beyond usability*, In: S. Robertson (Ed.), *Contemporary Ergonomics 1995*, Taylor and Francis in P. M. A. Desmet (2002).
- [31] S. Wensveen, C. Overbeeke, T. Djajadiningrat: Push Me, Shove Me and I Show You How You Feel. Recognizing Mood from Emotionally Rich Interaction, *Proceeding DIS '02 Proceedings of the 4th conference on Designing interactive systems: processes, practices, methods, and techniques*, pages 335–340, in P. M. A. Desmet (2002).
- [32] R. W. Picard: *Affective computing*, MIT Press, Cambridge in P. M. A. Desmet (2002).

ENGINEERING ANALYSES OF BIONICS STRUCTURES OF COMPONIBLE MODULES

Simona Taševska, Sofija Sidorenko

Faculty of Mechanical Engineering, "SS. Cyril and Methodius" University in Skopje,
P.O. Box 464, MK-1001 Skopje, Republic of Macedonia
sofija.sidorenko@mf.edu.mk

Abstract: The main goal of the research presented in this paper is creation of innovative concept for prefabricated houses for living, using the modular principal. The leading idea is assembling of prefabricated houses as structures of modules, with possibility for relatively easy changes during the exploitation: adding, removing or recombination of modules according to the space requirements of the users. Each of the modules would be fabricated as a fully prepared self standing room for living. The shape and construction of the modules, as well as their space arrangement are derived according to the principals of bionics. The quality of the presented concept is approved through several analyses: static analysis of the construction using finite elements method; solar analysis for election of perfect orientation and insulation; thermal analysis.

Key words: modular design; modular structures; bionic design

ИНЖЕНЕРСКИ АНАЛИЗИ НА БИОНИЧКИ СТРУКТУРИ ОД СОСТАВЛИВИ МОДУЛИ

Апстракт: Истражувањето презентирано во овој труд има за цел креирање иновативно решение, концепт, за монтажни објекти за живеење со примена на модуларен принцип. Водечката идеја е формирање на структури од готови модули, кои лесно се монтираат и демонтираат и имаат можност за релативно лесни промени во текот на нивната експлоатација како објекти за живеење: додавање, одземање или рекомбинација на модулите според просторните потреби на корисниците. Предвидено е секој модул да претставува целосно изведена самоносечка просторија за живеење или комбинација од неколку помали простории. Формата и конструкцијата на модулите, како и начинот на нивното комбинирање се изведени со примена на принципите на биониката. Квалитетот на презентираниот концепт е потврден преку неколку извршени анализи: статичка анализа на конструкцијата со помош на методот на конечни елементи; соларна анализа зарад избор на идеална ориентација и позиционирање; термичка анализа за испитување на енергетската ефикасност.

Клучни зборови: модуларен дизајн; бионички дизајн; енергетска ефикасност

1. INTRODUCTION

The existing of the problem of housing is as old as the existing of human being. Obtaining homes for the members of society is the crucial social problem for the governments. Designers and architects constantly search for new concepts for upgrading of human living conditions, but also for new building technologies. New technologies, new materials, new ways of reasoning are included in these researches with intention to make better homes, energy efficient, flexible and more functional.

The main goal of our research is creation of innovative solution for prefabricated houses for living, using the modular principal [1]. The leading idea is assembling of prefabricated houses as structures of fully prepared self standing modules, fabricated as rooms for living, or a set of few smaller ones. The innovation in this concept is a possibility for relatively easy changes of the whole structure in the phase of exploitation: addition, extraction or recombination of modules according to the space requirements of the users. Assembling of the house with modules as ready to live rooms is a perfect way to meet the needs of the users. As the family

become larger or smaller the house for living could become bigger or smaller with relatively simple addition or extraction of modules. The aspect of monotony living in the same space is also taken into consideration. Recombination of the modules in order to make new look and functionality of the house is another quality of the presented concept.

The shape and construction of the modules, as well as their space arrangement are derived according to the principals of bionics. Bionics as a science discipline engages itself in technical realization and application of constructions, processes and evolutionary principles of biological systems. This relatively new interdisciplinary science synthesizes knowledge of biology with other sciences: physics, chemistry, design, medicine, mechanical engineering, architecture, design, psychology etc. [2, 3]. It includes the following disciplines:

- Structural bionics: studying constructions and structures in the nature.
- Bionics of processes: studying methods and processes in the nature.
- Informational bionic: studying tools for data transfer, developmental and evolutionary strategies.

According to W. Nachtigall [4], bionics as a science proposes two main research principals:

- bottom-up-process where the principles of biological systems are abstracted, independent of product usage. Engineers, designers, architects could afterwards find application of the extracted principal;
- top-down-process means definition of a technical problem and search for solutions in the biosystems in the nature.

2. APPLICATION OF BIONICS PRINCIPALS IN THE PROCESS OF CONCEPT DEFINITION

Several aspects of the concept for modular prefabricated houses for living are derived by application of the bionics top-down-process. Three main problems were defined at the beginning and the solutions from the nature were recognized afterwards.

PROBLEM No. 1: Definition of the most appropriate shape for the assembling modules.

Elected sample from the nature: the honeycomb.

Proposed solution to the problem: Hexagonal prism is the form of the honeycomb (Fig. 1). It

is proposed as the most appropriate shape for the space modules, suitable for efficient arrangement into space structures.



Fig. 1. Honeycomb

PROBLEM No. 2: Definition of the best arrangement of the assembling modules into structures.

Elected sample from the nature: the schedule of crystals in the metal crystal lattice (Fig. 2).

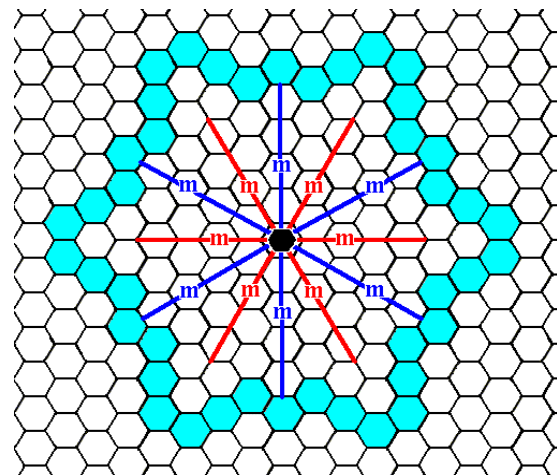


Fig. 2. Crystal structure of the metal

Proposed solution to the problem: There are a great number of different arrangements of the hexagonal crystals. All of them could be applied as a solution of the problem. The crystal lattice hexagons are usually symmetrical or mirrored (m) in multiple directions, which will contribute to a simpler arrangement of the modules to form structures for the proposed prefabricated houses.

PROBLEM No. 3: Definition of the supporting structure of the assembling module.

Elected sample from the nature: the structure of mammalian bone (Fig. 3). Bones are rigid organs that form parts of the skeleton. The internal structure of the bone is densely connected bone tissue.

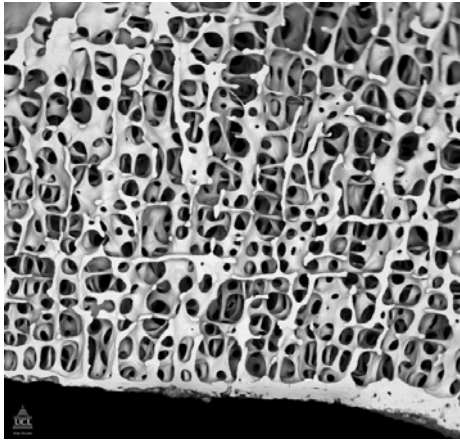


Fig. 3. The mammalian bone structure

Mechanical properties of the bones and the bones structure are excellent. Bones are classified in breakable materials, but their hardness is excellent. Bones can be compared with the hardness of steel at low temperatures and wood, measured parallel to their fibres. They are much stronger than artificial ceramics owing to the presence of collagen fibres in the bones. The elasticity of the bones is the result of the fibrous protein.

Proposed solution to the problem: metal lattice structure. This type of construction is nowadays very often applied in architecture and design because of the remarkable features.

3. DETAILED ELABORATION AND ANALYSIS OF THE MODULE STRUCTURE

According to the selected solutions for the shape, arrangement and structure of the modules using bionics top-down process the final shape of the modules is a hexagonal prism that would be fabricated as a metal lattice structure.

According to the space requirements for different rooms for living [5], the final dimensions of the typical module are established, presented on the technical drawing on Fig. 4. The diagonal of the circumscribed hexagon in the floor plan is 7.2 m long, the side of a hexagon is 3.6 m long, the area of a typical module is 33.6 m².

Technical drawing on Fig. 4 presents the adopted steel structure of the modules: 1. pillars, 2. beams, 3. auxiliary construction, 4. floor / ceiling structure [6]. Because of the adopted hexagonal shape of the module a triangular modular net is applied as a base (green lines).

The steel floor/ceiling structure of the modules is consisted of sticks which form triangles.

The floor and ceiling are connected with a ray of vertical sticks that allows application of glass windows through the whole height of the walls.

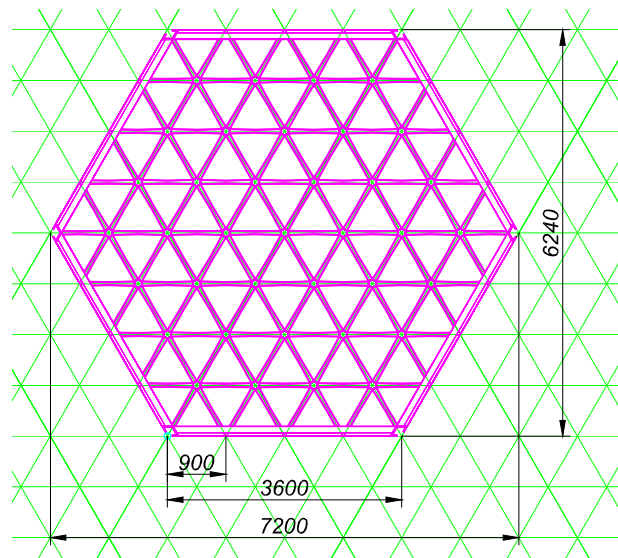
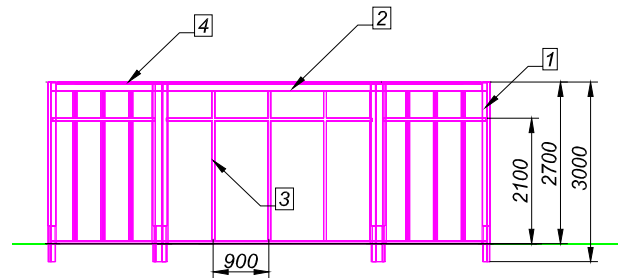


Fig. 4. Technical drawing for the steel structure of the module

The pillars of the module structure connected with the neighbour pillars of the modules form hexagonal shape (Fig. 5).

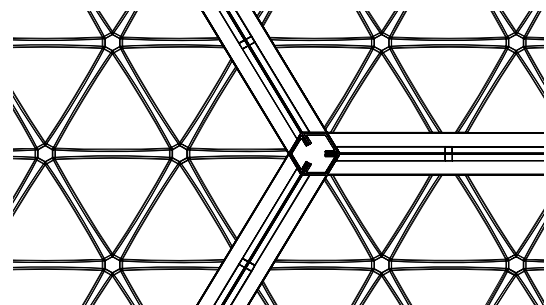


Fig. 5. Connection of three modules – detail

The pillars of the modules are connected with bolts and screws in horizontal direction. In vertical direction the both modules are connected with penetration of the upper pillars into the lower pillars at a height of the 300 mm, connected with bolts and screws (Fig. 6).

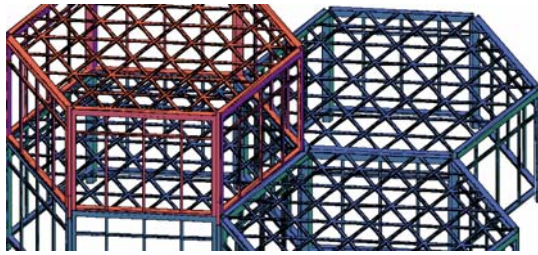


Fig. 6. Vertical arrangement of modules

4. STATIC ANALYSIS OF THE STRUCTURE USING THE FINITE ELEMENTS METHOD

The designed module steel structure enables solid rigidity. To confirm this statement static calculation and analysis with application of finite elements method is performed.

Predicted loads which will influence the structure are presented in Table 1:

Table 1

<i>Predicted loads</i>	
	N/m ²
Movable load for residential buildings	2000
Floor tiles of marble	200
Own weight	385
Total	2585

Adopted material for the structure is steel E360 (1.0070) with European standard EN 10025-2:2004.

The information and results from the analysis performed by the finite elements method, using the software package Solid Works, are presented in the next tables: model information (Table 2), material properties (Table 3), loads and fixtures (Table 4), resultant forces (Table 5), visual results of the structure loaded with 2585 N/m² (Fig. 7) and static displacement and nodal stress of the construction (Fig. 8).

Table 2

Model Information

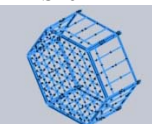
Name and reference	Formulation	Volumetric properties
Shell-1	Thin	Thickness: 6 mm
		Weight: 31427.7 N
		Volume: 0.411141 m³
		Mass: 3206.9 kg
		Density: 7800kg/m³

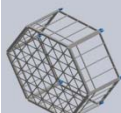
Table 3

Material properties

Name	1.0070 (E360)
Model type=:	Linear Elastic Isotropic
Default failure criterion	Max von Mises Stress
Yield strength	3.6e+008 N/m2
Tensile strength:	6.7e+008 N/m2
Elastic modulus:	2.1e+011 N/m2
Poisson's ratio:	0.28
Mass density:	7800 kg/m3
Shear modulus:	7.9e+010 N/m2
Thermal expansion coefficient:	1.1e-005 /Kelvin

Table 4

Loads and fixtures

Fixture name	Fixture image	Fixture details
Fixed-1		Entities: 30 faces Type{: Fixed geometry

Resultant forces

Components	X	Y	Z	Resultant
Reaction force (N)	5.1919	-5.18537	26546.7	26546.7
R. moment (N·m)	4.26816	0.913873	-9.22565	10.2061

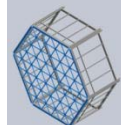
Load name	Load image	Load details
Pressure-1		Entities: 1 face Type: Normal to selected face Value: 2585 Units: N/m ²

Table 5

Resultant forces

Selection set	Units	Sum X	Sum Y	Sum Z	Resultant
<i>Reaction forces</i>					
Entire model	N	5.1919	-5.18537	26546.7	26546.7
<i>Reaction moments</i>					
Entire model	N·m	4.26816	0.913873	-9.22565	10.2061

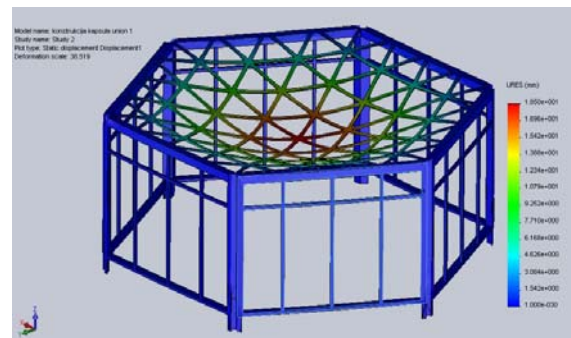


Fig. 7. Visual results of the loaded structure

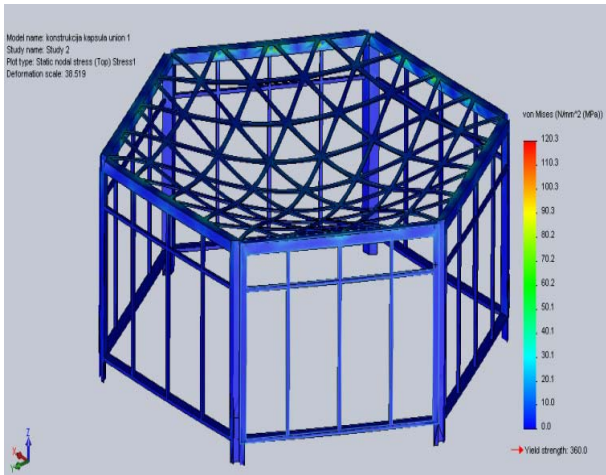


Fig. 8. Static displacement and nodal stress of the structure

5. SOLAR ANALYSIS – SELECTION OF PERFECT ORIENTATION AND INSULATION

The structures of arranged modules are modular prefabricated houses as apartments of closed structural type with internal yards - atriums. In order to confirm the good quality of living conditions of the designed apartments it was necessary to perform important analyses: lighting, shadows, insulation, ventilation and also thermal analysis. For that purpose the software package Ecotect was applied.

In the first phase the determination of the optimal orientation of the apartment (Fig. 9) was performed. The result shows that the best orientation of the living room is to the south.

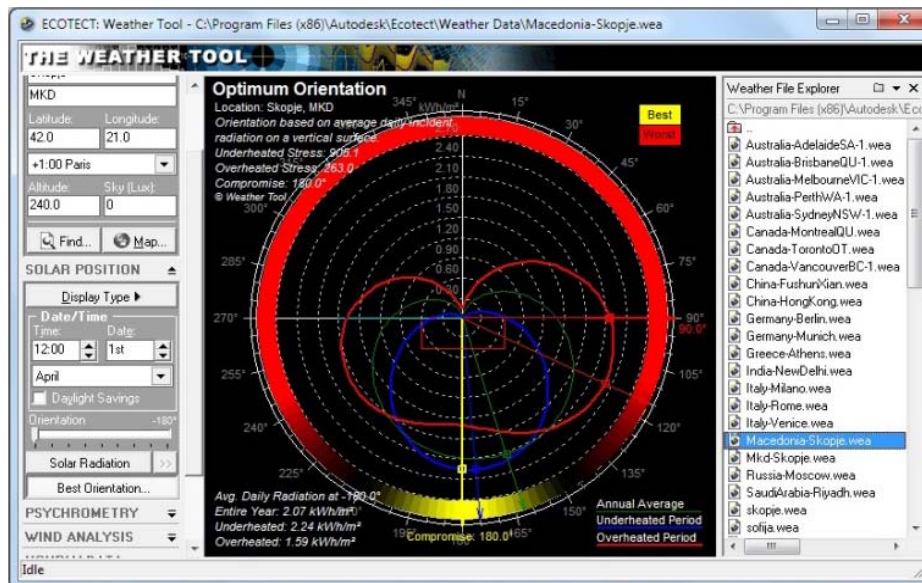


Fig. 9. Determination of the optimal orientation of the apartment

The analysis of shadows on June 22 at 12:45h shows that the atriums are properly dimensioned to ensure enough sunlight for the apartments, they are not overshadowed (Fig. 10).

The analysis of the shadows on June 22 at 12.45 h (Fig. 11) shows that insulation and shading of the interior ensure enough sunlight for the apartment and enough shadows for the warmest period of a summer day.

Insulation is the amount of energy on the Earth received from the Sun. This radiation contains the most of the emitted energy in the form of short wave radiation and light. In order to check the insulation for the whole apartment two analyses were performed for June 22: the first one for the ground floor of the apartment (Fig. 12), the

second one for the upper floor of the apartment (Fig. 13). The results for the both cases show the good insulation for the whole apartment.

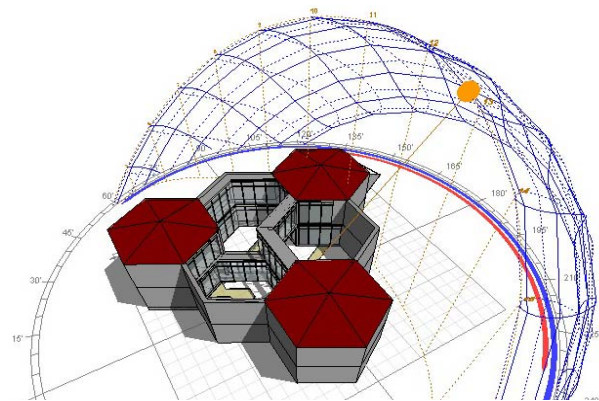


Fig. 10. Analysis of shadows on June 22 at 12.45 h

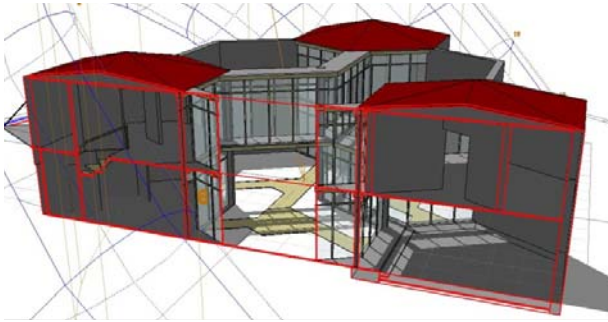


Fig. 11. Analysis of shadows in the interior on June 22 at 12.45 h

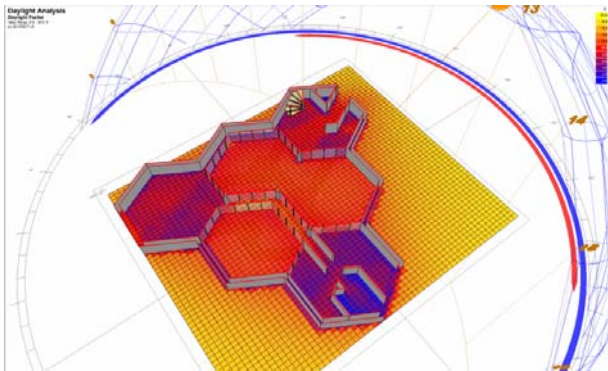


Fig. 12. Insulation analysis on the ground floor of the apartment on June 22

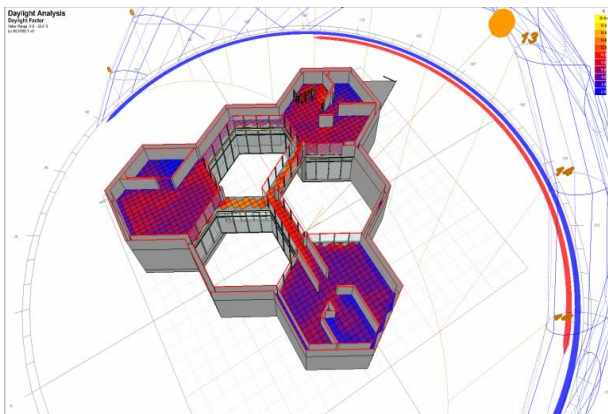


Fig. 13. Insulation analysis on the upper floor of the apartment on June 22

6. THERMAL ANALYSIS FOR ASSESSMENT OF ENERGY EFFICIENCY

The first step for the thermal analysis was setting the type of the walls for the modules – rooms. All of them are bordered with sandwich walls on four sides and with double thermo pane glass on the remaining two sides. Ecotect software auto-

matically calculates the coefficient of the heat transfer. The received result shows outstanding value of $0.180 \text{ W/m}^2\text{K}$.

The second step was zone management of the energy. The period of heating and cooling, using the system with mixed mode, in the rooms on weekdays is between 6:00 and 23:00 h and for weekends between 7:00 and 24:00h, with projected temperature of 22°C to 26°C .

It was also important for each module/room individually to predict the number of people who are expected to stay in the room in different periods of the day, the way people are expected to be dressed, the expected wind speed, the expected relative humidity, the way of lighting etc.

Hourly operational profile is an analysis that shows the energy flow according to the percentage of person attendance (number of persons in a certain period of day) in the room for a standard weekday (Fig. 14).

The obtained results are presented in the diagram (Fig. 15 and Table 6), which shows the amount of energy (Wh) required for heating and cooling for all zones, for all six modules respectively.

Gains breakdown is calculated also for all of the rooms. It is presented with the diagram on Fig. 16.

The results present the required energy for heating and cooling per month, for the whole apartment (Table 6). This data are necessary for calculation of the required devices for heating and cooling.

Example: required maximum energy for heating of the living room is 1022 W. Recommended device is aluminum radiator “Optimum”, Algreta, Resen, with smallest thermal effect. One radiator rib has a capacity of 120 W. According to the calculation $1022 \text{ W} / 120 \text{ W} = 8.52$, for heating of the living room there is a necessity of 9 ribs.

To improve the energy efficiency additional sources of energy are recommended. The designed roof of the house is a pyramid with six small slope segments, which is convenient for installing of solar devices. It is recommended to install three solar collectors and three photovoltaic panels with triangular form, where each of the triangles is with area of 6.36 m^2 .

The additional energy efficiency effect is the selection of proper windows and outside doors. Plastic profiles with double thermo pane glass are recommended.

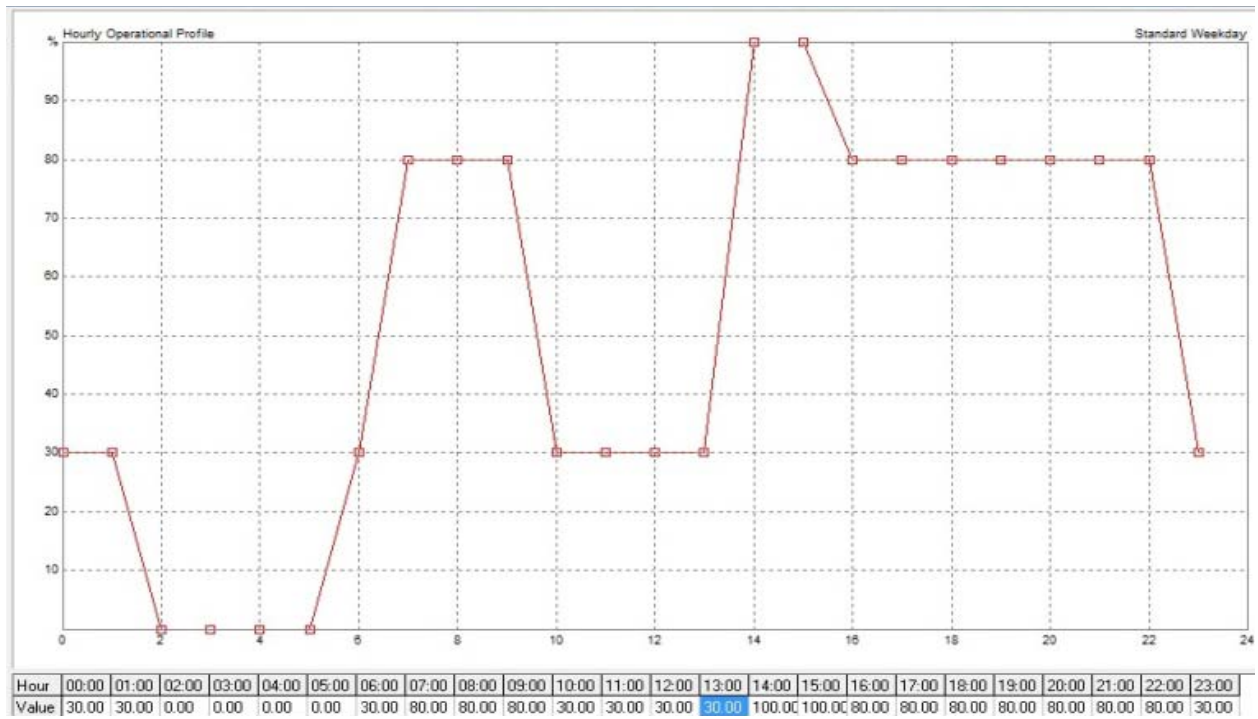


Fig. 14. Hourly operational profile

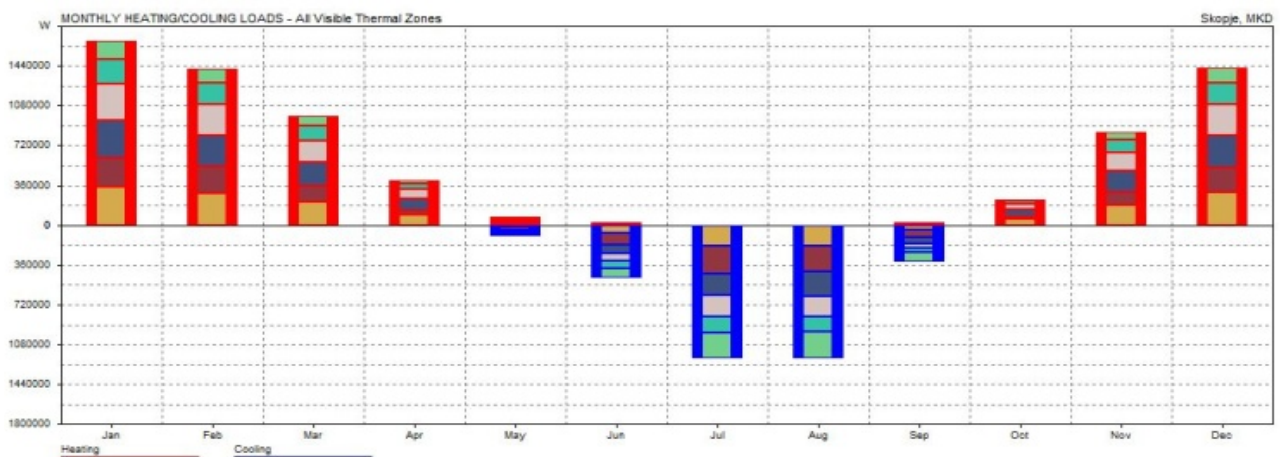


Fig. 15. Required monthly energy for all zones

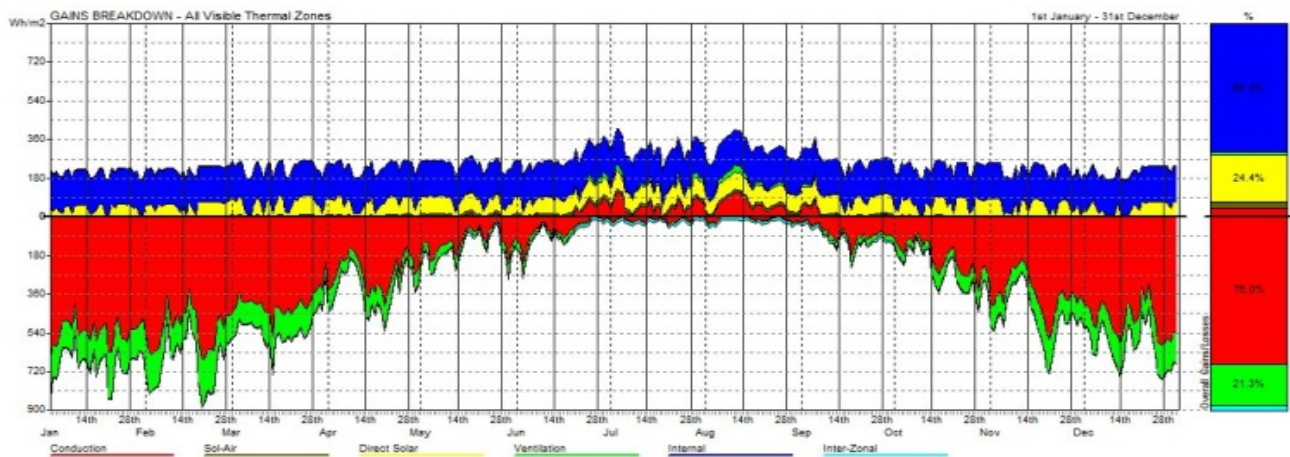


Fig. 16. Gains breakdown for all zones

Table 6.

Monthly heating /cooling loads

MONTH	HEATING Wh	COOLING Wh	TOTAL Wh
Jan	1664840	0	1664840
Feb	1416148	0	1416148
Mar	982211	0	982211
Apr	403538	0	403538
May	71651	95980	167631
Jun	27313	479669	506982
Jul	0	1200879	1200879
Aug	0	1205947	1205947
Sep	22598	326976	349575
Oct	233047	2469	235516
Nov	844221	0	844221
Dec	1423703	0	1423703
TOTAL	7089274	3311920	10401193
Per m ²	37618	17574	55193
Floor area	188.453 m ²		

All Visible Thermal Zones Comfort: Zonal Band.
 Max Heating: **6862 W** at 07:00 on 1st January
 Max Cooling: **7378 W** at 14:00 on 13th August

7. CONCLUSIONS

The presented concept in this paper, based on contemporary design methods modularity and bionics, propose a new way of building for prefabricated houses for living. The basic idea is to follow the space requirements of modern families without unnecessary moving from place to place, from house to house.

This concept is not so simple for realization from engineering aspect. There are many engineering problems to be solved: transportation, elevation, connection of the modules. The intention of the further researches is

to find appropriate decisions for the core engineering problems.

The aspect of energy efficiency today is very important. The presented idea could not be serious one if this aspect is not taken into consideration. All of the applied engineering analysis illustrate that the design and all of the applied materials and solutions have energy efficient house for living as a result. Our future researches will be directed into design of more effective energy efficient homes and products.

REFERENCES

- [1] W. Lidwell, K. Holden, J. Butler: *Universal Principles of Design*, Rockport Publishers, Inc., Massachusettes, USA (2003).
- [2] R. Neurohr, C. Dragomirescu: *Bionics in Engineering – Defining New Goals in Engineering Education at “Politehnica” University of Bucharest*, International Conference on Engineering Education – ICEE 2007, Coimbra, Portugal (2007).
- [3] M. Dickinson: *Bionics: Biological insight into mechanical design*, Proceedings of the National Academy of Sciences of the United States of America – PNAS, vol. **96**, no. 25, pp. 14208–14209, USA (1999).
- [4] W. Nachtigall: *Bionics, principles and examples for engineers and scientists*, Springer Verlag (2nd edition), Berlin, Germany (2006).
- [5] E. and P. Neufert: *Architects' Data*, Third edition, School of Architecture, Oxford Brookes University, Oxford (1999).
- [6] A. Agkathidis: *Modular Structures in Design and Architecture*, BIS Publishers Amsterdam and the editor / authors, USA (2009).

GEO-BASED SYSTEMS IN AUGMENTED REALITY

Taško Rizov, Risto Taševski

*Faculty of Mechanical Engineering, "SS. Cyril and Methodius" University in Skopje,
P.O. Box 464, MK-1001 Skopje, Republic of Macedonia
risto.tashevski@mf.edu.mk*

Abstract: Today's life is different to the one that existed not so many years ago. Our everyday life is constantly changing. The use of new technologies play major role in this change. Augmented Reality (AR) is looking to be the 8th mass market to evolve, following print, recordings, cinema, radio, TV, the Internet and mobile. In combination with geo-based technologies, augmented reality provides a completely new way of execution of the everyday activities. This paper presents the basic concepts and key characteristics of these two technologies. Also, the paper presents an example of a use of the technologies in an application meant for students for navigation through the campus of the Faculty.

Key words: augmented reality; 3D objects; geopositioning; visualization

СИСТЕМИ БАЗИРАНИ НА ГЕОГРАФСКО ПОЗИЦИОНИРАЊЕ ВО АУГМЕНТНАТА РЕАЛНОСТ

Апстракт: Животот денес драстично се разликува од оној што постоеше пред не толку многу години. Нашиот секојдневен живот постојано се менува. Употребата на нови технологии има клучна улога во оваа промена. Аугментната реалност (АР) има изгледи да биде осмиот масовен пазар кој се развива по печатењето, аудио продукцијата, киното, радиото, телевизијата, интернетот и мобилната телефонија. Во комбинација со технологиите за географско позиционирање, аугментната реалност обезбедува комплетно нов начин на извршување на секојдневните активности. Овој труд ги претставува основните концепти и клучните карактеристики на овие две технологии. Исто така, трудот претставува и еден пример за употреба на овие технологии во апликација наменета за студентите за навигација низ кампусот на Факултетот.

Клучни зборови: аугментна реалност; 3Д објекти; географско позиционирање; визуелизација

1. INTRODUCTION

Today's life is different to the one that existed not so many years ago. Our everyday life is constantly changing. The most important characteristics of our era may be the transformation, transmission and dominion of information. We live in an information society where the leading role has been given to new technologies. Our society could not be imagined without new technologies and their role both in this society and in human life in general.

With a growing amount of applications relying on spatial information systems, there is a corresponding increase in the number of naïve users of

such systems. Recognized for handling complex decision-making processes, spatial information systems need to be enhanced with real-world views in order to present the information in an understandable, user-friendly way [1]. Hence, the combination of the two emerging technologies of geo-based spatial information systems and augmented reality.

Augmented reality (AR) is a technology that enables digitally stored spatial information to be overlaid graphically on views of the real world [2]. AR holds enormous promise to enhance human management of complex systems, such as power plant maintenance procedures, cardiac surgery but also navigation through complex environments.

AR can be used as an enhancement in decision-making and operational efficiency in dealing with the intricacies of both natural and build environments. Considerable work is in progress around the world on hardware and software to develop AR systems.

2. AUGMENTED REALITY

Augmented Reality (AR) is a variation of Virtual Environments (VE), or Virtual Reality as it is more commonly called. VE technologies completely immerse a user inside a synthetic environment. While immersed, the user cannot see the real world around him. In contrast, AR allows the user to see the real world, with virtual objects superimposed upon or composited with the real world. Therefore, AR supplements reality, rather than completely replacing it. Ideally, it would appear to the user that the virtual and real objects coexisted in the same space. Azuma [3] gives a more comprehensive definition of AR as a system that has the following characteristics: (1) combines real and virtual world, (2) interactive in real time and (3) registered in 3D. Augmented Reality enhances a user's perception of and interaction with the real world. The virtual objects display information that the users cannot directly detect with their own senses. The information conveyed by the virtual objects helps a user perform real-world tasks.

Augmented Reality might apply to all senses, not just sight. So far, researchers have focused on blending real and virtual images and graphics. However, AR could be extended to include sound, smell or tactile.

A basic design decision in building an AR system is how to accomplish the combining of real and virtual. Two basic choices are available: optical and video technologies. Each has particular advantages and disadvantages.

Focus can be a problem for both optical and video approaches. Ideally, the virtual should match the real. In a video-based system, the combined virtual and real image will be projected at the same distance by the monitor. However, depending on the video camera's depth-of-field and focus settings, parts of the real world may not be in focus. In typical graphics software, everything is rendered with a pinhole model, so all the graphic objects, regardless of distance, are in focus. To overcome this, the graphics could be rendered to simulate a limited depth-of-field, and the video camera might have an autofocus lens.

In the optical case, the virtual image is projected at some distance away from the user. This distance may be adjustable, although it can be fixed if the display is mounted to the user. Therefore, while the real objects are at varying distances from the user, the virtual objects are all projected to the same distance. If the virtual and real distances are not matched for the particular objects that the user is looking at, it may not be possible to clearly view both simultaneously.

Contrast is another issue because of the large dynamic range in real environments and in what the human eye can detect. Ideally, the brightness of the real and virtual objects should be appropriately matched. Unfortunately, in the worst case scenario, this means the system must match a very large range of brightness levels. The eye is a logarithmic detector, where the brightest light that it can handle is about eleven orders of magnitude greater than the smallest, including both dark-adapted and light-adapted eyes. In any one adaptation state, the eye can cover about six orders of magnitude. Most display devices cannot come close to this level of contrast. This is a particular problem with optical technologies, because the user has a direct view of the real world. If the real environment is too bright, it will wash out the virtual image. If the real environment is too dark, the virtual image will wash out the real world.

A key measure of AR systems is how realistically they integrate augmentations with the real world. The software must derive real world coordinates, independent from the camera, from camera images. That process is called image registration. Image registration is one of the most basic problems currently limiting Augmented Reality applications. The objects in the real and virtual worlds must be properly aligned with respect to each other, or the illusion that the two worlds coexist will be compromised. More seriously, many applications demand accurate registration. Without accurate registration, Augmented Reality will not be accepted in many applications. Registration errors are difficult to adequately control because of the high accuracy requirements and the numerous sources of error. These sources of error can be divided into two types: static and dynamic. Static errors are the ones that cause registration errors even when the user's viewpoint and the objects in the environment remain completely still. Dynamic errors are the ones that have no effect until either the viewpoint or the objects begin moving.

Image registration uses different methods of computer vision, mostly related to video-tracking.

Many computer vision methods of augmented reality are inherited from visual odometry. Usually those methods consist of two parts. First detect interest points, or fiducial markers, or optical flow in the camera images. First stage can use feature detection methods like corner detection, blob detection, edge detection or thresholding and/or other image processing methods.

The second stage restores a real world coordinate system from the data obtained in the first stage. Some methods assume objects with known geometry (or fiducial markers) present in the scene. In some of those cases the scene 3D structure should be pre-calculated beforehand. If part of the scene is unknown simultaneous localization and mapping (SLAM) can map relative positions. If no information about scene geometry is available, structure from motion methods like bundle adjustment are used. Mathematical methods used in the second stage include projective (epipolar) geometry, geometric algebra, and rotation representation with exponential map, Kalman and particle filters, nonlinear optimization, and robust statistics.

However, video-based approaches can use image processing or computer vision techniques to aid registration. Since video-based AR systems have a digitized image of the real environment, it may be possible to detect features in the environment and use those to enforce registration. They call this a "closed-loop" approach, since the digitized image provides a mechanism for bringing feedback into the system. For example, in some AR applications it is acceptable to place stationeries in the environment. These stationeries may be LEDs or special markers. The locations or patterns of the stationeries are assumed to be known. Image processing detects the locations of the stationeries, and then those are used to make corrections that enforce proper registration.

According to Young [1] there are three broad components of AR systems: track, retrieve and inform. AR systems operate by tracking events and then providing users with information about those events. For visual AR systems, event monitoring is primarily based on user pose (position and attitude of the user). This information is required to enable the registration of augmented information to the user's view. Registration refers to the process of combining the user's view of the physical environment with additional information provided by the AR system. There are several types of sensors used for tracking, and often a hybrid approach is

implemented to enable the AR system to operate in different environments and to provide not only user position, but also attitude. In the retrieve component, event information is used to query the AR system's database. Information can be chosen and sorted according to the restrictions and requirements generated from the event data. The inform component presents the retrieved data in a manner useful to the user. The format of this presentation may vary, and could be visual, audible, haptic or combination of all [1].

3. GEOBASED SYSTEMS

The growing amount of applications relying on spatial information systems is mainly due to the availability of these systems to a wider range of users. This was primarily evoked by the decision of the U.S. Department of Defense and U.S. Department of Transportation in 1997 that civil users will have uninterrupted access to the carrier phase portion of the L2 signal which was only for military use prior to that [4]. In addition, the huge popularity and constantly growing number of users of smart phones and similar hand-held devices enabled to use different geobased systems resulted in high acceptance of this technology at every day user level.

The development of the geobased systems started with the military technologies developed in 1972 when the USAF conducted developmental flight tests of two prototype GPS receivers using ground-based pseudo-satellites and continues with today's development of Satellite-based Augmentation Systems (SBAS) all around the world.

The Global Positioning System (GPS) is consisted of 24 satellites orbiting in 6 orbits around the Earth providing high accuracy and global coverage, with a position fix generally available within 60 seconds of turning the receiver on [1]. GPS receivers for position determination are common additions to AR systems that are used in outdoor environments. There are two improvements to a standalone GPS receiver that have made GPS technology suitable for AR applications. They are Differential GPS (DGPS) and RTK GPS.

DGPS relies on the establishment of a GPS base station, which transmits C/A-code pseudo range corrections to the rover receiver, or the user. Accuracies of up to 0.3 meters are possible. For RTK GPS, the carrier phase is used for range measurement, providing a much more accurate

satellite range. Using this technique, real-time positioning at 10 Hz with an accuracy of up to 0.005 meter is achievable [5].

One more enabler in the development of the geobased systems is the advances in sensor technologies. The abilities of the sensors have changed dramatically in the past 15 years, from use of inertial sensors, accelerometers, gyroscopes and compass to the use of Fiber Optic Gyroscopes (FOG) and Micro-Electro-Mechanical Systems (MEMS). The advances in production processes of these sensors have provided the ability of having accurate, small, low consuming and low cost devices. Still, there is no single sensor available that will provide all the necessary data for geobased systems. This is the expected direction of further research and development in this technology.

With geobased augmented reality systems the most important element is to determine user's position and attitude (heading, pitch and roll). The input from the geobased systems is crucial in the tracking component in the AR systems. Its sole purpose is to provide information about the user's environment. Using GPS technology, it is possible to determine the position of user's device with an accuracy of around 1 centimeter [1]. This surely depends on the mode and type of GPS equipment that one will use. Still, by using GPS technology we can only determine the longitude and latitude of the user's device, but we cannot determine his attitude. Meaning, the user can be near the historical monument, and this can trigger to retrieve and present information about the monument in vicinity, while the user is oriented towards the other side turning his back to the point of interest. That is why, in geobased systems for augmented reality, systems for determining the heading, pitch and roll of the user's device is of same importance as the systems for determining the position. Using inertial sensors and dead reckoning tracking systems the relative position and orientation of the user's device can be determined.

4. GEOBASED SYSTEMS IN AUGMENTED REALITY

By combining these two technologies users are provided with a solution that solves number of issues that neither geobased systems nor augmented reality can solve as single technologies. This combination provides users with ability to visually navigate through urban environments, to

visually get information on touristic monuments or similar points-of-interest, to visually get information from various GIS systems and databases etc.

In this paper the system for visual navigation through the campus of the Faculty of Mechanical Engineering – Skopje is described. Existing students, but more often the new students have difficulties in finding the classrooms, laboratories or other point of interest along the campus. Since the campus is consisted of 7 different buildings spread on an area of approximately 45000 m² often finding the right location of a classroom is difficult if you do not know which classrooms are in which building. Also, students often have to find their way to a classroom fast in order to get to a lecture on time.

In order to solve the above described problem a comprehensive solution had to be created. The solution is consisted of hardware and software with specifically designed architecture. The system is designed primarily to assist students to easily find their way through the campus to various classrooms, laboratories, student's organizations etc. The systems was developed using only of-the-shelf software and usual hardware that is used by this target group.

On the market today a variety of software packages exist for augmented reality. They are developed with a main goal to help the users to easily create an augmented reality scene. Depending on the level of computer literacy, especially on the level of knowledge of computer programming, different software is available.

Basically, no matter which of the existing software for creation of AR scenes is going to be used the procedure for its use and the design of the complete system is pretty much the same. One always needs a personal computer, regardless of its physical shape (desktop, laptop, tablet or smart phone). Depending on the AR software used different operating systems are compatible. The majority of the available software is compatible with Windows, Android and iOS. The final required element to create the AR scene is the 3D virtual object. This can also be video or even a picture. In order to make the system faster and to lower the data traffic over the internet, the solution described in this paper uses pictures with accompanying text as elements for augmenting the reality (Fig. 1).

The first step, in creating the geobased augmented reality is to define the type of virtual objects that are going to be used as augmentation of the user's reality. As mentioned previously, the

augmentation can be done using 3D model, a video, a picture or text, or as in this case, it can be done using a combination of the above mentioned. In this case a combination of picture and accompanying text is used. The pictures represent the building of the campus of the Faculty of Mechanical Engineering – Skopje, and the accompanying text describes which classrooms or laboratories are inside that building.

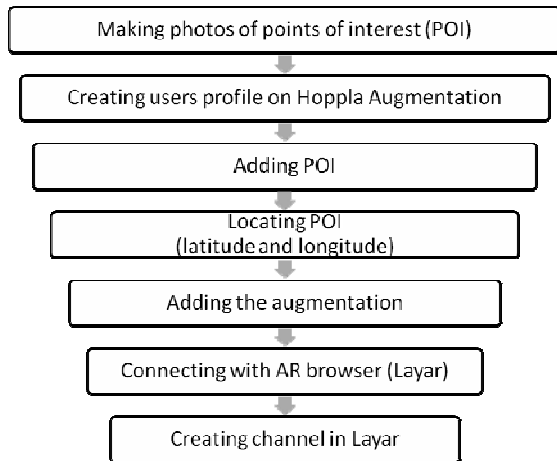


Fig. 1. Flow diagram of creating geo-based application

There are various ways how to combine a geobased system with augmented reality. In any case, one has to map data from a GIS system to data from the augmented reality application (Fig. 2). This is to execute the first component of augmented reality and that is tracking. Since this type of AR applications are marker-less and used in unprepared outdoor environment, the tracking component is done by data from the user's sensors determining the position and attitude.



Fig. 2. Design and operating diagram of the application

The system described in this paper is meant for hand held devices that are equipped with devices for position and attitude determination. In order to identify the position of the point of interest, in this case the system of *Hoppala Augmentation* is used (Fig. 3). *Hoppala* is a web based entry point content platform for mobile augmented reality applications. The platform offers seamless support for the three biggest mobile AR browsers: Layar, Junaio and Wikitude. Hoppala provides easy-to-use graphical web interface to create augmented reality contents. It provides a full screen map interface with ability to add images and 3D models as augmentations by uploading them to a personalized inventory.

After creating the content, again using Hoppala users can publish their geobased augmented reality application to all major mobile augmented reality browsers (Fig. 4). Publishing content on mobile AR browser today still requires creating program code, and without any established standards, content creation not only becomes a technology decision, but even a platform decision as well [6].

Next step is to create the application that will be displayed and operated by user on user's device. In this case the application was created using the system of Layar. Using the web based application Layar Creator any registered user can create a layer or a channel that is going to be used by users to display the augmentations. The Layar Creator offers ability to customize the channel by adding picture, logo, short and long text description etc. In addition, it uses metrics for the creators of channels to monitor the use of the created channel.

After that, the Layar Creator is checking and verifying the API Url provided by the Hoppala Augmentation platform. If the checks are verified, than the layer can be published. With that, end-users are able to open the layer on their handheld device using the Layar app. (Fig. 5).

When the described layer is searched using the Layar app, the layer basic description is displayed on the user's handheld device. After starting the layer the handheld device displays the video from the camera showing what is in line of sight of the user. The app sends spatial data collected by the sensors to the server and queries any point of interest in vicinity relative to the user's position and attitude. After retrieving the data, information is registered on user's display augmenting the video of the real world displayed on the hand held device

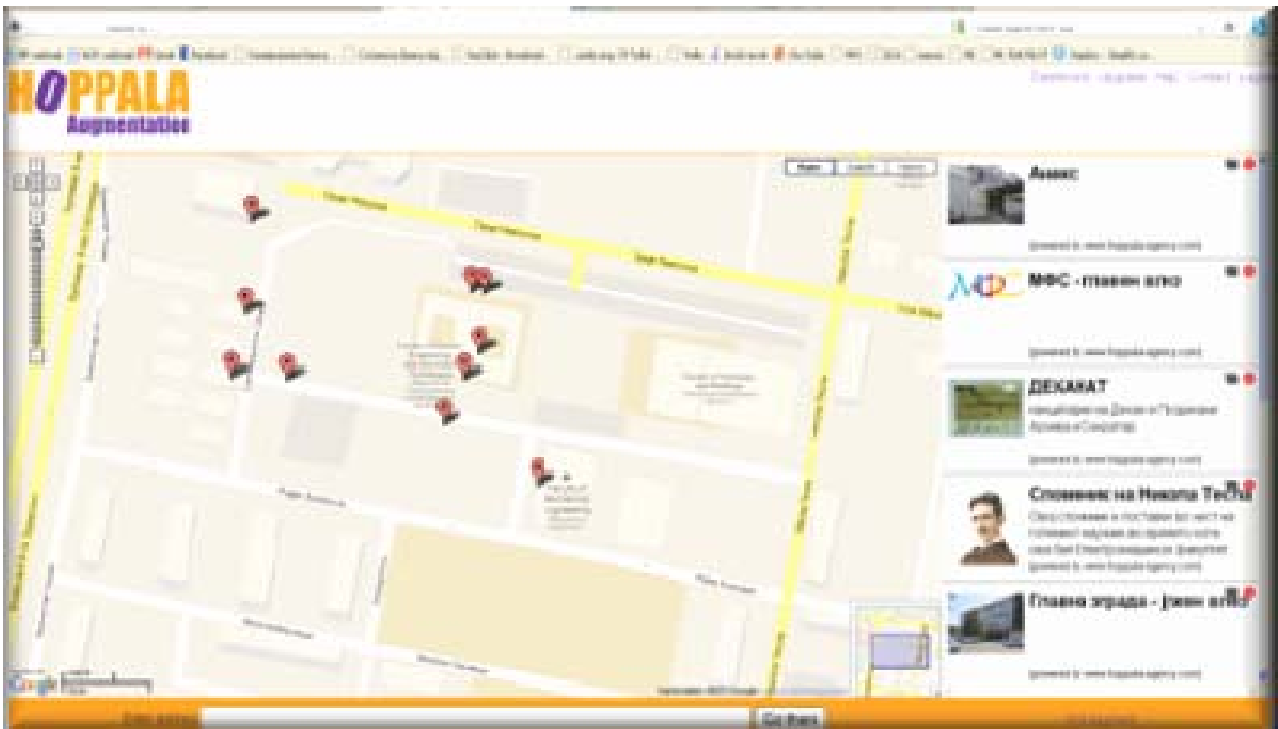


Fig. 3. Interface of Hoppala Augmentation content platform

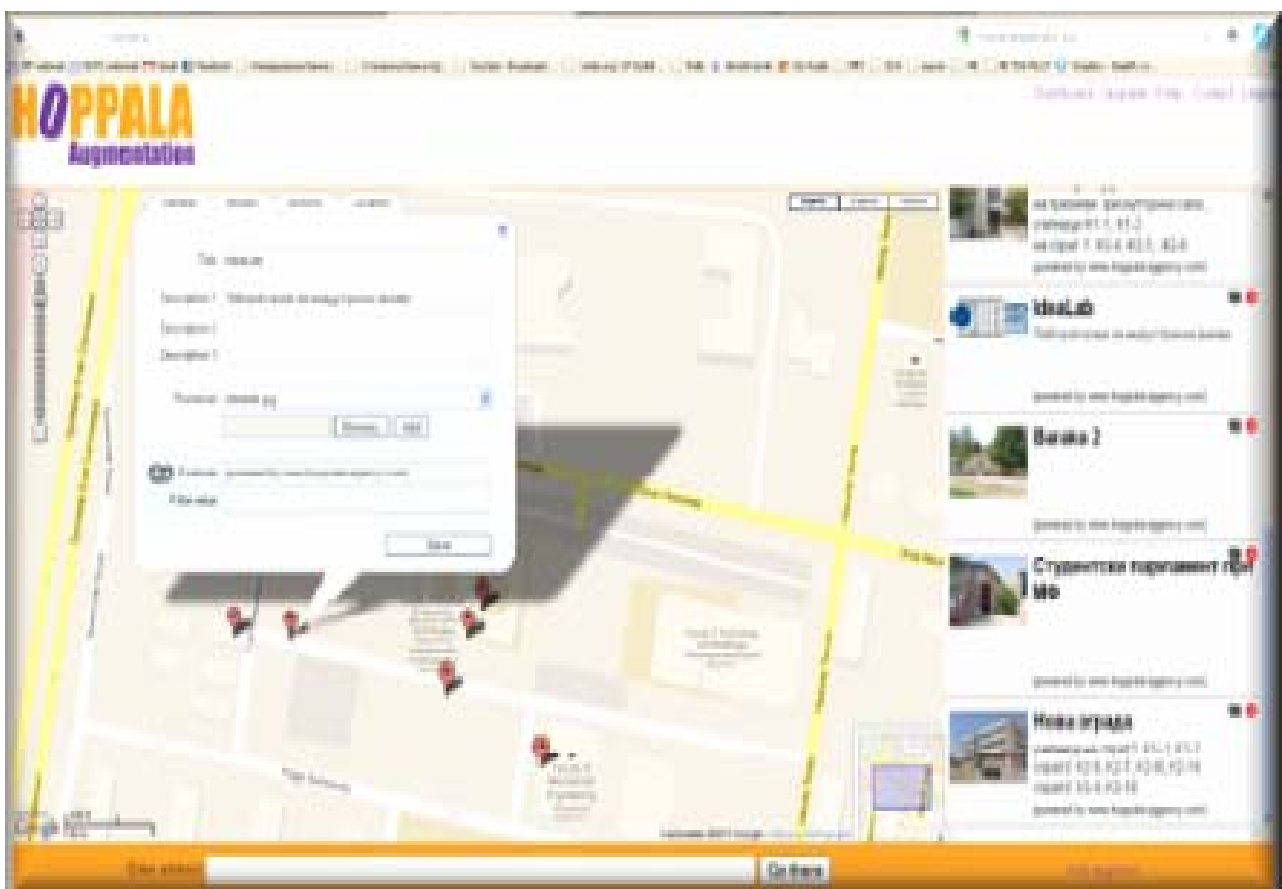


Fig. 4. Adding augmentations using Hoppala Augmentation content platform

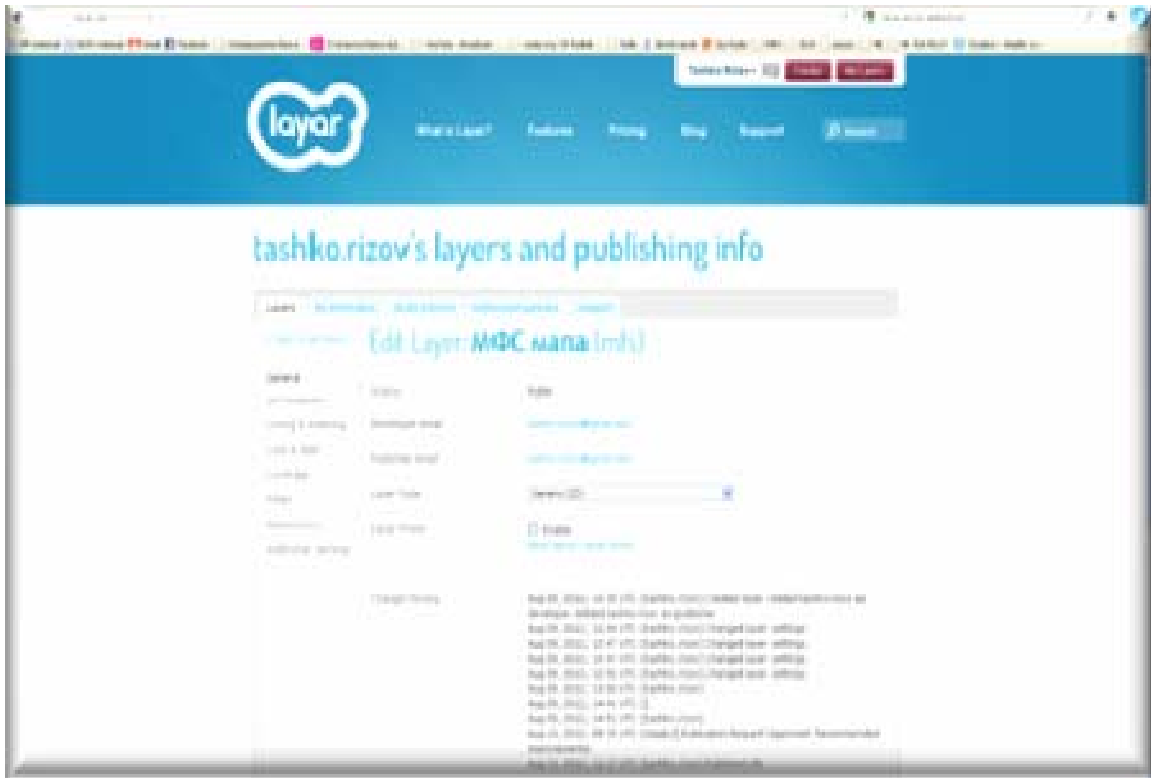


Fig. 5. Creating channel using Layar Creator

The layer augments the user’s reality by displaying the pictures of the points of interest along with text explaining which classrooms or laboratories are located at that building (Fig. 6). At the same time, the app provides the ability to navigate the user from the current position to the desired point of interest either by foot or by car displaying the distance, needed time to reach the destination.

In that way, students can find their way through the campus in easy manner and fast. With this tool they can reach their destination on time, hence they can be in the classroom before the class starts (Fig. 7).

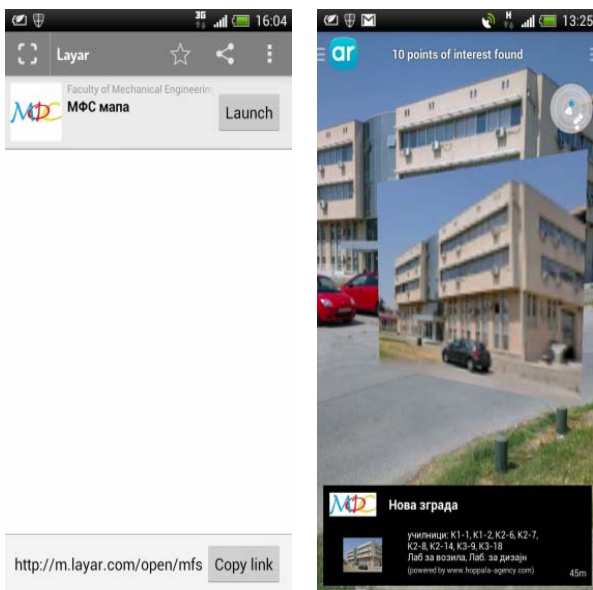


Fig. 6. Screen shots from application MFS map

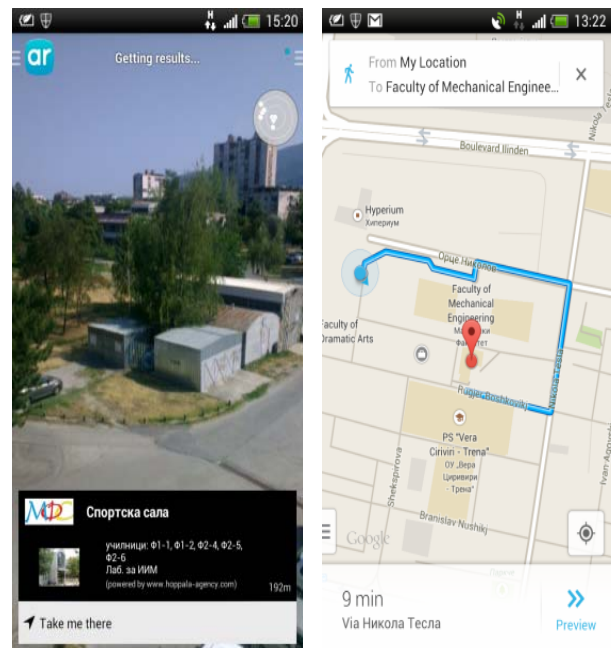


Fig. 7. Navigation using application MFS map

Also, they like using new technologies and things that make them look more technology aware. Last but not least, the majority of students like the design and user friendliness of the application. It is simple and it does exactly what it says it does. The negative aspects of the application are that users will use it only limited number of times. Meaning, students need to find their way around the campus only during their first two weeks of their first semester. After that, they pretty much have been in all classrooms and know their location on the campus. Using the application afterwards, when they are acquainted with the campus is only in rare occasions. The second negative aspect is the internet connection. The use of the application is fully dependable on access to internet. The campus has wireless signal, but sometimes it is weak and users are not able to connect to it. Although, internet is available through the mobile networks its speed is still very low and the prices by the mobile providers are still not competitive for a target group as students.

5. CONCLUSION

This paper presents the basics of geo-based systems in augmented reality and the ability to use this technology as an everyday tool. According to Dan Farber from CBSNews and CNET News “The next big thing in technology: Augmented reality”. This statement is getting its verification by every passing day. The “big thing” is getting even bigger mostly due to the enormous spread of use of smartphones and other smart hand-held devices. Augmented Reality (AR) is looking to be the 8th mass market to evolve, following print, recordings, cinema, radio, TV, the Internet and mobile, according mobile industry analyst Tomi Ahonen. The ability this technology is providing to users is unimaginable. Its applications spread each day as more peo-

ple are becoming aware of it and as they start understand how it can augment their lives.

But still, all this is mainly limited by the key characteristic of the augmented reality – and that is how real the virtual objects are presented. In order for the AR to work, it has to persuade its user that the virtual and real objects coexist in the environment. Here is where geometry has to complete its role. By using various geometric projections a various level of reality is achieved. It is clear that best results would be provided by stereo-metric perspective, but than one should consider the complexity, price and time consumed to produce the virtual objects for AR. Since this technology is mostly used by wearable computers and hand-held devices with limited power of graphical processors the focus is put on lean methods for providing geometrical projections that result with virtual objects that are at the same time real enough and simple enough.

6. REFERENCES

- [1] S., Young: *Integrated Position and Attitude Determination for Augmented Reality Systems*, Department of Geomatics, University of Melbourne, 2004.
- [2] G. Roberts, A. Evans, A. Dodson, B. Denby, S. Cooper, R. Hollands: Integrating GPS, INS and Augmented Reality for sub-surface visualization, *Proceedings of the 14th International Technical Meeting of the Satellite Division of The Institute of Navigation (ION GPS 2001)* – Salt Lake City, USA, 233-266 (2001).
- [3] Azuma R.: A Survey of Augmented Reality, *Teleoperators and Virtual Environments*, August 1997, USA, pp. 355–385.
- [4] Wikipedia, available at: en.wikipedia.org/wiki/Global_Positioning_System (accessed at 15.08.2013).
- [5] Leica: *GPS Surveying System 500 Technical Reference Manual*, Leica Geosystems AG, Heerbrugg, Switzerland, 1999.
- [6] Hoppala AR Content Platform, available at: www.hoppala-agency.com/article/augmented-reality-content-platform/#more-1392 (accessed at 15.08.2013)..

COMFORT ANALYSIS OF DRIVER'S SEAT FOR PASSENGER CAR THROUGH SIMULATION OF THE SITTING PROCESS

Ile Mircheski, Tatjana Kandikjan, Sofija Sidorenko, Petar Simonovski

Institute of Engineering Design, Mechanization and Motor Vehicles, Faculty of Mechanical Engineering, "SS. Cyril and Methodius" University in Skopje, P.O. Box 464, MK-1001 Skopje, Republic of Macedonia
ile.mircheski@mf.edu.mk

Abstract: In this paper, a method in two phases for ergonomic analysis of the seating comfort in the driver's seat for passenger vehicles is presented. In the first phase, the comfort seating postures of the driver are analyzed considering the comfort angles for the placement of human body and necessary space for foot controls in vehicles, as well as the ranges of adjustments of the driver's seat and steering wheel. According to the determined comfort postures, the seat-human body virtual system is modeled. In the second phase, virtual testing of the seating comfort is performed with two different body sizes for 50th and 80th percentiles of virtual mannequins. The results can be used further to improve the arrangement of the basic comfort components for the driver's seat in vehicles. Virtual solid model of a driver's body and driver's seat was created, especially for analysis of the pressure distribution on the contact surface of the virtual human body and the seat cushion foam. The virtual testing was performed using software package ABAQUS, simulating processes with finite element analysis method (FEA). The testing includes variation of the spatial mechanical properties of polyurethane foam and variation of the male body sizes for 50th and 80th percentiles. The results from the virtual testing were verified experimentally using pressure distribution mapping sensors. Using to the virtual testing system for seating comfort, design changes of the seat can be introduced and verified.

Key words: Comfort angles; driver's seat; ergonomics; pressure distribution; virtual human model; virtual mannequin

АНАЛИЗА НА УДОБНОСТА НА ВОЗАЧКОТО СЕДИШТЕ ЗА ПАТНИЧКИ АВТОМОБИЛ СО СИМУЛАЦИЈА НА ПРОЦЕСОТ НА СЕДЕЊЕ

Апстракт: Во овој труд е презентирани метод кој содржи две фази на ергономски анализи на удобноста при седење на возачко седиште од патнички автомобил. Во првата фаза се анализирани положбата на возачот при седење и агли на местоположбата на човековото тело при седење, како и просторот потребен за управувачките педали во возилото, распонот на нагодување на возачкото седиште и управувачкиот волан. Во согласност со определените удобни положби е моделиран виртуелниот систем на седиште и човеково тело. Во втората фаза е направено виртуелно тестирање на удобноста при седење со две различни големини на тело за 50 и 80 проценти на виртуелни манекени. Резултатите можат да бидат користени за понатамошно подобрување на оценувањето на основните компоненти на удобноста за возачкото седиште. Креирани се виртуелни модели на човеково тело и возачко седиште за анализирање на распределбата на притисок на контактната површина помеѓу виртуелното човеково тело и седиштето од полиуретанска пена. Виртуелното тестирање е извршено со употреба на софтверскиот пакет ABAQUS кој служи за симулирање на процеси со методот на конечни елементи (FEA). Тестирањето вклучува промена на одредени механички особини на полиуретанската пена и промена на големината на човековото тело за 50 и 80 проценти на човек. Резултатите од виртуелното тестирање се експериментално верифицирани со користење на сензори за мерење на распределбата на притисокот. Дизајнерските промени кои се прават на седиштето во процесот на тестирање можат да бидат потврдени и верифицирани со употребата на системот за виртуелно тестирање на удобноста при седење.

Клучни зборови: Удобни агли; возачко седиште; ергономија; распределба на притисок; виртуелен модел на човек; виртуелен манекен

1. INTRODUCTION

The choice of passenger car depends on a variety of factors, such as vehicle type, brand, trend,

safety, performance, interior space, interior design, additional equipment and other. The seat comfort is very important issue for the drivers. Long time

driving usually affects on manifestation of low back pain or other musculo-skeletal disorders, caused by the discomfort of the seats. According to this fact, the expectations of customers regarding the seat comfort are continuously increasing [1, 2]. The manufacturers of seats for passenger automobiles have to respond on market requirements fast and appropriate and offer seats with higher quality and comfort.

The process of manufacturing of automobile seats, from the beginning of product development until the final fabrication, requires a great amount of time and financial resources. The manufacturers of automobile seats usually make prototypes for testing of the comfort in order to achieve the desired results. Testing with prototypes is time and money consuming process [3].

The contemporary vehicle development process is based on the virtual design of the vehicle structure and its verification. Using appropriate software products for virtual modeling of vehicle structure, as well as software products for simulation of processes and system behavior, the time required for testing of the new vehicle today is reduced. Contemporary testing of new vehicles starts with virtual testing of virtual models, using virtual humans. The errors and inconveniences are reduced in the early phase. As a consequence, time and price for testing of new or improved vehicles are reduced. The final tests are applied on real models - prototypes.

The first phase of our research is determination of the basic components of the automobile's driver comfort: angles for placement of the human body and necessary space for the foot controls, as well as the ranges of adjustments of the driver's seat and the steering wheel. The second phase of our research is to determine the influence of variation of the spatial mechanical properties of polyurethane foam, such as thickness and density, and also the shape of contact surface between driver and seat, to the seating comfort for automobile's driver.

2. DETERMINATION OF THE COMFORT SEATING AND HANDLING CONDITIONS FOR THE DRIVER

Sitting of the driver and other passengers, arrangement of all handling devices and controls, as well as application of all safety regulations and legislation [4, 5], are very important initial points in order to perform the overall dimensioning of the vehicle. The process of design starts with defini-

tion of a user population and with obtaining human body data.

In order to obtain comfort posture for the drivers of different sizes, many components of the vehicle have to be adjustable. Contemporary vehicles are equipped with adjustable seats, adjustable steering wheel, and adjustable mirrors. Other components, like the floor under the foot pedals, are not yet adjustable, because of the complicated and expensive mechanisms.

The first part of our research was committed to the definition of the best position of the seat and all handling devices in the vehicle. We started with adoption of comfort criteria and definition of four different testing conditions with different initial fixed point: fixed eye point, fixed hip point, fixed hand point and fixed heel point.

2.1. Adoption of the comfort criteria

The ranges of seat and steering wheel adjustments are directly dependent on the body sizes of the smallest and biggest representative of the selected user population. The analyses were applied on two extreme human sizes: 5th percentile woman and 95th percentile man.

In the case of driver's work position the workspace envelope depends on the position of the driver's body. Several functional measurements are very important parameters in the vehicle: the angles in elbow joint, shoulder joint, hip joint, knee joint, ankle joint and torso orientation (Fig. 1).

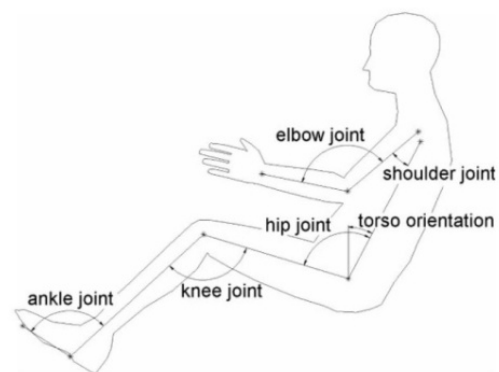


Fig. 1. Parameters of driver's work position

In order to obtain driving comfort the driver's seating posture have to be always in the comfortable range [3]. Many researchers during the past few years have offered their recommendations about the ranges of comfortable angles [6]. There are big differences between their recommendations

about the comfort angles. Some of them recommend discrete comfort angles, and the others recommend ranges of comfort. Using the fact that RAMSIS software [7] is specialized for ergonomics in vehicles we decided to adopt the recommended discrete comfort angles included in the RAMSIS data bases (Table 1).

Table 1

Adopted comfortable angles for the driver's seating posture

Torso orientation	27°
Angle of shoulder joint	22°
Angle of elbow joint	127°
Angle of hip joint	99°
Angle of knee joint	119°
Angle of ankle joint	103°

2.2. Examination of the proposed testing concepts

Virtual mannequins of two extreme anthropometric sizes with adopted comfortable posture were examined in four different testing conditions with different initial fixed point: fixed eye point, fixed hip point, fixed hand point and fixed heel point. The results of the testing were the ranges of necessary horizontal and vertical adjustments of the vehicle's components in order to accommodate drivers of different human sizes.

The concept of fixed eye point for all anthropometric sizes requires the following adjustments (Fig. 2):

- adjustment of the seat in the horizontal range of 43 mm and vertical range of 85 mm;
- adjustment of the steering wheel in the horizontal range of 119 mm and vertical range of 58 mm;
- adjustments of the foot pedals in the horizontal range of 218 mm and in the vertical range of 129 mm.

The driver's seat has to be fixed in the vehicle in the concept of fixed hip point (Fig. 3). This concept for all anthropometric sizes requires the following adjustments:

- adjustments of the steering wheel: horizontal adjustment of 75 mm and vertical adjustment of 425 mm;
- adjustments of the foot pedal: horizontal adjustment of 175 mm and vertical adjustment of 44 mm;

- because of the fixed seat, the eye position could not be positioned on the recommended height: missing horizontal adjustment of 31 mm and vertical adjustment of 85 mm.

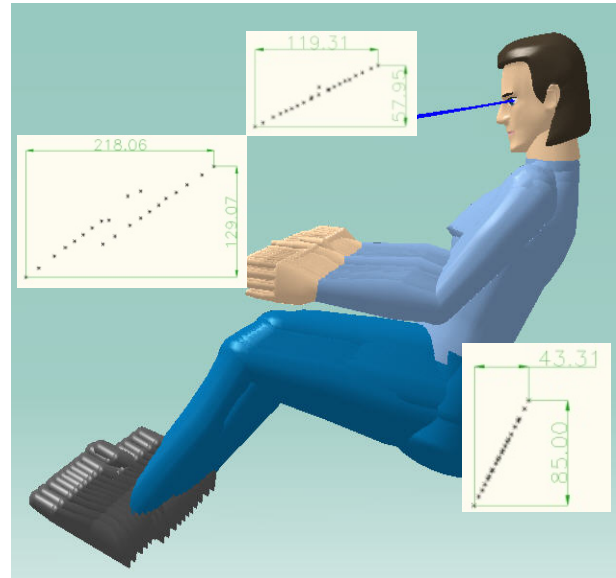


Fig. 2. Concept with fixed eye point

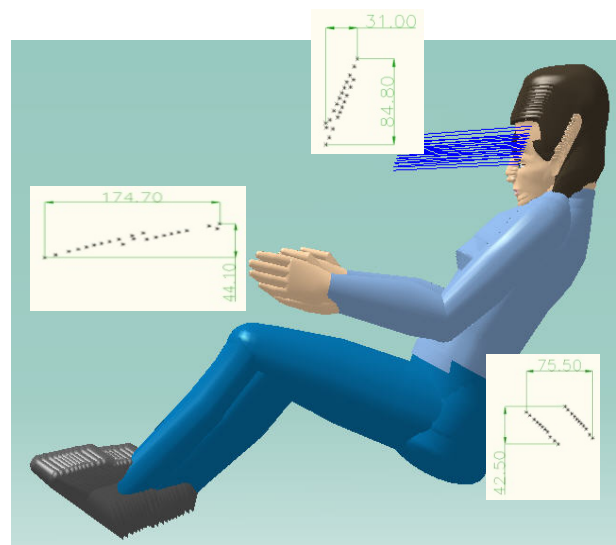


Fig. 3. Concept with fixed hip point

The steering wheel has to be fixed in the vehicle in the concept of fixed hand point (Fig. 4). This concept for all anthropometric sizes requires the following adjustments:

- adjustments of the seat: horizontal adjustment of 80 mm and vertical adjustment of 44 mm;
- adjustments of the foot pedal: horizontal adjustment of 94 mm and vertical adjustment of 72 mm;

- because of the fixed steering wheel, the eye point could not be positioned on the recommended height, but it could be neglected because the difference is only 57 mm.

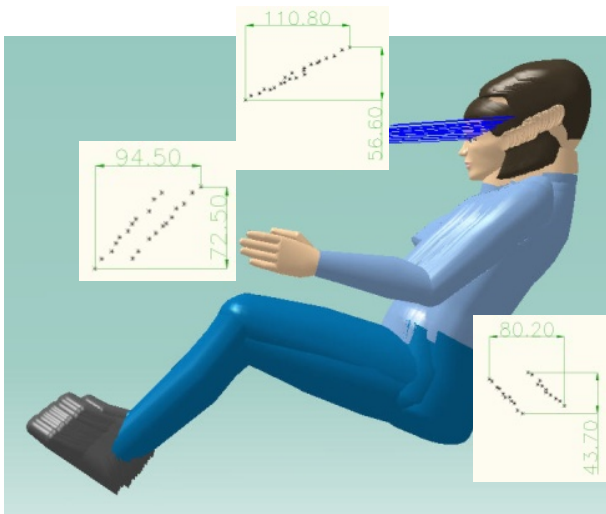


Fig. 4. Concept with fixed hand point

The concept with fixed heel point proposes fixed foot controls (Fig. 5). This concept for all anthropometric sizes requires the following adjustments:

- adjustment of the seat: horizontal adjustment of 173 mm and vertical adjustment of 58 mm;
- adjustments of the steering wheel: horizontal adjustment of 97 mm and vertical adjustment of 87 mm;
- because of the fixed foot controls, the eye point could not be positioned on the recommended height. The difference of 143 mm could not be neglected.

The concept with fixed heel point was accepted as a concept with the best balance between function and driver's comfort.

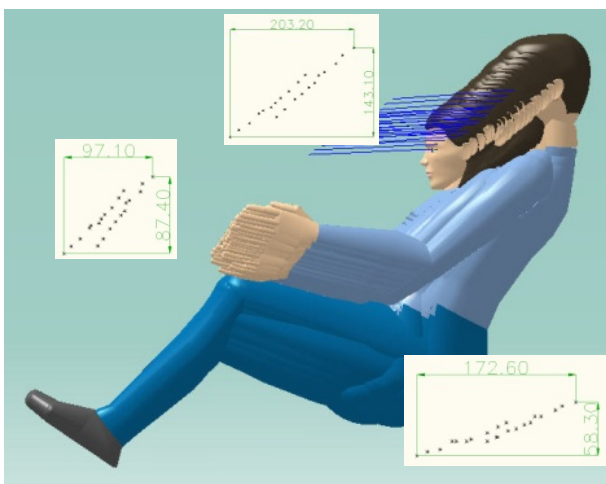


Fig. 5. Concept with fixed heel point

2.3. Improvement of the selected concept

In order to ensure perfect visibility on the road the eye points of all of the anthropometric sizes have to be placed on or over the line that touches the front profile of the car's shell. The visual line can be defined as a tangent line over the front profile of the car's shell that begins in the eye point of a 95th percentile man. The anthropometric size of 95th percentile man has a best view as a result of his highest eye position in comparison with other anthropometric sizes.

In order to obtain a good driving comfort the positioning of the pedals for foot controls has to be in accordance with the comfort knee angle. Several situations of different leg positions, as a result of different pressing forces applied on the pedals were also examined.

The first examined situation was: the right foot in pressing position on the acceleration pedal and the left foot in relaxing position. The results were: comfort positions of two legs and no problems with the visual control (Fig. 6). The problem appeared in the case of clutch pressing: the angle in the left knee was 180°, not comfortable (Fig. 7).

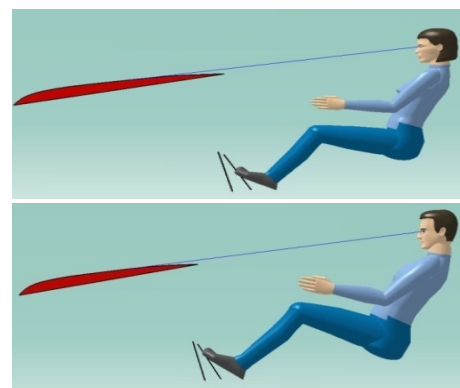


Fig. 6. The first examined situation

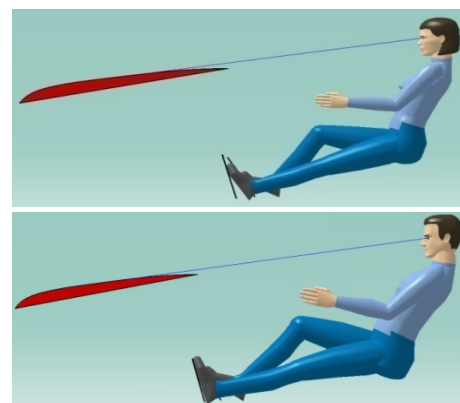


Fig. 7. The problem with clutch pressing

The second examined situation was: the right foot in pressing position on the acceleration pedal and the left foot in pressing position on the clutch pedal.

Both of the models are not acceptable for the final concept: the first one is too far from the pedals, the other one is too close to the pedals. In the first case the left leg is too extended – the knee angle is 180° , in the second case the right knee angle is 90° (Fig. 8). The final decision about the positioning of the pedals was obtained as result of taking into consideration the importance of the right foot control. Because of the long duration of the pressing position of the right leg on the acceleration pedal, the comfort angle of the right leg in pressing position have to be the initial point.

The left leg is used temporarily for pressing clutch pedal and it's not necessary to obtain comfort angle. After the examination of two extreme anthropometric sizes, the obtained knee angle for the left pedal was 150° as an acceptable solution.

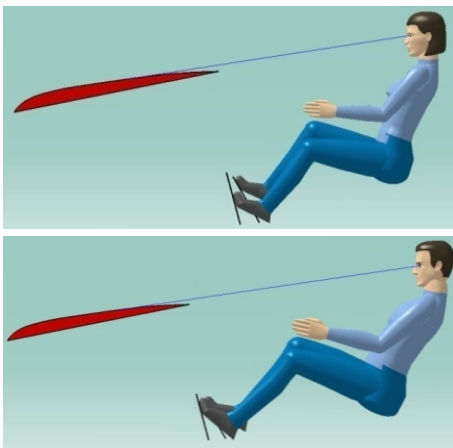


Fig. 8. The second examined situation

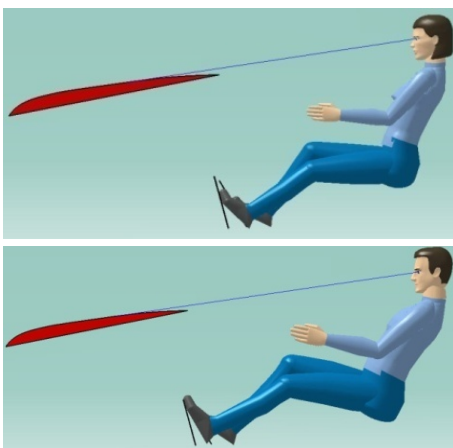


Fig. 9. Final concept

Finally, the concept with fixed heel point was accepted with initial comfort angle for the right leg. According to the fact that the determined adjustable ranges for the seat and for the steering wheel obtain perfect vision control for all anthropometric sizes, all of the ergonomic criteria for the accepted concept were fulfilled.

3. VIRTUAL MODEL OF HUMAN BONES AND MUSCLES

Geometric data of virtual models of human are taken from the data base of the software module Human Builder in Catia [6–8]. The virtual human model is composed of two parts, muscle tissue and skeleton. The human skin is not taken in the analysis because it is geometrically very complicated and has small impact on the results of the pressure distribution analysis [9]. The geometry of the skeleton is simplified with the aim to reduce the time needed for calculation of the numerical model with FEA, but the model should not be oversimplified because it will influence the validity of the received values from pressure distribution. Pelvis, femurs and simplified model of skeleton from virtual model of human are shown in the Figure 10. The FEA model for numerical calculation is represented with the meshed model of the human with the characteristics of muscles tissue and bones. The mesh is created with tetrahedron elements, which are suitable for complicated geometric models.

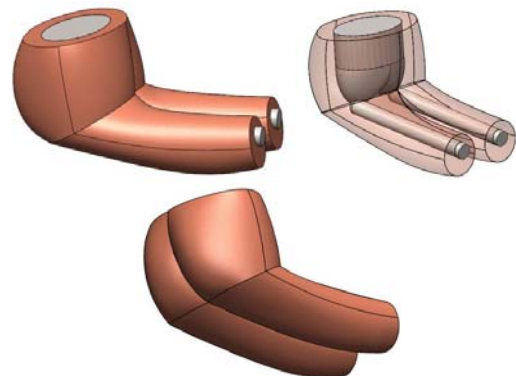


Fig. 10. Geometrical representation of part of virtual model of human – pelvis, femurs and simplified muscle tissue

The mesh of human muscle tissue is composed of smaller finite elements than the mesh of simplified model of human skeleton (Fig. 11). The human skeleton is not the goal of this analysis. The goal of the analysis is the human muscle tissue where the real contact with the seat occurs, and

from where the values for pressure distribution are read.

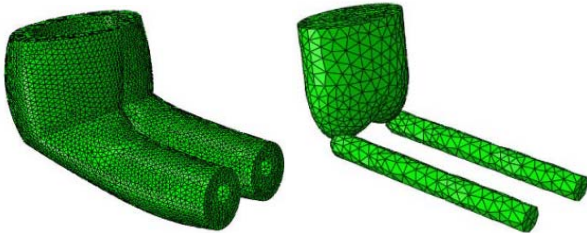


Fig. 11. The FEA mesh model of the seating human

For human bone structures, the skeleton is assumed to be a rigid body. The human skeleton is a rigid body because the bones are not being deformed when the human body is in the seating position.

The influence of clothing on the pressure distribution is very low and is excluded from the model.

Few of the authors that worked with virtual testing of human muscle tissue are (A. Siefert, S. Pankoke, H. P. Wolfel [10]; and Verver, M. [11]). The authors give different kinds of definition of the human muscle tissue. Verver, M. [11] in her doctoral dissertation describes the parameters which define the non-linear mechanical behavior of human muscle tissue with the software package ABAQUS [12–15], with hyperelastic isotropic material model of Mooney – Rivlin. The strain energy function is defined by [11] as:

$$W = A_1(J_1 - 3) + A_2(J_2 - 3) + A_3(J_3^2 - 1) + A_4(J_3 - 1)^2 \quad (1)$$

where J_1 , J_2 and J_3 are the invariants of the right Cauchy-Green strain tensor. The right Cauchy-Green strain tensor is defined by [11]:

$$\underline{C} = \underline{F}^T \cdot \underline{F}, \quad (2)$$

where \underline{F} is the deformation tensor. J_1 , J_2 and J_3 have been defined [9] as:

$$\begin{aligned} J_1 &= \text{trace}(\underline{C}), \\ J_2 &= \frac{1}{2} \left(\text{trace}^2(\underline{C}) - \text{trace}(\underline{C})^2 \right), \\ J_3 &= \det(\underline{C}). \end{aligned} \quad (3)$$

The second Piola-Kirchhoff stress tensor is obtained by differentiating the strain energy function W with respect to the right Cauchy-Green strain tensor [11]:

$$\underline{S} = 2 \frac{\partial W}{\partial \underline{C}}. \quad (4)$$

The material parameters A_3 and A_4 are function of the coefficients A_1 and A_2 :

$$A_3 = \frac{1}{2} A_1 + A_2$$

and

$$A_4 = \frac{A_1(5\nu - 2) + A_2(11\nu - 5)}{2(1 - 2\nu)}. \quad (5)$$

The values for A_1 , A_2 and ν have been set to: $A_1 = 0.00165$ MPa, $A_2 = 0.00335$ MPa and $\nu = 0.49$. These values for material parameters are used by Verver, M, [11].

The value for density of human muscle tissue is defined with volume and body mass. The density of human muscle tissue is 0.0026 kg/m³.

4. VIRTUAL MODEL OF DRIVER'S SEAT CUSHION WITH CHARACTERISTICS OF THE USED MATERIALS

The driver's seat for passenger automobile consists mainly of three parts: seat cushion, seat back and head restraint. In the Figure 12, the seat cushion assembly is represented with the sheet metal holder and the polyurethane foam. The polyurethane foam from the seat cushion is placed on the sheet metal holder. The sheet metal is with thickness of 1 mm and is supported by the seat mechanical structure on four small perpendicular support area.

The driver's seat cushion for the driver's seat, shown in Figure 12, is made by Johnson Controls. The geometrical data are used for the analysis of the influence of the thickness and density of the polyurethane foam on the seating comfort.



Fig. 12. Sheet metal holder and the foam from seat cushion

The investigation begins with a virtual model of the seat cushion which is the same with the real seat, shown in Figure 12. The virtual model of the seat cushion in Figure 12 is shown in Figure 13. In

Figure 13 we can see also two elliptical holes, which have a significant influence on the seat comfort. In the Figure 14 the dimensions of the seat cushion are shown.

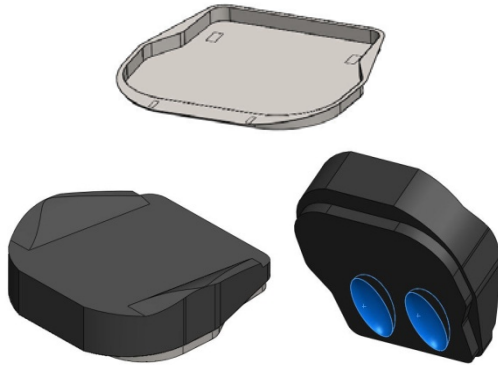


Fig. 13. Virtual model of seat cushion

The meshed model with tetrahedron elements is prepared to be used in FEA. The meshed model of the seat cushion, which corresponds to the virtual model of the seat in Figure 13 is shown in Figure 15.

The influence of covering on the pressure distribution is very low and is excluded from the model.

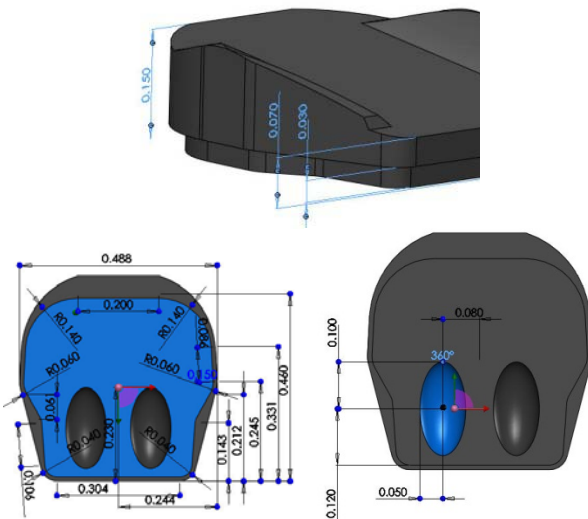


Fig. 14. Dimensions of the seat cushion

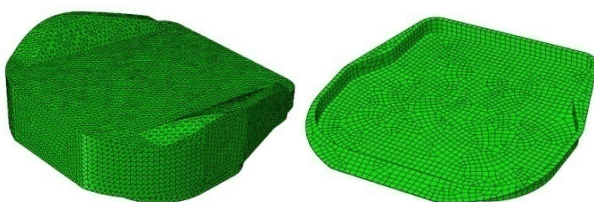


Fig. 15. The meshed model of seat cushion

As means for the description of foam materials in ABAQUS [12–15], a hyper-elastic law is used. The elasticity of the material is described via the potential energy U of elastic deformation. The applied potential function for foams (Eq. (6)) considers nearly full compressibility of polyurethane foams.

Strain energy potential of compressive foams is computed as Ogden function:

$$U = \sum_{i=1}^N \frac{2\mu_i}{\alpha_i^2} \left[(\lambda_1^{\alpha_i} + \lambda_2^{\alpha_i} + \lambda_3^{\alpha_i} - 3) + \frac{1}{\beta_i} (J^{-\alpha_i \beta_i} - 1) \right], \quad (6)$$

The potential energy U is defined by the following parameters: μ_i are the coefficients of initial shear modulus, λ_{1-3} the principal stretches, α_i the standard material parameter, β_i the coefficients for degree of compressibility and J the elastic volume ratio. The free material parameters μ_i , α_i and β_i are determined experimentally, with the average values out of loading and unloading.

With bold line in Figure 16, are represented the nonlinear characteristic of polyurethane foam which is described with Ogden function with $N = 1$, $\mu = 10$ kPa, $\alpha = 8$ and Ogden function with $N = 2$, $\alpha_1 = 17,4$, $\mu_1 = 18,3$ kPa, $\alpha_2 = -2,0$, $\mu_2 = 0,21$ kPa and Poisson ratio $\nu = 0$ [16].

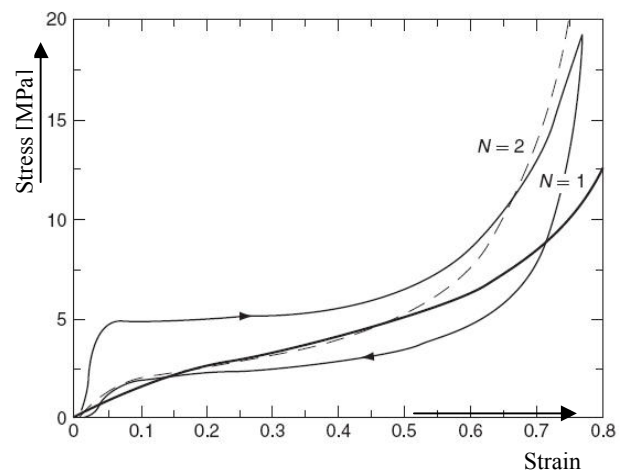


Fig. 16. Nonlinear characteristic for flexible polyurethane foam [16]

Ogden function from second degree with $N = 2$ is used for description of nonlinear behavior of flexible polyurethane foam [12].

The density of polyurethane foam is given from the manufacturer Johnson Controls Inc. and is 50 kg/m^3 .

5. MEASUREMENT EQUIPMENT AND TESTING OF THE MODEL

5.1. Measurement equipment

For obtaining of pressure distribution in the contact surface between the driver's seat and the driver the equipment from manufacturer XSENSOR Technology Corporation is used. The measurement equipment consist of few elements such as: sensor platform X3 PRO, sensor pad for measuring of pressure distribution, Mini – B USB cable, 12 VDC 3.75 A AC/DC power supplier, electronic

for connection of sensor pad and PC, X3 node, PC and software XSENSOR – X3 MEDICAL v6.0 used for data acquisition. The sensor pad is of type PX100:36.36.02 composed of a seat sensor with resolution of 1296 sensible points, with excellent flexibility and endurance. The measurement pressure range is between 10 – 200 mmHg. The resolution of pressure measurement is 1,27 cm. The elements which are included in the measurement equipment for measuring of pressure distribution between two bodies in contact are shown in Figure 17.



Fig. 17. XSENSOR – X3 PRO system for measuring of pressure distribution

5.2. The results from the experimental measuring and virtual testing

For measuring of the pressure distribution between the driver's seat cushion from passenger automobile and the man, we use the seat described in Figure 12. The measuring is performed with men from 50th and 80th percentile. The human weight of 50th percentile man before the testing was 71 kg and for 80th percentile man was 78.5 kg. The measured weights are the same with the weights of the corresponding virtual models. Before the measuring the participants were seated according to the comfort angles. The measured pressure distribution and the values for maximum contact pressure are shown in Figure 18.

The boundary conditions in the simulation are defined on the seat geometry. In reality, the seat is fixed from below on four supports (in precisely

defined areas) located on the sheet mental. The fixing is defined with translations and rotations equal to zero.

The initial conditions in the simulation is defined for the time $t = 0$ s. In the initial moment of the simulation, the virtual model of the human is placed above the seat without a contact between them, and the initial speed is set to 0.

The loading condition in the simulation is defined with gravity of 9810 mm/s².

The contact between the virtual model of human and the seat cushion is defined with selecting of surfaces that come in contact. In reality, there is friction between contact surfaces. The coefficient of friction between contact surfaces is 0.75 and is obtained experimentally [16].

The pressure distributions on the seat contact surface resulting from the analyses for 50th (left) and 80th (right) percentile are shown in Figure 19,

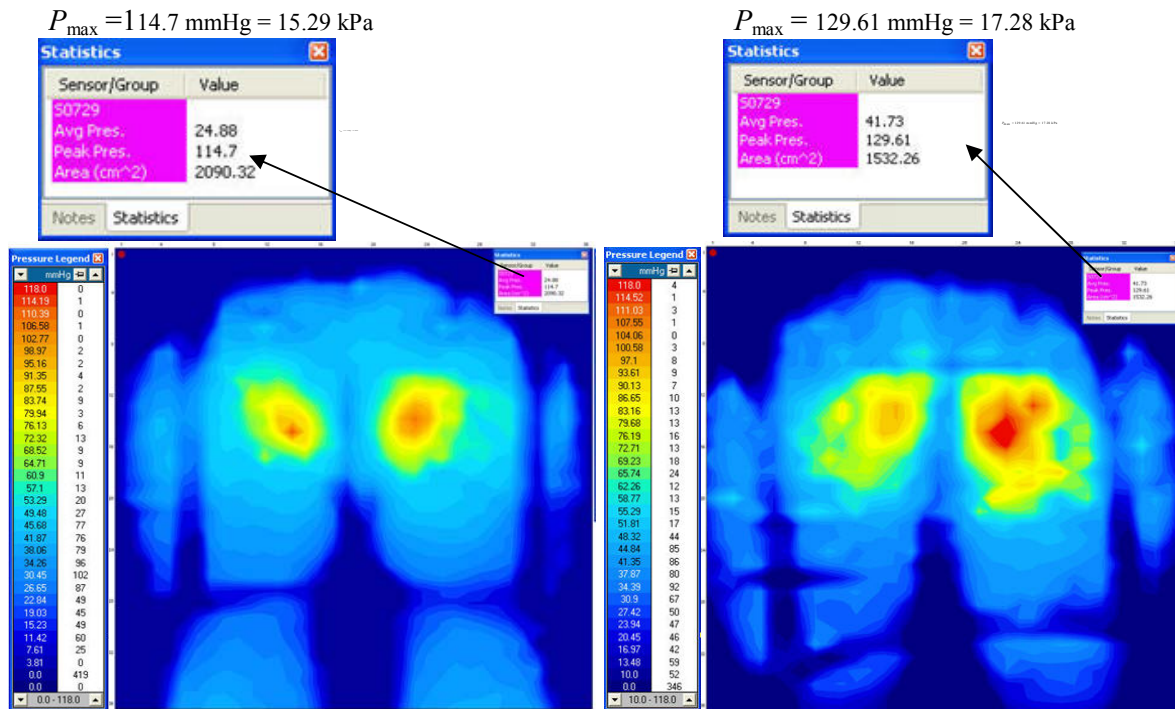


Fig. 18. Pressure distribution between seat cushion and participants from 50th and 80th percentile

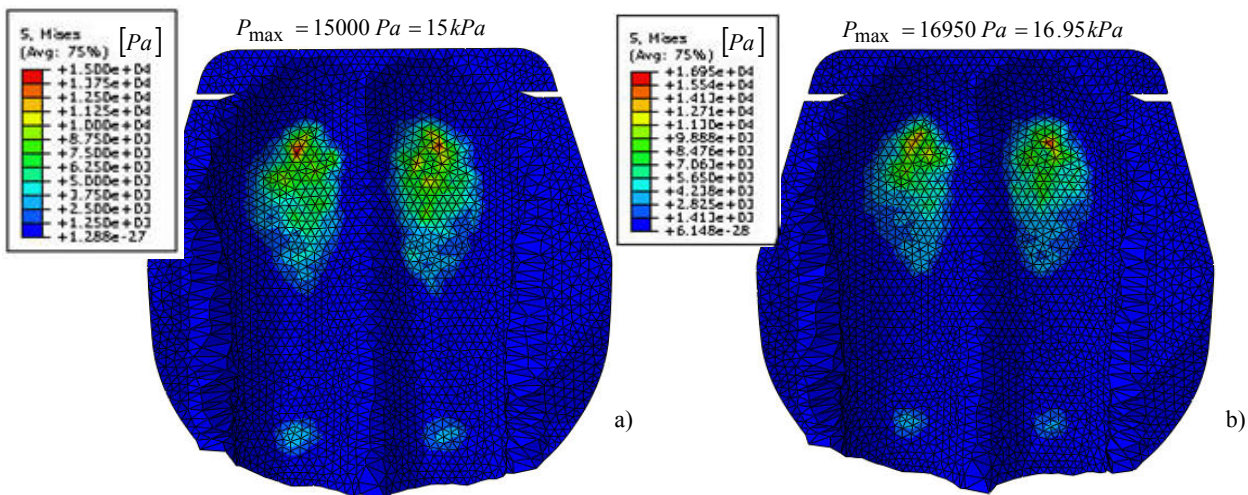


Fig. 19. Pressure distributions on the contact surface of virtual seat cushion and virtual model of human from a) 50th and b) 80th percentile

The experimental values of the maximum contact pressure in the contact surface between the seat cushion and the human are given in Table 2. The measured values are close to the values obtained from the virtual testing.

The human skin and seat cover are not considered in the virtual testing. For this reason, there is a difference in the results obtained from the experiment and the virtual testing of about 2%. This difference is small and approves the use of the virtual model instead of the experimental testing of seat prototypes.

Table 2

Values for maximum contact pressure

Human percentile	Maximum contact pressure from experimental measurement (kPa)	Maximum contact pressure from virtual testing (kPa)
50th percentile	15,29	15,00
80th percentile	17,28	16,95

6. INFLUENCE OF THICKNESS AND DENSITY OF POLYURETHANE FOAM ON THE SEATING COMFORT

According to the data found in literature [16], comfortable seats are seats with max contact pressure less from 12 kPa.

For the seat geometry shown in the Figure 13 and 14, the influence of the foam thickness on the maximum contact pressure is examined using the virtual models of the seat and human from 50th and 80th percentile. The initial seat has foam thickness of 70 mm. If the foam thickness is reduced to 60 mm, 50 mm, and 40 mm, than the contact pressure increases, first slowly and than rapidly, such as shown in Figure 20.

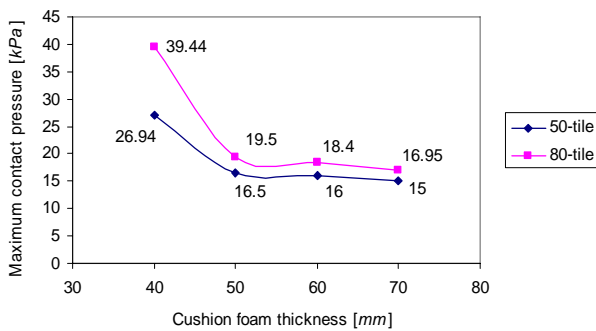


Fig. 20. Relationship of maximum contact pressure and seat cushion thickness

To examine the influence of the density of the polyurethane foam on the contact pressure, six virtual testing for design shown in the Figure 13 and 14 are performed with the foam thickness of 70 mm. The results obtained from virtual testing of six virtual models of seats with density of 30 kg/m³, 40 kg/m³ and 50 kg/m³ and two types of virtual models of human from 50th and 80th percentile are shown in Figure 21.

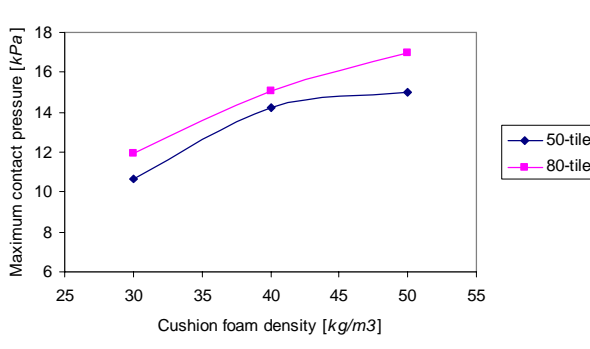


Fig. 21. Relationship of maximum contact pressure and density of the polyurethane foam

7. INFLUENCE OF SHAPE FROM CONTACT SEAT SURFACE ON THE SEATING COMFORT

With changing of the seat design is known that pressure distribution map and value of maximum contact pressure also are changing. In the Figure 22 is shown car seat, which has same dimensions as seat shown in the Figure 13, with correction in upper contact surface of the seat. On the upper seat surface which is in contact with virtual model of human is add more material from polyurethane foam. For seat design shown in the Figure 22 four virtual testing are made, with different densities of the polyurethane foam at 30 kg/m³ and 50 kg/m³ and with 50th and 80th percentile of mannequin.

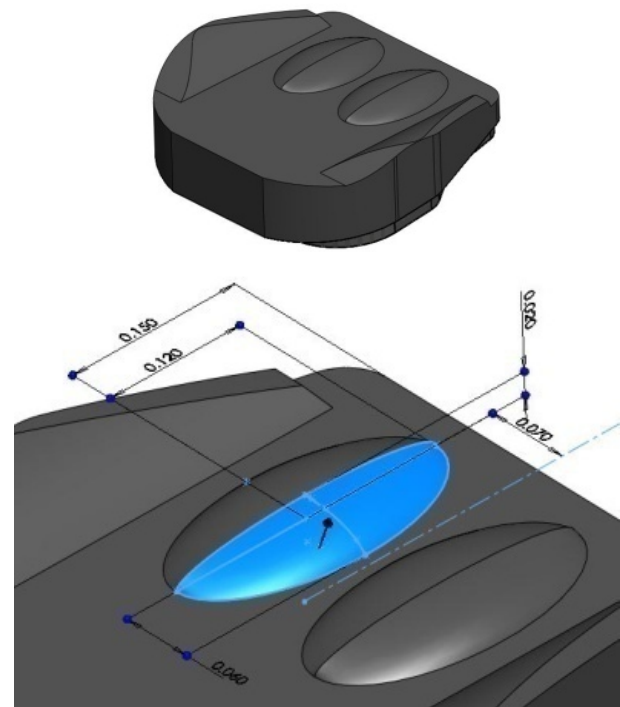


Fig. 22. Virtual model of new seat cushion

Maximum contact pressure in the contact between virtual model of seat and virtual model of human is reading from pressure distribution map. In the Table 3 is given preview of obtained results with change of upper contact surface of seat.

Table 3 shows that for lower density of polyurethane foam are obtain lower maximum pressures of contact surface of seat. It can also be concluded that for lower density of polyurethane foam have greater difference in maximum pressures for 50th percentile and 80th percentile of human.

Table 3

Maximum contact pressure for virtual model of seat shown in Figure 22

Human percentile	Virtual model of seat with density of polyurethane foam from:	
	30 kg/m ³	50 kg/m ³
50 th percentile	5,05 kPa	7,85 kPa
80 th percentile	8,43 kPa	10.83 kPa

With comparing of values of maximum contact pressure from Table 3 is shown big difference in results. So, with adding of material on the upper surface on the seat also as shown in the Figure 22, value of maximum pressure is reduced for about 50%. The design has significant impact on pressure distribution map and value of maximum contact pressure.

8. CONCLUSIONS

The virtual testing of seating process in driver's seat for passenger automobile allows fast and simplified review of the phenomena that occur during the seating. This virtual testbench provides a mechanism for investigation of new design ideas for new types of seats. Using this virtual testbench, the new design of seat can be validated in the product development phase, thus avoiding the financial costs and saving time for making physical prototypes.

The influence thickness of the seat cushion foam on the maximum contact pressure is examined. From the diagram shown in the Figure 20, it is obvious that with reducing of the foam thickness below certain limit value, the seating comfort is deteriorating gradually.

The foam density has an important influence of the value of the maximum contact pressure. As shown in Figure 21, with reducing of the foam density the value of the maximum contact pressure is decreasing slowly, and with that the seating comfort is improving.

The design has significant impact on pressure distribution map and value of maximum contact pressure. With local adding of material corresponding with seat design, shown in Figure 22, we can greatly affect on the value of maximum contact pressure between virtual models of seat and human in order to improve seating comfort.

REFERENCES

- [1] D. A. Attwood, J. M. Deeb, M. E. Danz-Reece: *Ergonomic Solutions for the Process Industries*. Elsevier Inc. (2004).
- [2] K. H. E. Kroemer: "Extra-ordinary" *Ergonomics*, Taylor and Francis, Vol. 1 (2006).
- [3] J. D. Bernaer: *Ergonomic for Beginners*, Taylor and Francis, Second Edition (2001).
- [4] Council Directive 74/60/EEC, *Official Journal of the European Communities*, December 17, 1973
- [5] Council Directive 77/649/EEC, *Official Journal of the European Communities*, December 17, 1973
- [6] (2008): *CATIA V5 Tutorial*, SIMULTIA Inc.
- [7] S. Dickson (2007): *CATIA V5 Design with Analysis*, The Hong Kong Polytechnic University.
- [8] F. Karam, C. Kleismit (2006): *CATIA V5*, SDC Publications.
- [9] K. Ebe, J. M. Griffin (2001): *Factors affecting static seat cushion comfort*, Taylor and Francis.
- [10] A. Siefert, S. Pankoke, H. P. Wolfel (2008): Virtual optimization of car passenger seats: Simulation of static and dynamic effects on driver' seating comfort, *International Journal of Industrial Ergonomics*, Vol. 38, pp. 410-424, Science Direct.
- [11] M. M. Verver (2004): *Numerical tools for comfort analysis of automotive seating*, Ph.D. thesis (English language), Technische Universiteit Eindhoven.
- [12] C. C. Spyarakos, J. Raftoyiannis: Linear and Nonlinear Finite Element Analysis, In: *Engineering Practice*. Algor Inc. (1997).
- [13] *ABAQUS Example Problems Manual*, ABAQUS Inc. (2008).
- [14] *Getting Started with ABAQUS/Standard*, ABAQUS Inc. (2008).
- [15] G. R. Liu, S. S. Quek: *The Finite Element Method: A Practical Course with Abaqus*, Department of Mechanical Engineering, National University of Singapore (2003).
- [16] J. M. Nigel: *Polymer Foams Handbook: Engineering and Biomechanics Applications and Design Guide*, Butterworth-Heinemann (2007).

WATER HAMMER ANALYSIS USING CHARACTERISTICS METHOD AND NUMERICAL SIMULATION

Viktor Iliev, Predrag Popovski, Zoran Markov

*Institute of Hydraulic Engineering and Automation, Faculty of Mechanical Engineering,
"SS. Cyril and Methodius" University in Skopje,
P.O. Box 464, MK-1001 Skopje, Republic of Macedonia
viktor.iliev@mf.edu.mk*

Abstract: Sudden change in the velocity of fluid induces substantial increase or decrease of pressure which are transmitted through the system with speed equal to the speed of sound. When it comes to incompressible fluid flow, pressure surges and consequences are described with process called water hammer. Water hammer can be result of normal system operation, such as valves closure, pumps and turbines turning off, turbine regulation, as well as abnormal system operation such as electrical defect or emergency shut-down of operating elements (turbine run-away). Characteristic of water hammer is dull humming sound and can result in catastrophic component effect. Because of this, possibility of water hammer appearance in the system has to be considered during the system design and determine the normal operation conditions of elements. The main aim of this paper is to analyze and to determine conditions for water hammer appearance in hydraulic systems. Mathematical model of system is presented and solution of water hammer is made in conditions of quicker closure the valve and turbine guide vanes closure. Several solution are performed according to method of characteristics and numerical simulation with specialized software packages. Also, analysis and validation of results obtained is made.

Key words: water hammer; pressure wave speed; method of characteristics; numerical simulation; hydroelectric power plant

АНАЛИЗА НА ХИДРАУЛИЧЕН УДАР СО ПРИМЕНА НА МЕТОДОТ НА КАРАКТЕРИСТИКИ И НУМЕРИЧКА СИМУЛАЦИЈА

Апстракт: При нагла промена на брзината на струење на флуидот се иницира значително зголемување или намалување на притисокот, кој се шири низ системот со брзина еднаква на брзината на протирање на звукот. Кога станува збор за струење на некомп्रेसибилан флуид, ударните бранови на притисокот и настанатите појави се опишуваат со процес наречен хидрауличен удар. Хидрауличниот удар може да настане како последица на нормална работа на системот, на пример затворање на вентили, исклучување на пумпи, регулација на турбини, или при услови на неправилна работа како што се електричен дефект или нужно исклучување на работните елементи (побег на турбина). Хидрауличниот удар се карактеризира со тап шум и може да резултира со катастрофални последици врз работните елементи на системот. Поради тоа можноста од појава на хидрауличен удар во системот мора да се има во предвид при проектирањето и определувањето на нормални услови на работа на работните елементи. Основната цел на овој труд е да се направи анализа и да се определат условите при кои настанува хидрауличен удар во хидрауличните системи. Претставено е математичко моделирање на системот и извршена е пресметка во услови на работа при појава на хидрауличен удар поради нагло затворање на вентил и нагло затворање на лопатките на спроводен апарат кај турбина. Пресметките се извршени со примена на методот на карактеристики и нумеричка симулација со специјализиран софтверски пакет. Наедно, е извршена анализа и верификација на добиените резултати.

Клучни зборови: хидрауличен удар; брзина на пропација на притисок; метод на карактеристики; нумеричка симулација; хидроелектрана

1. INTRODUCTION

Water hammer is result of sudden change in flow velocity that results in large increase of pressure. For example when flows velocity changes suddenly, kinetic energy of fluid is transformed in potential energy result of which is pressure increase up to a point that can cause large tensile force in the pipe walls cross sections. This change of pressure spreads as a wave through the pipeline with speed equal to the speed of sound, i.e. pressure wave speed.

Reasons for flow velocity change can be different regimes of operation such as closing of valves, normal turning off of turbines and pumps, turbine regulation and shutdown of the system components because of defect. Because of this, investigation and ability to prediction water hammer conditions is of great importance during the hydraulic system design.

GOVERNING EQUATION OF WATER HAMMER

Application of Newton's second law of motion to the case of unsteady flow of a incompressible fluid in an elastic pipe leads ultimately to the momentum equation [1]:

$$g \frac{\partial H}{\partial x} + v \frac{\partial v}{\partial H} + \frac{\partial v}{\partial t} + \frac{\lambda v |v|}{2D} = 0. \quad (1)$$

In accordance with conservation of matter law, the continuity equation is obtained in the form, [1]:

$$v \frac{\partial H}{\partial x} + \frac{\partial H}{\partial t} - v \sin \alpha + \frac{a^2 \partial v}{g dx} = 0. \quad (2)$$

In equations (1) and (2), v is average velocity of flow, H denotes the piezometric head at the centreline of the pipeline at location x and time t , D is the pipeline diameter, λ is the friction factor in the Darcy-Weisbach formula [2], x is the distance along the centreline of the pipe, α is the angle between the horizontal and the centreline of the pipe, g is the gravity acceleration and a is pressure wave speed. The positive direction for flow velocity is in direction of x axis.

Equations (1) and (2) represent governing mathematical models that describe water hammer and they represent hyperbolic partial differential equations with two dependent variables v and H , and two independent variables x and t .

All methods of water hammer solution begin with these two governing equations. Following assumptions were made during their derivation:

- The velocity and the pressure are equal through whole cross section of the pipeline, i.e., one-dimensional model is used.
- The pipeline is full of liquid at all times.
- In equation (1) the effects of density variation is neglected.
- Friction factor λ is calculated for steady flow apply to unsteady flow.
- Angle $\alpha = 0$, i.e. axis of pipe is in direction of x axis.

Pressure wave speed is calculated according to following equation [3]:

$$a^2 = \frac{K / \rho}{1 + \left[\left(\frac{K}{E} \right) \left(\frac{D}{\delta} \right) \right] c_1}. \quad (3)$$

In equation (3) K represents bulk modulus of elasticity of the liquid in the pipe, ρ is density of the fluid, E is young's modulus of material that the pipes are made of, δ is pipe equivalent wall thickness, c_1 is a coefficient that takes in consideration the type of the pipeline stiffening, i.e. [3]:

Case 1: For pipeline that is stiffened on one end only, $c_1 = (1 - \mu)/2$.

Case 2: For pipeline that is stiffened on two ends, $c_1 = 1 - \mu^2$.

Case 3: For pipeline that is not stiffened $c_1 = 1$.

In c_1 expressions, μ represents Poisson's ratio that depends on material that pipes are made of.

METHOD OF CHARACTERISTICS

Method of characteristics as numerical method of unsteady flow solution provides transformation of the hyperbolic partial differential equations in ordinary differential equations i.e. their transformation in characteristic form and determining equations of characteristic-line in $x-t$ plane in which ordinary equations apply. If momentum and continuity equations transformed in simpler form are represented as L_1 and L_2 [4] then:

$$L_1 = \frac{\partial Q}{\partial t} + gA \frac{\partial H}{\partial x} + \frac{\lambda}{2DA^2} Q |Q| = 0, \quad (4)$$

$$L_2 = gA \frac{\partial H}{\partial x} + a^2 \frac{\partial Q}{\partial x} = 0. \quad (5)$$

The linear combination of equations (4) and (5) $L_1 + \varphi L_2 = 0$, result are two pairs of ordinary differential equations:

$$C^+ \left\{ \frac{\partial Q}{\partial t} + \frac{gA}{a} \frac{dH}{dt} + \frac{\lambda}{2DA^2} Q|Q| = 0, \quad (6)$$

$$\left\{ \frac{\partial x}{\partial t} = +a, \quad (7)$$

$$C^- \left\{ \frac{\partial Q}{\partial t} - \frac{gA}{a} \frac{dH}{dt} + \frac{\lambda}{2DA^2} Q|Q| = 0, \quad (8)$$

$$\left\{ \frac{\partial x}{\partial t} = -a. \quad (9)$$

In this way two real values for $\varphi = \pm 1/a$ are used for transformation of the two hyperbolic partial differential equations in two ordinary differential equations, equation (6) and (8), which are true only when equations (7) and (9) are true.

For easier solution $x-t$ plane is created, in which ordinary differential equations are presented with characteristic lines. In most cases, pressure wave speed in incompressible fluid flow is constant, so equations (7) and (8) in $x-t$ plane give approximately straight characteristic lines with slope $dx/dt = \pm a$ (Fig. 1). These lines in $x-t$ plane represent characteristic straight lines with slope a and equations (6) and (8) are applicable.

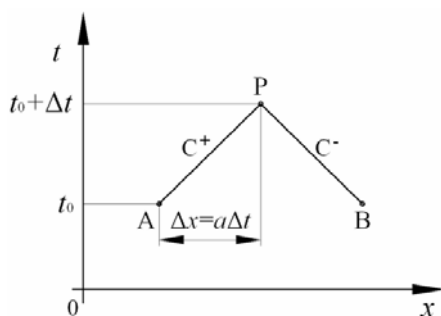


Fig. 1. Characteristic lines in $x-t$ plane

Equations (6), (7), (8) and (9) can be solved with numerical method if initial and boundary conditions are known. With finite difference method differentials dh , dv , dx , and dt are replaced with finite differences Δh , Δv , Δx and Δt . These equations are applicable for characteristics C^+ and C^- that can be presented in $x-t$ plane. Length of

pipeline L is divided in N equal parts, each with length Δx (Fig. 2).

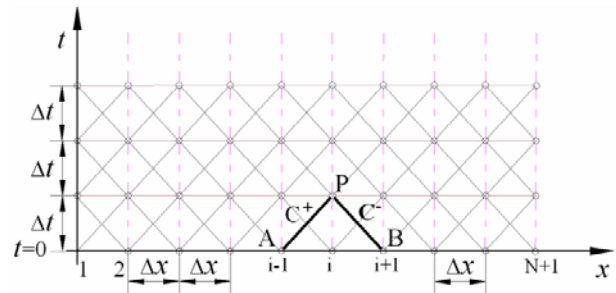


Fig. 2. Families characteristic curves (MOC)

Time step for calculation is $\Delta t = \Delta x/a$. Line AP (positive characteristic) represents diagonal in the matrix and equation (6) is applicable. If dependant variables v_A and H_A are known (initial and boundary conditions), then equation (6) is applicable for positive characteristic C^+ , that can be integrated between A and P, in such way result is equation with two unknown variables v_P and H_P in point P. Line BP (negative characteristic) represents diagonal in the matrix for which equation (8) is applicable.

By integrating equation (8) that represents line BP, with known conditions in point B (v_B and H_B) and unknown in point P, result is the other equation with unknown variables in point P (v_P and H_P).

By transformation of equation (6) with expression $adt/g = dx/g$, and if flow velocity is expressed through discharge ($Q = vA$), equation (6) can be presented in a form suitable for integrating along the positive characteristic C^+ , result is [4]:

$$\int_{H_A}^{H_P} dH + \frac{a}{gA} \int_{Q_A}^{Q_P} dQ + \frac{\lambda}{2gDA^2} \int_{x_A}^{x_P} Q|Q| dx = 0. \quad (10)$$

By integrating of equation (10) along positive C^+ and negative characteristic C^- , between A and P and between P and B limits respectively we get:

$$H_P - H_A + \frac{a}{gA} (Q_P - Q_A) + \frac{\lambda \Delta x}{2gDA^2} Q_A |Q_A| = 0, \quad (11)$$

$$H_P - H_B + \frac{a}{gA} (Q_P - Q_B) + \frac{\lambda \Delta x}{2gDA^2} Q_B |Q_B| = 0. \quad (12)$$

Equations (11) and (12) are basic algebraic equations for calculating the flow velocity and pressure change during unsteady flow of liquid (water hammer).

CASE STUDIES

In this paper the main aim is to analyze the condition of water hammer for systems with different hydraulic configuration.

a) Case study 1#: Elementary plant

Configuration of this hydraulic system, so called “elementary plants“ consisting of reservoir-pressure pipeline-valve (Fig. 3) is shown in Table 1.

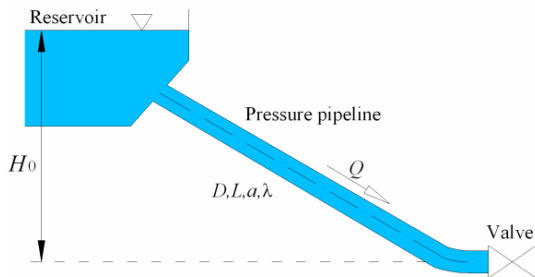


Fig. 3. Case study 1# (reservoir-pressure pipeline-valve)

Table 1

System configuration case study 1#

Reservoir	Pressure pipeline	Valve
$H_0 = 150$ m	$L = 660$ m	$D_v = 0.6$ m
	$D = 0.6$ m	$\tau = f(t)$
	$\lambda = 0.03$	$(c_Q)_0 = 0.0465$
	$a = 1219$ m/s	$Q_0 = 0.47$ m ³ /s

Such systems can be found in all water supply systems, but the water hammer investigations are particularly important for hydroelectric power plant’s penstocks.

Pressure pipeline is made of steel and is stiffened at both ends (case 3, $c_1 = 1 - \mu^2$) and in accordance with it, pressure wave speed calculated with equation (3) is $a = 1219$ m/s.

Valve closing schedule $\tau(t)$ (Fig. 4) is given with following equation:

$$\tau_{(t)} = 1 - \left(\frac{t - t_s}{t_c} \right) 0.75. \quad (13)$$

In equation (13) t_s represents valve time at the start of the closure and t_c is valve closure time.

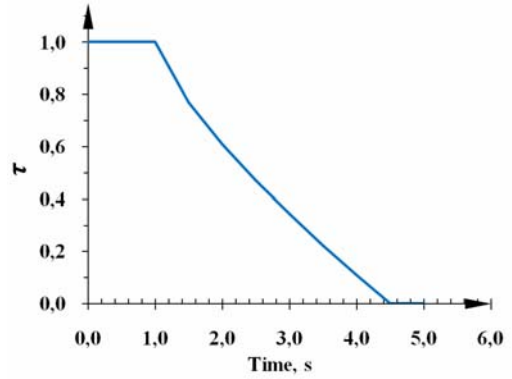


Fig. 4. Valve closing schedule

Valve discharge coefficient (c_Q) depending on closing schedule is given on Fig. 5 or with equation [5]:

$$c_{Q(t)} = \tau c_{Q(0)} = \frac{\tau Q_0}{A \sqrt{2gH}}. \quad (14)$$

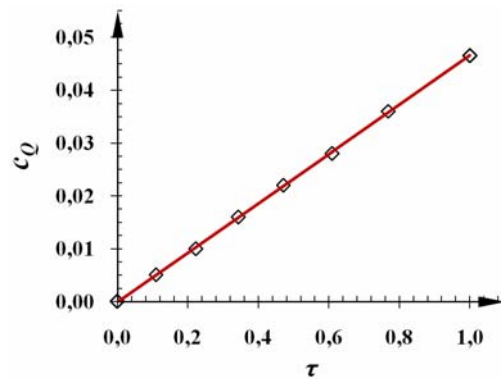


Fig. 5. Valve discharge coefficient

Pressure losses in the valve are defined with equation, [5]:

$$h_{zv} = \frac{Q_v |Q_v|}{c_Q^2 2gA_Q^2}. \quad (15)$$

In equations (14) and (15) Q_0 represents discharge at the fully opened valve, H is hydrostatic pressure (head) before valve with discharge Q_0 , A is surface of valve cross section at Q_0 , A_Q cross section of valve at Q_v , Q_v and c_Q represent values of discharge and discharge coefficient depending on valve state of openness.

a.1) Solution by method of characteristics (case study 1#)

Water hammer solution by characteristic method (MOC) starts with equations (6), (7), (8) and (9) expressed as finite differences, while we

assume that losses are concentrated at the end of the pipeline [4]:

$$C^+ \begin{cases} \frac{\Delta h}{\Delta Q} = -\frac{a}{gA}, \end{cases} \quad (16)$$

$$\begin{cases} \frac{\Delta x}{\Delta t} = +a, \end{cases}$$

$$C^- \begin{cases} \frac{\Delta h}{\Delta Q} = -\frac{a}{gA}, \end{cases} \quad (17)$$

$$\begin{cases} \frac{\Delta x}{\Delta t} = +a. \end{cases}$$

Equations (15) and (16) define straight lines in diagram $[Q,H]$ with slope $\pm a$. Calculation is made for closing the valve for time $t_c = 3.5$ s. Calculation is performed in two diagrams $[x,t]$ and $[Q,H]$ and is based on observation of movement (path) of two points A and B in time, respectively for reservoir and valve (Fig. 6), [6].

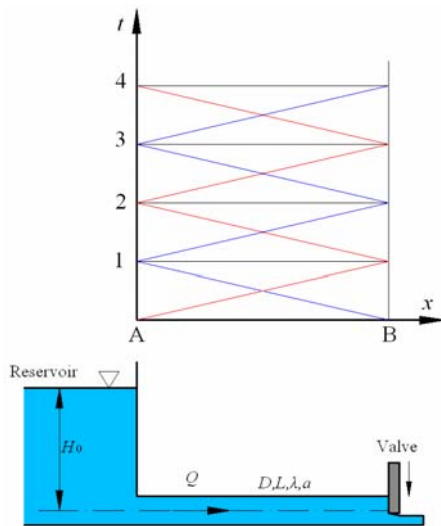


Fig. 6. Diagram $[x,t]$

Movement of points A and B is with speed equal to the wave speed according to the characteristic lines in diagram $[x,t]$, in forward and backward direction towards characteristics of valve h_v (eq.18) and characteristics of reservoir $(H_0 - h_2)/H_0$.

Equation of valve characteristic is:

$$h_v = \frac{Q_v |Q_v|}{c_0^2 2gHA^2}. \quad (18)$$

By combining the path of these two points of diagrams $[x,t]$ and $[Q,H]$, pressure and discharge time evolution is attained (Figs. 7 and 8).

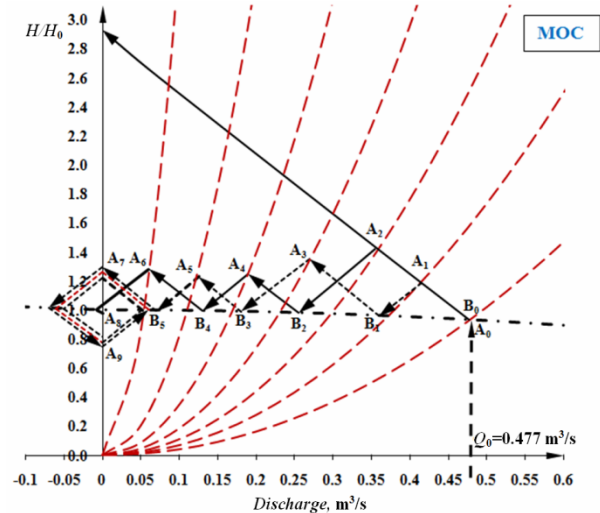


Fig. 7. Graphical solution by MOC

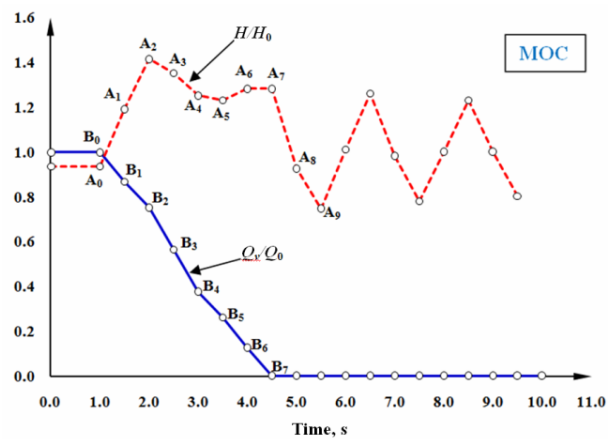


Fig. 8. Time evolution of the head and discharge at the valve

Maximum amplitude of the pressure can be seen on the diagram at instant closure of valve through characteristic line that starts from point A_0 (relates to steady regime of work for discharge Q_0) up to the vertical axis H/H_0 .

Maximum pressure for rate of closure according to equation (13) is $H_{max}(\tau) = 1.42H_0$ and appears at time $t_s + 2L/a$ (s). Critical time of the valve closure is $t_{cr} = 2L/a = 1$ s and is called phase of water hammer at the valve.

From the calculation following can be concluded:

- Valve closing faster than the critical time ($t_c < t_{cr}$) induces maximum pressure H_{max} , or real water hammer.
- In order to prevent water hammer time of the valve closing needs to be longer than critical time ($t_c > t_{cr}$).

For minimal pressure at the valve value of $H_{min}(\tau) = 0.75H_0$ is calculated.

Maximum pressure for quicker the valve closure is $H_{\max} = 2.94H_0$ (real water hammer).

This value of pressure is adequate to value the calculated according to Zhukovski [8]:

$$H_{\max} = H_0 - h_{z(Q_0)} + av_0/g = 442.5 \text{ m} \quad (19)$$

a.2) *Solution by numerical simulation
(case study I#)*

For numerical simulation software package WHAMO (Water Hammer and Mass Oscillation) is used [5]. This simulation software uses an implicit finite difference method for calculating time-varying flows and pressures in the hydraulic systems (hydroelectric power plants, pumping facilities, jet fueling systems, wastewater collection systems, etc.).

Numerical techniques used to approximate water hammer partial differential equations can be classified as implicit or explicit. Implicit methods generally require simultaneous solution of a set of equations while explicit methods can be solved directly. Explicit methods are constrained according to hydraulic system geometry to work at computational time steps which are typically very small, while the implicit methods are not so constrained. Implicit methods require greater computational effort per time step because of the necessity of solving simultaneous equations.

The amount of effort required for a simulation can be reduced with WHAMO by varying the length of the time step during the simulation. Any initial, high frequency water hammer response in a system should be modelled with short time steps, but in simulations where the water hammer dissipates and mass oscillation becomes predominant, the time step can be greatly increased during the simulation with no significant loss of accuracy [5]. The main assumptions of numerical model (one-dimensional flow) in WHAMO are the same as those shown in **heading II**.

First, for simulation, minimum time step Δt needs to be determined for iterative calculation. This time step is determined from condition of complying to the Lewy-Courant [7] criteria, that is $Cr < 1$:

$$\Delta t < L/(a \cdot N) = 660/(1219 \cdot 50) = 0.01 \text{ s}. \quad (20)$$

Cr number must be less than 1:

$$Cr = a \cdot \Delta t / \Delta x = 1219 \cdot 0.01 / 14 = 0.87 < 1. \quad (21)$$

In equation (20), N represents number of segments that pipeline is divided in, while Δx is length of one segment.

The simulation parameters are summarized in Table 2.

Table 2

Simulation parameters				
N	Δt (s)	t (s)	a (m/s)	C_r
100	0.001	3.5	1219	0.2

Results of the numerical simulation for same rate of closing (eq. 13) are given on Fig. 9.

It can be seen that maximum pressure appears at time $(t_s + 2L)/a$ with $H_{\max}(\tau) = 1.42H_0$ and minimum pressure value at the valve is $H_{\min}(\tau) = 0.72H_0$. After valve closure time t_c discharge through the valve Q_v decrease until zero, involve large head (pressure) pulsations and excessive mass oscillations in the pipeline.

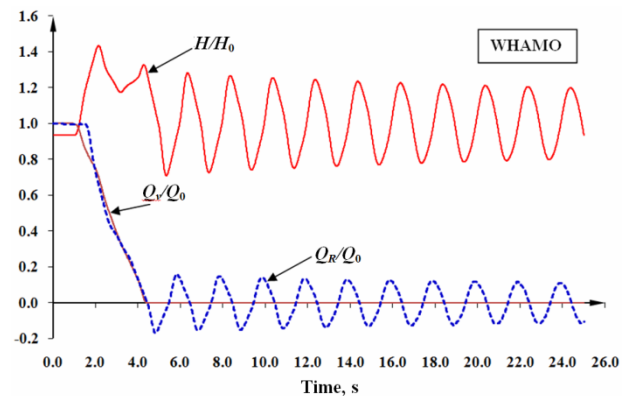


Fig. 9. Time evolution of the head (H), the discharge at the valve Q_v and discharge at the reservoir Q_R

Numerical simulation results are compared with the simulation results obtained by MOC (Fig. 10).

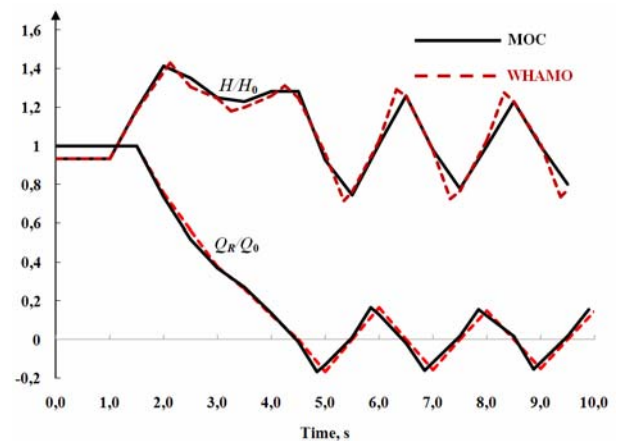


Fig. 10. Comparison of the results calculated by MOC and WHAMO

Figure 10 shows the comparison of the time evolution for head at the valve and discharge at the reservoir. It can be seen that results obtained by numerical simulation show good agreement with the ones obtained with method of characteristics.

Very important is that the value of maximum pressure at the valve (water hammer) are getting the best agreements of the results (deviation from 1.4%, MOC: $H_{max} = 1.41H_0$, WHAMO: $H_{max} = 1.43H_0$).

Results from numerical simulation for case of valve closing of 0.1 s ($0.1 = t_{cr}$) are presented on Fig. 11. Maximum value of pressure at the valve $H_{max} = 2.95H_0$ is achieved at time $T = 4L/a$.

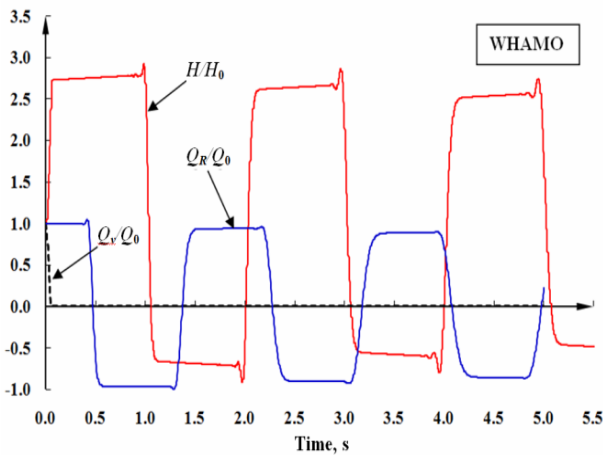


Fig. 11. Time evolution of H , Q_v and Q_R for valve closure time of 0.1 s

After that with every period T value of pressure drops because of influence of friction of fluid with walls of pipeline.

When the calculation is performed with different spatial discretization of the pipeline numerical instabilities on the pressure signal and discharge signal at the reservoir is obtained. The longer the simulations, is the higher numerical instabilities occurs.

Figure 12 shows the time evolution of the pressure obtained through numerical simulation with different spatial discretization of the pipeline ($N = 15, 30, 60, 100$).

It can be concluded that with segment number increase numerical instabilities decreases. Because of this it is very important to consider this factor while spatial discretization of pipeline is performed as well as time step Δt determination.

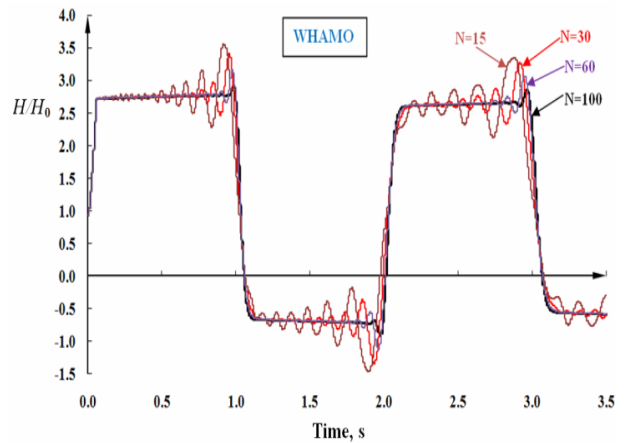


Fig. 12. Comparison of the time evolution of the head H/H_0 at the valve for different spatial discretizations of the pipe

b) Case study 2#: Hydroelectric power plant

This case study focuses on a hydroelectric power plant (HPP) consisting of the following components (Fig. 13): upstream reservoir, gallery, surge tank, penstock, valve, units (two 40 MW vertical Francis turbines) and downstream reservoir. Technical characteristics of the HPP are presented in Table 3.

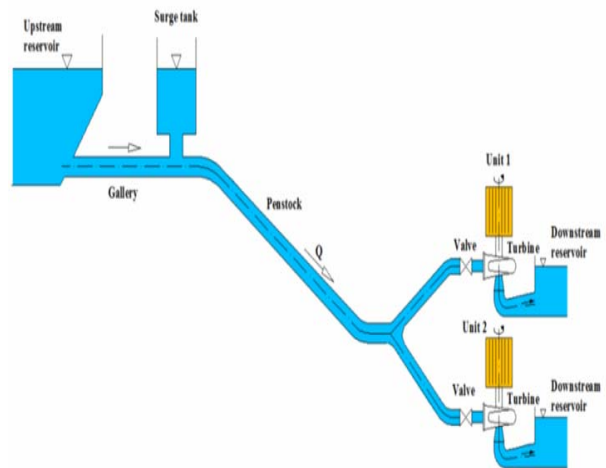


Fig. 13. Layout of the HPP

b.1) Solution by numerical simulation (case study 2#)

The following transient computation scenarios of hydroelectric power plant are analyzed:

Scenario 1: normal shut down of the turbine 1 while turbine 2 is in standby mode.

Scenario 2: load rejection (simultaneously) of the turbine 1 (40 MW) and turbine 2 (40 MW).

Table 3
 Characteristics of hydroelectric power plant
 (rated values)

Upstream reservoir	$H_0 = 109$ m
Gallery	$L = 98$ m; $D = 5.0$ m
	$\lambda = 0.02$; $a = 1050$ m/s
Penstock	$L = 220$ m; $D = 5.0/3.12$ m
	$\lambda = 0.02$; $a = 1020$ m/s
Turbine	$H_R = 92$ m; $Q_R = 50$ m ³ /s
	$P_R = 40$ MW; $n = 300$ min ⁻¹
Unit	$J = 1500$ t·m ²

The influence of the turbine’s water passage (Fig. 14) on the hydraulic system can be defined by one-dimensional approach for modelling of the pipeline through the continuity and motion equation. The head (pressure) pulsations in hydraulic installation from the turbine are represented as [5]:

$$\Delta H = 2 \left[\frac{1}{k_Q^2 D^4 g} \right] Q_2 |Q_1| - \left[\frac{1}{k_Q^2 D^4 g} \right] Q_1 |Q_1|, \quad (22)$$

where: ΔH is the head (pressure) fluctuations between two point of computation, k_Q is discharge turbine coefficient computed from turbine characteristics (hill chart – Fig. 15) and expressed as function of guide vane opening and discharge value, Q_1 and Q_2 are the discharge values in the previous step from the computation and current discharge, D is the turbine runner diameter.

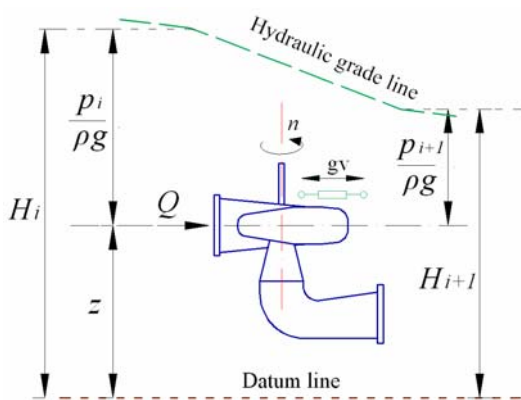


Fig. 14. Francis turbine model

Turbine discharge control is performed by closing/opening of the guide vanes. Opening of the guide vanes is defined by its absolute size a_0 mm, or by the non-dimensional characteristic

$$gv = a_0/a_{0max}.$$

The speed factor n_{11} , discharge factor Q_{11} and torque factor M_{11} can be defined as function of guide vane position a_0 using turbine characteristics:

$$n_{11} = \frac{nD}{\sqrt{H}}; \quad Q_{11} = \frac{Q}{D^2 \sqrt{H}}; \quad M_{11} = \frac{30 \rho g Q_{11} \eta_T}{n_{11} \pi}; \quad (23)$$

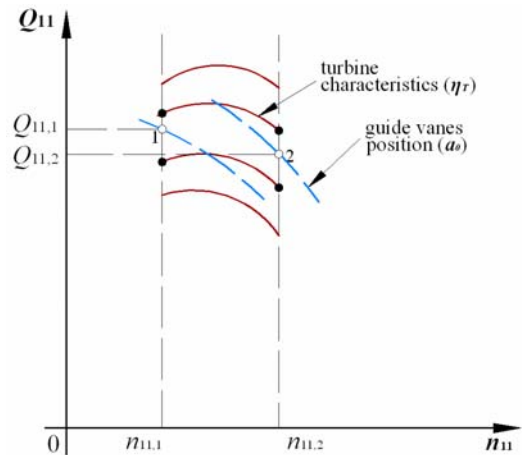


Fig. 15. Turbine characteristics (hill chart)

Dynamic equilibrium (balance) of the moments and masses of rotating parts of the unit is given using the following equation [9]:

$$M_n = J \frac{d\omega}{dt} \quad (24)$$

where: M_n is net torque applied to the unit, $d\omega/dt$ is the angular acceleration, and J is the polar moment of inertia of rotating fluid and mechanical parts in the turbine-generator (unit) combination ($J = GR^2/g$, where G is weight, R is radius of gyration).

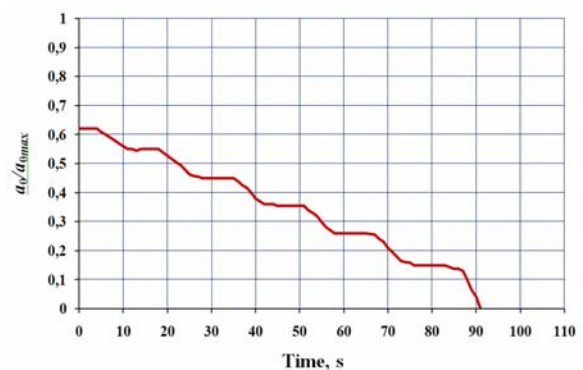


Fig. 16. Guide vane closing law during normal shut-down of the turbine

The guide vane closing law during normal shut-down of the turbine is shown in Fig. 16 and

the guide vane closing law after load rejection of the turbine is shown in Fig. 17.

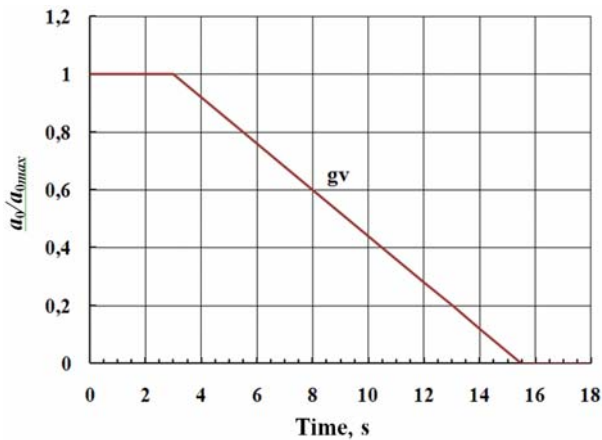


Fig. 17. Guide vane closing law after load rejection of the turbine

The results from numerical simulation and experimental [10] are presented in Fig. 18 (scenario 1) and Fig. 19 (scenario 2), using non-dimension characteristics:

$$h = \frac{H}{H_0}; \quad \alpha = \frac{n}{n_0}; \quad gv = \frac{a_0}{a_{0max}}, \quad (25)$$

where H_0 , n_0 and a_{0max} are rated values for head at the inlet of turbine, rotational speed and guide vane opening.

By comparing the simulation results with experimental data for scenario 1, the following can be concluded:

- the steady state conditions (before the guide vanes closing – first 7 seconds) are predicted with a error of 0.1%, which is extremely accurate;
- the time evolution of the heads differ for approximately 5%;
- the time of occurrence of the head peaks are at a good agreement;
- the maximum amplitude of the head are at even better agreement.

The corresponding comparison for scenario 2 shows that:

- the maximum amplitudes (water hammer) at the turbine are in a very good agreement (the error is 1.8%);
- results for the maximum increase of rotational speed of the turbine have a discrepancy of 2.5%.

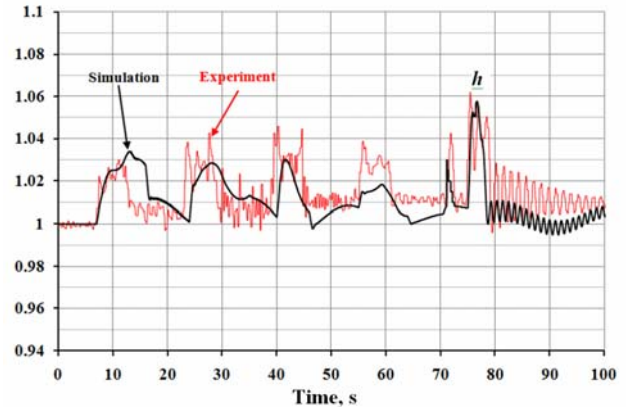


Fig. 18. Results of the simulation and experimental for head (pressure $h = H/H_0$) at the inlet of turbine 1 for scenario 1

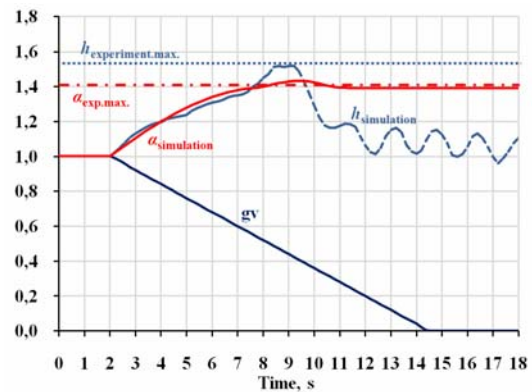


Fig. 19. Results of the simulation and experimental for head (pressure) $h = H/H_0$ at the inlet of turbine 1 and speed of revolution $\alpha = n/n_0$ (runaway) for scenario 2

CONCLUSIONS

Water hammer occurrence as a result of a quicker valve closure in a elementary plant and turbine guide vanes closure in a hydroelectric power plant is analyzed in this paper. For this purpose, mathematical models obtained with one dimensional approach that describe unsteady fluid flow are used. Solving of mathematical models is performed with method of characteristics and numerical simulation with WHAMO software package. By analysis can be concluded that for hydraulic systems with very complex initial boundary conditions water hammer computation (prediction) with method of characteristics is very complicated and it takes more time to perform the computation.

By comparing the results it can be concluded that modern software packages for numerical simulation represent a reliable tool for modeling and computation of water hammer in hydroelectric power plants. It has also been concluded that the

used numerical models are appropriate for water hammer analysis in different configuration of hydroelectric power plants and this would reduce the number of the necessary experimental runs in the future. This is particularly important having in mind that such experiments are very hard to organize, require a lot of precaution measures and are costing time and resources the energy producer.

The performed computations will contribute to a much more accurately determination of the following parameters in the design of new HPPs: guide vane closing law after load rejection, normal guide vane closing/opening law and accurately determine the increase of the pressure (water hammer). Thus, the accurate numerical modelling greatly increases safety and reliability in the design and construction of new HPPs, especially those with more complex hydraulic configuration.

NOMENCLATURE

a_0	– absolute opening of guide vanes, mm
A	– cross section, m^2
a	– wave speed, m/s
c_Q	– discharge coefficient
Cr	– Lewy–Courant number
D	– diameter, m
E	– young’s modulus of the pipe wall material, N/m^2
g	– gravity, m/s^2
g_v	– guide vane opening non-dimensional characteristic
h	– piezometric head non-dimensional characteristic
h_z	– pressure losses, m
H	– piezometric head, m
J	– polar moment of inertia, kgm^2
K	– bulk modulus of the liquid, N/m^2
k_Q	– discharge turbine coefficient
L	– length, m
M_{11}	– torque factor
M	– torque, Nm
n	– rotational runner speed, min^{-1} , rpm

n_{11}	– speed factor
P	– power, W
Q	– discharge, m^3/s
Q_{11}	– discharge factor
t	– time, s
v	– velocity, m/s
α	– runner speed non–dimensional characteristic, angle
δ	– thickness of the pipe wall, m
Δx	– length, m
Δt	– time step iteration, s
η_T	– turbine efficiency
λ	– friction factor (Darcy–Weisbach)
μ	– Poisson’s ratio
ρ	– water density, kg/m^3
ω	– angular speed, rad/s

REFERENCES

- [1] M. Hanif Chaudhry: *Applied Hydraulic Transients*, Oxford University (1979).
- [2] S. Pejovic, A. P. Boldy, D. Obradovic: *Guidelines to Hydraulic Transients Analysis*, Gower Technical Press.
- [3] A. B. Almeida, E. Koelle (1992): *Fluid Transients in Pipe Networks*, C. M. P., Elsevier (1987).
- [4] E. Benjamin Wylie, V. L. Streeter: *Fluid Transients*, University of Michigan (2001).
- [5] R. Fitzgerald, V. L. Van Blaricum: *Water Hammer and Mass Oscillation*, US Army Corps of Engineers, Research Laboratories (1998).
- [6] M.H. Chaudry: *Applied Hydraulic Transients*, British Columbia Hydro and Power Authority, Vancouver, Canada (1979).
- [7] M. Savar: *Pipeline Hydro-Dynamics*, Faculty of Mechanical Engineering and Naval Architecture, Zagreb, Croatia (2005).
- [8] C. Jaeger: *Fluid Transients in Hydro-Electric Engineering Practice*, University of Glasgow (1977).
- [9] Shavelev, D.S., *Hydroelectric Power Plants* (in Russian). Leningrad State University (1981).
- [10] V. Iliev: *Analysis of the influence of the unsteady phenomena in the intake structures, penstocks and units of the HPPs during transient regimes*. Master Thesis (in Macedonian), Faculty of Mechanical Engineering, University of Skopje, Macedonia (2011).

DEVELOPING SIMULATION APPLICATION USING GRAPHICAL PROGRAMING LANGUAGE FOR OPTIMIZATION OF SOLAR COLLECTOR POSITION

Igor Šešo, Done Taševski

*Institute of Thermal Engineering, Faculty of Mechanical Engineering,
"SS. Cyril and Methodius" University in Skopje,
P.O. Box 464, MK-1001 Skopje, Republic of Macedonia
igor.seso @mf.edu.mk*

Abstract: The sun radiation is the main energy input for the solar collectors. Thus the tilt greatly influences on the performance of solar collectors. Maximum output can be obtained if they are installed at an optimum tilt or have track the sun path in order to minimize the incident angle. In this paper, a mathematical models for the sun radiation are implemented into simulation applications by which is determined solar radiation incident on an inclined surface, optimized the tilt angles for each month, season, year, for collectors with and without tracking mechanism. Simulation application as input use global solar radiation data for solar collectors located in areas with latitude of 41.12° and longitude of 20.8° such as Ohrid, Macedonia. Results from the optimization indicates that for solar collector with fixed position the optimal tilt angle is 30° inclined from the horizontal, and considered by seasons, for winter months optimal tilt is 50° and for summer months 20° . Deviations of $\pm 5^\circ$ are allowed from optimal tilt angles since they don't affect on the total solar radiation gains with more than 1%. One axis tracking solar collector systems are recommended to track the azimuth angle inclined on angle of 50° from the horizontal. Two axis tracking system which generally use azimuth tracking together with tilt-roll tracking mechanism can provide harvesting of 2354 kWh/m^2 solar radiation per year.

Key words: solar radiation; optimization; azimuth; tilt angle; solar collector; tracking mechanism

РАЗВОЈ НА СИМУЛАЦИОНА ПРОГРАМА ЗА ОПТИМИЗАЦИЈА НА ПОСТАВЕНОСТА НА СОНЧЕВ КОЛЕКТОР СО КОРИСТЕЊЕ НА ГРАФИЧКИ ПРОГРАМСКИ ЈАЗИК

Апстракт: Сончевото зрачење е главен детерминирачки фактор за функционалноста на сончевите колектори. Затоа наклонот под кој се поставуваат има големо влијание врз нивните термички перформанси. Максимална термичка моќност може да се добие доколку сончевите колектори се поставени под оптимален наклон или ако имаат механизам со кој ја следат сончевата патека овозможувајќи сончевите зраци да паѓаат нормално на апсорберската површина. Во овој труд математички модели за сончевото зрачење се имплементирани во симулациона програма со што е овозможено: за секој час да се определи аголот на сончевите зраци во однос на нормалата на наклонетата површина, со што се овозможува да се оптимизира аголот односно наклонот, на колекторите за секој месец, за годишно време или година, притоа анализирајќи случаи со и без механизам за следење на сончевата патека. Во симулационата програма за оптимизацијата како влезни податоци се семени вредностите за глобалното сончево зрачење за градот Охрид кој се наоѓа на северна географска ширина од $41,12^\circ$ и источна географска должина $20,80^\circ$. Резултатите од оптимизацијата укажуваат дека на годишно ниво оптималниот агол на поставување на колекторите во однос на хоризонталата е 30° , додека во однос на годишното време зима оптималниот агол изнесува 50° , а за летните месеци тој агол е 20° . Во однос на пресметаните оптимални агли дозволени се промени во границите од $\pm 5^\circ$ кои не влијаат со повеќе од 1% врз вкупните сончеви добивки. За сончевите колектори кои имаат механизам за следење на сонцето по една оска се препорачува следењето да биде по азимут, а оптималниот агол на поставување (наклонот) треба да биде 50° . Системите на сончеви колектори со две оски на следење на сонцето односно со механизам за истовремена промена на наклонот и ротација на колекторот овозможуваат искористување на 2354 kWh/m^2 сончева енергија на годишно ниво за разгледуваната локација.

Клучни зборови: сончево зрачење; оптимизација; азимут; наклон; сончев колектор; механизам за следење

1. INTRODUCTION

According the IEA (International Energy Agency) buildings represents 32% of the total final energy consumption and converted in terms of primary energy this will be around 40%. Inspected deeper, the heating energy consumption represents over 60% of the total energy demand in the building. Space heating and hot water heating account for over 75% of the energy used in single and multifamily homes. Solar energy can meet up to 100% of this demand [1].

Solar technologies can supply the energy for all of the building's needs – heating, cooling, hot water, light and electricity – without the harmful effects of greenhouse gas emissions created by fossil fuels thus solar applications can be used almost anywhere in the world and are appropriate for all building types. The major share of the energy, which is needed in commercial and industrial companies for production, processes and for heating production halls, is below 250°C. The low temperature level (< 80°C) complies with the temperature level, which can easily be reached with flat plate solar thermal collectors.

The performance of a solar collector is highly influenced by its angle of tilt with the horizontal. This is due to the facts that tilt angle change the solar radiation reaching the surface of the collector, the tilt angle, defined as the angle of collectors with respect to horizontal, is a dominant parameter affecting the collectible radiation of a fixed collector. In general, the optimal tilt angle of a fixed collector is related to the local climatic condition, geographic latitude and the period of its use. Hence, different places will have different optimal tilt angles for a yearly-used solar collector.

Also sun-tracking system plays an important role in the development of solar energy applications. High degree of sun-tracking accuracy is required to ensure that the solar collector is capable of harnessing the maximum solar energy throughout the day. Azimuth-elevation and tilt-roll tracking mechanisms are among the most commonly used sun-tracking methods for aiming the solar collector towards the sun at all times.

For achieving high degree of tracking accuracy, sun-tracking systems normally employ sensors to feedback error signals to the control system for continuously receiving maximum solar irradiation on the receiver. Over the past two decades, various strategies have been proposed and they can be classified into the following three categories,

i.e. open-loop, closed-loop and hybrid sun-tracking [2].

Prior to mathematical derivation, it is worthwhile to state that the task of the on-axis sun tracking system is to aim a solar collector towards the sun by turning it about two perpendicular axes so that the sunray is always normal relative to the collector surface. Under this circumstance, the angles that are required to move the solar collector to this orientation from its initial orientation are known as sun-tracking angles. In the derivation of sun-tracking formula, it is necessary to describe the sun's position vector and the collector's normal vector in the same coordinate reference frame, which is the collector-centre frame.

There are already plenty of investigations dealing with this subject to optimize solar power systems according to the correct tilt angle or orientation. Many authors have provided empirical or analytical models to calculate the optimum tilt angle (β_{opt}) by searching for the maximum total solar radiation on the collector surface. In reference to a specific period of time and purpose, daily, monthly, seasonal or yearly values have been calculated [3].

2. SOLAR ANGLES AND DIRECTION OF BEAM RADIATION

Knowledge of sun path through the sky is necessary to calculate the solar radiation falling on a surface, the solar heat gain, the proper orientation of solar collectors, the placement of collectors to avoid shading etc. The variation of solar incidence angle and the amount of solar energy are analyzed for a fixed and trackings surfaces. The general weather of a location is required in many energy calculations. This is presented with typical meteorological year (TMY).

The geometric relationship between a plane of any particular orientation relative to the earth at any time (whether that plane is fixed or moving relative to the earth) and the incoming beam solar radiation, that is the position of the sun relative to that plane, can be described in terms of several angles (Fig. 1) [4]:

φ – **latitude**, the angular location north or south of the equator, north positive;

δ – **declination**, the angular position of the sun at solar noon with respect to the plane of the equator, north positive;

β – **slope** (tilt), the angle between the plane of the surface in question (collector) and the horizontal ($\beta > 90$ means that the surface has a downward facing component);

ω – **hour angle**, the angular displacement of the sun east or west of the local meridian due to rotation of the earth on its axis at 15° per hour;

θ – **angle of incidence**, the angle between the beam radiation on a surface and the normal to that surface;

Additional angles are defined that describe the position of the sun in the sky:

θ_z – **zenith angle**, the angle between the vertical and the line to the sun, i.e. the angle of incidence of beam radiation on a horizontal surface;

α_s – **solar altitude angle**, the angle between the horizontal and the line to the sun, i.e. the complement of the zenith angle.

γ_s – **solar azimuth angle**, the angular displacement from south of the projection of beam radiation on the horizontal plane. Displacement east of south are negative and west of south are positive.

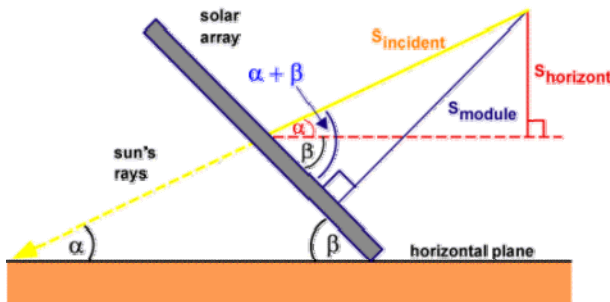


Fig. 1. Schematic view of solar collector with the characteristic angles

Equation used for calculation of the incident angle for every hour of the year is introduced with the following expression:

$$\begin{aligned} \cos \theta = & \sin \varphi \cos \beta - \sin \delta \cos \varphi \sin \beta \cos \gamma \\ & + \cos \delta \cos \varphi \cos \beta \cos \omega \\ & + \cos \delta \sin \varphi \sin \beta \cos \gamma \cos \omega \\ & + \cos \delta \sin \beta \sin \gamma \sin \omega. \end{aligned} \quad (1)$$

The solar azimuth angle γ_s can have values in the range of 180° to -180° . For north or south latitudes between 23.45° and 66.45° , γ_s will be between 90° and -90° for the days less than 12 hours long; for days with more than 12 hours between sunrise and sunset γ_s will be greater than 90° or

less than -90° early and late in the day when the sun is north of the east-west line in the northern hemisphere.

Thus to calculate γ_s it must be known in which quadrant the sun will be. A general formulation for γ_s from Braun and Mitchel (1983) is written for pseudo solar azimuth angle γ_s in the first or fourth quadrant [5]:

$$\gamma_s = C_1 C_2 \gamma'_s + C_3 \left(\frac{1 - C_1 C_2}{2} \right) 180, \quad (2)$$

where

$$\begin{aligned} \tan \gamma'_s &= \frac{\sin \omega}{\sin \varphi \cos \omega - \cos \varphi \tan \delta}, \\ C_1 &= \{1 \text{ if } |\omega| < \omega_{ew}; \quad -1 \text{ otherwise}\}, \\ C_2 &= \{1 \text{ if } \varphi(\varphi - \delta) \geq 0; \quad -1 \text{ otherwise}\}, \\ C_3 &= \{1 \text{ if } \omega \geq 0; \quad -1 \text{ otherwise}\}, \\ \cos \omega_{ew} &= \frac{\tan \delta}{\tan \varphi}. \end{aligned} \quad (3)$$

If a collector is installed toward south in the northern hemisphere, the equation for calculation of the cosine of the incidence angle can be simplified as follows:

$$\cos \theta = \cos(\varphi - \beta) \cos \delta \cos \omega + \sin(\varphi + \beta) \sin \delta. \quad (4)$$

3. SOLAR ANGLES FOR TRACKING SURFACES

There are solar collectors with systems that track the sun by moving in prescribed ways to minimize the angle of incidence of beam radiation on their surfaces and thus maximize the incident beam radiation. As input for tracking devices are needed the angles of incidence and the surface azimuth angles.

Rotation can be around one axis (horizontal east-west, horizontal north-south, vertical or parallel to the Earth axis) or it can be around two axis. In the following paragraph will be presented the set of equations which are applicable for surfaces that rotate on axes that are parallel to the surface.

For a plane rotated about the horizontal east-west axis with a single daily adjustment so that the beam radiation is normal to the surface at noon each day [6]:

$$\cos \theta = \sin^2 \delta + \cos \delta \cos \omega. \quad (5)$$

With each day fixed slope defined with:

$$\beta = |\varphi - \delta|. \quad (5.1)$$

For a plane rotated about horizontal east-west axis with continuous adjustment to minimize the angle of incidence:

$$\cos \theta = (1 - \cos^2 \delta \sin^2 \omega)^{1/2}. \quad (5.2)$$

Where the slope of this surface is given by the equation:

$$\tan \beta = \tan \theta_z |\cos \gamma_s|. \quad (5.3)$$

The plane, i.e. the collector with a fixed slope rotated about vertical axis, the angle of incidence is minimized when the surface and solar azimuth are equal. Thus the angle of incidence is:

$$\cos \theta = \cos \theta_z \cos \beta + \sin \theta_z \sin \beta. \quad (5.4)$$

The slope is fixed $\beta = \text{const}$ and the surface azimuth is $\gamma = \gamma_s$.

For a solar collector rotated about north-south axis parallel to the Earth's axis with continuous adjustment to minimize the angle of incidence θ , $\cos \theta = \cos \delta$ where the slope varies continuously and is determined with the equation:

$$\tan \beta = \frac{\tan \varphi}{\cos \gamma}. \quad (5.5)$$

And the surface azimuth angle is:

$$\gamma = \tan^{-1} \frac{\sin \theta_z \sin \gamma_z}{\cos \theta \sin \varphi} + 180 C_1 C_2, \quad (5.6)$$

where

$$\cos \theta' = \cos \theta_z \cos \varphi + \sin \theta_z \sin \varphi \quad (5.7)$$

$$C_1 = \begin{cases} 0 & \text{if } (\tan^{-1} \frac{\sin \theta_z \sin \gamma_s}{\cos \theta \sin \varphi} + \gamma_s = 0; \\ 1 & \text{otherwise} \end{cases}$$

$$C_2 = \{1 \text{ if } \gamma_s \geq 0; -1 \text{ if } \gamma_s \leq 0\}.$$

It is often necessary to calculate the hourly radiation on a tilted surface of a collector from measurements or estimates of solar radiation on a horizontal surface. The official measurements of solar radiation in most cases provides data for radiation on horizontal surface, whereas the need is for beam and diffuse radiation on the plane of a collector. Therefore is introduced the geometric factor R_b , which is the ration of beam radiation on

the tilted surface to that on a horizontal surface at any time. The angle of incidence of beam radiation on the horizontal and tilted surfaces. It is calculated with the equation [7]:

$$R_b = \frac{G_{bt}}{G_b} = \frac{G_{b,n} \cos \theta}{G_{b,n} \cos \theta_z}. \quad (5.8)$$

The optimum azimuth angle for flat plate collectors is usually 0° in the northern hemisphere. Thus is a common situation that $\gamma = 0^\circ$. Determination of R_b for the northern hemisphere for $\gamma = 0^\circ$ can be done with the equation:

$$R_b = \frac{\cos(\varphi - \beta) \cos \delta \cos \omega + \sin(\varphi - \beta) \sin \delta}{\cos \varphi \cos \delta \cos \omega + \sin \varphi \sin \delta}. \quad (5.9)$$

A special case of interest is $R_{b,noon}$ the ratio of south facing surfaces at solar noon. For the northern hemisphere

$$R_{b,noon} = \frac{\cos|\varphi - \delta - \beta|}{\cos|\varphi - \beta|}. \quad (5.9.1)$$

In this regard Hottell and Woertz [7] pointed that equation 5.9 provides a convenient method for calculating R_b for the most common cases. They also showed graphical method for solving those equations. The graphical method plots $\cos \theta_z$ as a function of φ and $\cos \theta$ as a function of $|\varphi - \beta|$ for various dates, i.e. declination.

For a plane rotated about a horizontal east-west axis to maximize the beam radiation on the plane, from the following equation can be calculated the ratio of the beam radiation on the plane to that on a horizontal surface at any time:

$$R_b = \frac{(1 - \cos^2 \delta \sin^2 \omega)^{1/2}}{(\cos \varphi \cos \delta \cos \omega + \sin \varphi \sin \delta)}. \quad (5.9.2)$$

When there is need to calculate the radiation on tilted surfaces with only total radiation data is available then is needed to be known the directions from which the beam and diffuse components reach the surface in question. The direction from which the diffuse radiation is received, i.e. the distribution over the sky dome is a function of conditions of cloudiness and atmospheric clarity, which are highly variable. The diffuse radiation can be described with three parts. First is isotropic part received uniformly from all of the sky dome. The second is circumsolar diffuse resulting from forward scattering of solar radiation and concentrated in the sky around the sun. The third referred to as horizon brightening is concentrated near the hori-

zon and is most pronounced in clear skies. The angular distribution of diffuse is to some degree a function of the reflectance ρ_g (the albedo) of the ground.

The total incident solar radiation is the sum of a set of radiation streams including beam radiation the three components of the diffuse radiation from the sky and radiation reflected from the various surfaces "seen" by the collector surface can be written-calculated as:

$$I_T = I_{T,b} + I_{T,d,iso.} + I_{T,d,hz} + I_{T,refl}, \quad (5.9.3)$$

where the subscripts *iso*, *cs*, *hz*, and *ref* refer to the isotropic, circumsolar, horizon and reflected radiation streams. The ratio of the total radiation on tilted surface to that on the horizontal surface can be determine as $R=I_T/I$.

Determine the value for I_T is the main difficult in the above equations, i.e. the difference in calculating it's values are largely in the way that the diffuse terms are treated.

It can be assumed that the diffuse radiation is isotropic where the calculation is represented by the isotropic diffuse model with the equation:

$$R = \frac{I_b}{I} R_b + \frac{I_d}{I} \left(\frac{1 + \cos \beta}{2} \right) + \rho_g \left(\frac{1 - \cos \beta}{2} \right). \quad (5.9.4)$$

For the anisotropic model the calculation of the total radiation on the tilted surface is:

$$I_T = (I_b + I_d A_i) R_b + I_d (1 - A_i) \left(\frac{1 + \cos \beta}{2} \right) + I \rho_g \left(\frac{10 + \cos \beta}{2} \right), \quad (5.9.5)$$

where A_i is the anisotropy index which is a function of the transmittance of the atmosphere for beam radiation. The anisotropy index determines a portion of a horizontal diffuse which is to be treated as forward scattered; it is considered to be incident at same angle as the beam radiation.

When the beam and ground-reflected terms are added the HDKR model (the Hay, Davies, Klutscher, Reindl model) results. The total radiation on the tilted surface is:

$$I_T = (I_b + I_d A_i) R_b + I_d (1 - A_i) \left(\frac{1 + \cos \beta}{2} \right) \cdot \left[1 + f \sin^3 \left(\frac{\beta}{2} \right) \right] + I \rho_g \left(\frac{10 + \cos \beta}{2} \right), \quad (5.9.6)$$

where f is modulating factor which with the form $f \sin^2(\beta/2)$ accounts for cloudiness.

$$f = \sqrt{\frac{I_b}{I}}. \quad (5.9.7)$$

For use in solar process design procedures also is needed the monthly daily average radiation on the tilted surface. There are several methods for calculating the monthly average daily radiation on sloped surfaces among which the widely used are the isotropic sky and *K-T* method. The first method isotropic sky is that of Liu and Jordan (1962) extended from Klein (1977). If the diffuse and ground reflected radiations are each assumed to be isotropic then the monthly mean solar radiation on an unshaded tilted surface can be expressed as:

$$R = \frac{\overline{H_T}}{H} = \left(1 - \frac{\overline{H_d}}{H} \right) \overline{R_b} + \frac{\overline{H_d}}{H} \left(\frac{1 + \cos \beta}{2} \right) + \rho_g \left(\frac{1 - \cos \beta}{2} \right), \quad (5.9.8)$$

where $\frac{\overline{H_d}}{H}$ is a function of K_T .

Another method for calculation of average radiation on sloped surfaces is developed by Klein and Theilacker called *K-T* method which valid for any azimuth angle is given with the following expression [8]:

$$R = D + \frac{\overline{H_d}}{H} \left(\frac{1 + \cos \beta}{2} \right) + \rho_g \left(\frac{1 - \cos \beta}{2} \right)$$

$$D = \begin{cases} \max\{0, G(\omega_{SS}, \omega_{SR})\} & \text{if } \omega_{SS} > \omega_{SR} \\ \max\{0, [G(\omega_S - \omega_S) + G(\omega_S, \omega_{SR})]\} & \text{if } \omega_{SR} > \omega_{SS} \end{cases} \quad (5.9.9)$$

$$a' = a - \frac{\overline{H_d}}{H}; \quad A = \cos \beta + \tan \varphi \cos \gamma \sin \delta$$

$$B = \cos \omega_S \cos \beta + \tan \delta \sin \beta \cos \gamma; \quad C = \frac{\sin \beta \sin \gamma}{\cos \varphi}$$

a) *Extra terrestrial radiation on a horizontal surface*

Using the normalized radiation levels can be calculated the ratio of radiation level to the theoretically possible radiation that would be available if there were no atmosphere.

At any point in time the solar radiation incident on a horizontal plane outside the atmosphere is the normal solar incident radiation calculated with the following equation [9]:

$$G_0 = G_{sc} \left(1 + 0.033 \cos \frac{360n}{365} \right) \cos \theta_z, \quad (6)$$

where G_{sc} is the solar radiation constant and n is the day of the year. Calculation of G_0 for a horizontal surface at any time between sunrise and sunset is provided with the equation:

$$G_0 = G_{sc} \left(1 + 0.033 \cos \frac{360n}{365} \right) \cdot (\cos \varphi \cos \delta \cos \omega + \sin \varphi \sin \delta). \quad (6.1)$$

It is often necessary for calculation of daily solar radiation to have the integrated daily extra-terrestrial radiation on a horizontal surface H_0 .

$$H_0 = \frac{24 \cdot 3600 G_{sc}}{\pi} \left(1 + 0.033 \cos \frac{360n}{365} \right) \cdot \left(\cos \varphi \cos \delta \sin \omega_s + \frac{\pi \omega_s}{180} \sin \varphi \sin \delta \right) \quad (6.2)$$

The monthly mean daily extra-terrestrial radiation \bar{H}_D is a useful quantity and for latitudes in the range +60 to -60 can be calculated with the equation 6.2 using n and δ for the mean day of the month.

b) Estimation of average solar radiation

For estimation of average incident radiation requires to be provided solar radiation data. Lacking of these data it is possible to use empirical relationships to estimate radiation from hours of sunshine or cloudiness. Data on average hours of sunshine or average percentage of possible sunshine hours are widely available in many stations with Campbell-Stokes. Page in 1964 suggested equations for estimation of the monthly average daily radiation base it on extra-terrestrial radiation on a horizontal surface:

$$\frac{\bar{H}}{H_0} = a + b \frac{\bar{n}}{\bar{N}}. \quad (7)$$

where H_0 is the extra-terrestrial radiation for the location, averaged over the time period in question and a and b are constants depending on location, \bar{N} is the average day length and \bar{n} is monthly average daily hours of bright sunshine.

c) Estimation of hourly radiation from daily data

Information on the frequency distribution is the link between the daily fraction of diffuse with

daily radiation and that of the monthly average fraction of diffuse with monthly average radiation.

The monthly average clearness index \bar{K}_T is the ratio of monthly average daily relation on a horizontal surface to the monthly average daily extra-terrestrial radiation.

$$\bar{K}_T = \frac{\bar{H}}{H_0}. \quad (7.1)$$

The most precise performance calculations for system are the hour-by-hour where it is necessary to start with daily data and estimate hourly values from daily numbers. It should be noted that daily total radiation values in the middle range between clear day and completely cloudy day values can arise from various circumstances such as intermittent heavy clouds, continuous light clouds or heavy cloud cover for part of the day. The method presented in this paper works best for clear days and those are the days that produce most of the output of solar processes that operate at temperatures significantly above ambient.

Statistical studies of the time distribution of total radiation on horizontal surfaces through the day using monthly average data for a number of stations have led to generalized charts of r_t , the ratio of hourly total to daily total radiation as a function of day length and the hour in question:

$$r_t = \frac{1}{H}. \quad (7.2)$$

Collares-Pereira and Rabl developed equation which calculates the above mentioned ratio:

$$r_t = \frac{\pi}{24} (a + b \cos \omega) \frac{\cos \omega - \cos \omega_1}{\sin \omega_s - \frac{\pi \omega_s}{180} \cos \omega_s}. \quad (7.3)$$

The coefficients a and b are given by:

$$a = 0.409 + 0.5016 \sin(\omega_s - 60). \quad (7.4)$$

In these equations ω is the hour angle in degrees for the time in question and ω_s is the sunset hour angle.

4. DESCRIPTION OF GRAPHICAL PROGRAMMING SOFTWARE

The software that is used in the thermal analysis is called INSEL which is acronym for Integrated Simulation Environment Language. IN-

SEL it's not a simulation program but provides an integrated environment and a graphical programming language for the creation of simulation applications. The basic idea of the software is to connect blocks to blocks diagrams that express a solution for a certain simulation task.

In the graphical programming language the data flow plays the key role. This language provides graphical symbols which can be interconnected to build a larger structures. The graphical symbols represent mathematical functions and real components like: solar thermal collectors, photovoltaic modules, wind turbines and batteries, for example, or even complete technical systems of any kind [11].

Fundamental blocks, basic operations and mathematical functions of the environment are provided in a dynamic library. It contains tools like blocks for date and time handling, access to arbitrary files, blocks for performing mathematical calculations and statistics, blocks for data fitting, plotting routines etc.

Energy meteorology and data handling are available as library. This library contains algorithms, like the calculation of the position of the Sun, spectral distribution of sunlight, and radiation outside atmosphere. A large data base provides monthly mean values of irradiance, temperature and other meteorological parameters. Generation of hourly radiation, temperature, wind speed, and humidity data from monthly means is possible. Further, diffuse radiation models, conversion of horizontal data to tilted are included.

5. OPTIMIZATION OF COLLECTOR AZIMUTH AND SLOPE ANGLE FOR OBTAINING MAXIMUM ANNUAL SOLAR ENERGY GAIN

For receiving maximum solar energy, the collector's surface should be perpendicular to the sun's rays, and this can be accomplished when the solar trackers are used to follow the sun instantaneously. The main problem in this regard is however the high cost of this kind of trackers, so instead of employing solar trackers, the angles of collector's surface could be changed manually every day or month or season in order to adjust the collector almost perpendicular to the sun's rays. In this paper the optimization of the collector slope angle is performed for a location in Ohrid, R. Macedonia, in regard obtaining maximum solar energy gain, i.e. useful thermal energy.

Most of the measurements or available data for solar radiation are for horizontal surfaces which should be converted into values of solar radiation on the tilted surface.

There are plenty of models which can be used to convert horizontal data to tilt. Most of them use the same approach: in a first step the radiation data are split up into their beam and direct use fractions by some statistical correlation, and in a second step both components are converted to the tilted surface. Concerning the beam part G_{bh} the conversion can be done by pure geometry, in the case of the direct use radiation some assumption about its distribution over the sky dome must be made.

Since it is for tilted surfaces this portion depends on the ground reflectance, or albedo which having a minor role will be set constant to $\rho = 0.2$.

The correlations which calculate the diffuse use fraction are based on the clearness index k_t , defined as the ratio between the global radiation that arrives at the Earth's surface on a horizontal plane G_h and its extra-terrestrial pendant G_{oh} .

The optimization procedure is an program assembly of several subprograms.

6. PLOTTING THE HOURLY TIME SERIES OF GLOBAL AND DIFFUSE RADIATION FOR THE DEFINED LOCATION

As the solar radiation passes through the Earth's atmosphere, some of it is absorbed or scattered by air molecules, water vapour, aerosols and clouds. The solar radiation that passes through directly to the Earth's surface is called Direct Solar Radiation and the radiation scattered out of direct beam is called Diffuse Solar Radiation. The direct component of sunlight and the diffuse component of skylight falling together on the horizontal surface make up the Global Radiation.

For this reason, many models have been developed to establish correlations between the diffuse fraction and various predictors.

In Figure 2 is presented the simulation sub-program scheme which plots the hourly time series of the horizontal global and diffuse solar radiation for Ohrid which geographically is located at latitude 41.1 °N longitude 20.8 °E (in the model the longitude value is inserted with minus sign because it concerns east) 23 time zone. Its structure is formed of several blocks such as:

- The "CLOCK" block connected with the "Hour of the year" which provides the program cycle counting each hour of the year.

- The “MTM” block is weather data base which provides weather monthly values for sun irradiation, ambient, minimum and maximum temperature for the specified location.
- The “GENG” block generates the series of hourly global radiation data from monthly mean values, using the inputs from the MTM block.
- The “GOH” block returns the radiation outside atmosphere on a horizontal surface for the defined location.
- The “G2GDH” block returns the diffuse radiation according to various correlations for radiation hourly data calculated according the model of Orgill and Hollands [10].

The “CLOCK” block provides program cycle counting for each hour, day and month of the year, i.e. simulates the year 2006 on hourly basis for the “GENG” and “GOH” blocks. The “GENG” block beside the clocks year, month, days and hour inputs requires input for the monthly mean horizontal irradiance in W/m^2 for the specified location – Ohrid, defined by its latitude, and longitude which data’s are provided from the “MTM” block. As an output from the “GENG” block is the hourly irradiance data for the location which is used as an input for the “G2GDH”. It should be noted that the Gordon-Reddy variance factor is set to one; the year-to-year variability is set to zero, such that the time series of generated irradiance data represents the monthly mean value as close as possible.

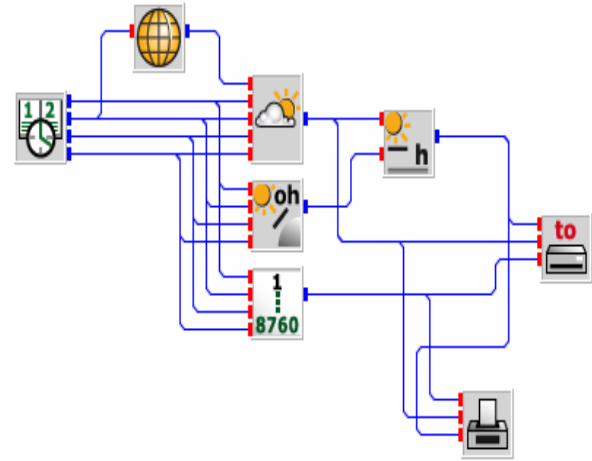


Fig. 2. Simulation program for total and diffuse horizontal radiation

In order to calculate the hourly diffuse radiation the “G2GDH” block requires input for the extra-terrestrial radiation for the given location. The values for the extra-terrestrial radiation are provided from the “GOH” block. The block calculates the fraction of hourly diffuse and global radiation on a horizontal surface mainly on the basis of the clearness index. Among the eight offered correlations models for calculation of the diffuse fraction in this paper is used the model of Orgill and Hollands.

The simulation results i.e. hourly plot for the global and diffuse radiation over one year period for the location of Ohrid is presented on Figure 3:

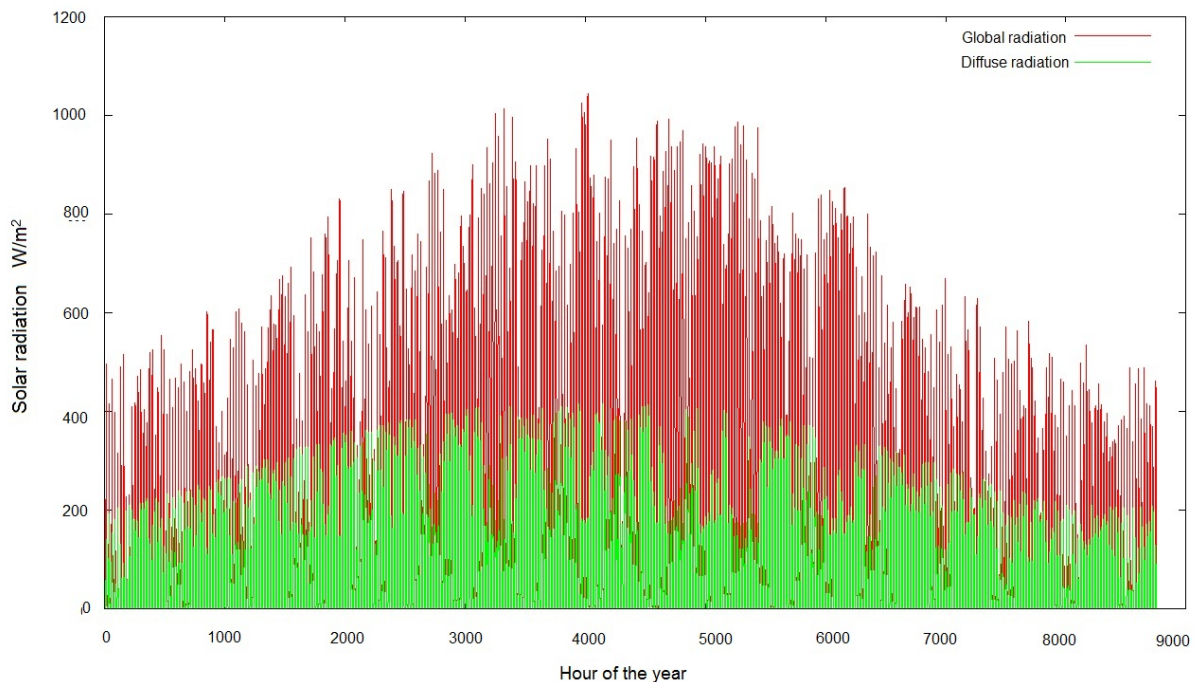


Fig. 3. Global and diffuse solar radiation on horizontal plane for Ohrid – hourly values

The x-axis shows the hour of the year, the y-axis shows synthetic hourly means of global irradiance on a horizontal plane (red) and diffuse irradiance on a horizontal plane (green) both given in W/m^2 .

7. OPTIMIZATION OF COLLECTOR TILT ANGLE AND AZIMUTH

Optimization program simulation is developed for four different cases which in detail analyzed in the following sections.

a) Optimization of collector tilt angle for azimuth tracking system

Optimization is made to determine the optimal collector tilt angle for collector with constant azimuth-orientation toward south 180° in order to harvest the maximum solar radiation energy on annual basis. The algorithm-block scheme of the simulation program for optimization of collector tilt angle is given on Figure 4.

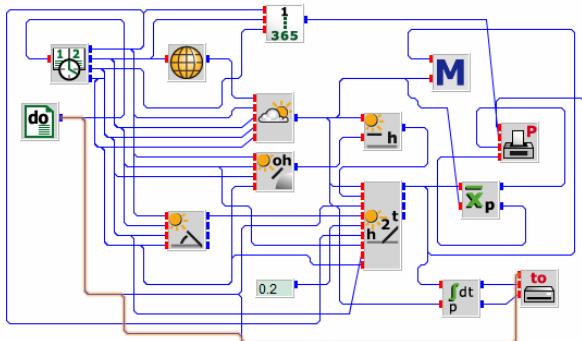


Fig. 4. Graphical scheme of the simulation program for determination of monthly solar radiation energy on horizontal plane and on several tilt angles with azimuth tracking

Information regarding the total and diffuse solar radiation is calculated with the previously described program (Fig. 5). The “GH2GT” block is used to calculate the radiation on a tilted surface from horizontal data which as an input data requires: the global solar radiation from “GENG”, hourly diffuse radiation from “G2GDH”. The tilt angle (slope) is varied and set as parameter with the “DO” block starting with the value of 20° ending with 60° changing them in the cycle with step of 10° . The azimuth tracking values are obtained from the “SUNAE” block which calculates the position of the sun for each hour of the year using Holland [10] approximation for the specified location and the albedo factor is taken as a constant

with value of 0.2 (Fig. 6). The output results for the global radiation on the horizontal and tilted plane are plotted graphically by the “PLOT” block and written as a file with the “WRITE” block which is presented in Table 1.

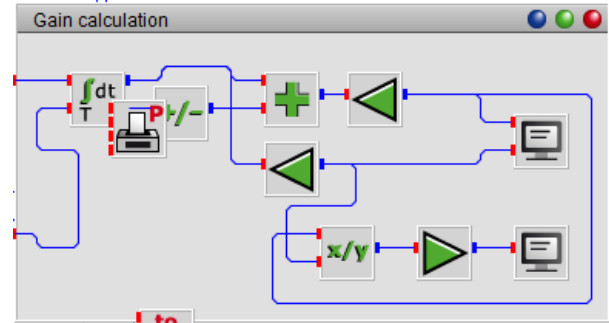


Fig. 5. Graphical scheme of the macroblock from Fig. 1



Fig. 6. One axis tracking system

Table 1

Monthly solar radiation values for different collector slope with one axis tracking system azimuth

	Collector slope, °				
	20	30	40	50	60
January	82.52	92.55	100.33	105.64	108.29
February	118.01	130.40	139.57	145.21	147.12
March	151.50	162.79	170.24	173.63	172.82
April	192.30	202.56	208.07	208.65	204.30
May	241.16	253.61	259.79	259.50	252.75
June	256.95	268.06	272.37	270.01	261.07
July	269.62	283.34	289.86	289.05	280.92
August	238.29	253.16	261.54	263.20	258.11
September	200.04	216.02	226.48	231.14	229.86
October	138.52	152.29	162.12	167.78	169.16
November	100.63	112.86	122.26	128.57	131.63
December	69.08	76.98	83.01	87.02	88.96
Total, kWh	2058.61	2204.63	2295.64	2329.38	2304.99
Horizontal, kWh	1616				
Gain	21.50%	26.70%	29.61%	30.63%	29.89%

v) *Optimization collector tilt angle for constant solar azimuth – south 180°*

It is an established fact that the solar radiation intensity falling on a horizontal flat surface, at a given time and location, increases with the increase in surface tilt angle at a solar hemispherical inclination.

It is generally known that in the northern hemisphere, the optimum collector orientation is south facing (= 0) and the optimum tilt depends upon the latitude and the day of the year. In winter months, the optimum tilt is greater (usually latitude +15°), whilst in summer months, the optimum tilt is less (usually latitude –15°). There are many papers in the literature which make different recommendations for the optimum tilt based only on the latitude. In practice, the collector plate is usually oriented south facing and at a fixed tilt which is set to maximize the average energy collected over a year.

This case considers situation where the collector has constant azimuth angle 180°, i.e. installed toward south. Optimization is done for the collector tilt angle in regard obtaining maximum solar radiation energy on annual basis.

The simulation program for optimisation consist almost all of the previously defined block for optimization of the one-axis tracking collector slope, i.e. the data for monthly solar radiation on horizontal (W/m^2) is given with the MTM block which with the application of “GH2GT”, “GENG” and “G2GDH” blocks is converted to hourly values. The block “GH2GT” using constant value for the azimuth of 180° and parametric values from the “DO” block for the tilt angle. As output from the block are given the hourly values for the incident solar radiation on the surface which with the “Parametric accumulation” block are averaged on monthly basis and the results are written in specific file. In Table 2 are presented the simulated results for the collector monthly received solar radiation in kWh/m^2 oriented toward south 180° for different tilt angles.

On Figure 7 is given graphical presentation of the above results which provides better visibility where are given the monthly values for solar radiation on to the collector plane tilted on angles starting from 20° up to 60° with step of 10°. For each of the tilt angles are simulated and calculated monthly values in one year period.

If the same system configuration is analyzed for the summer period, i.e. during the months from

May till September then the sum of received solar radiation in regard of the slope angle would be.

Table 2

Monthly solar gains on collector plane with constant azimuth toward south 180°

Collector slope, °	Solar gain, kWh/m ²				
	20	30	40	50	60
January	77.55	85.51	91.40	95.07	96.44
February	108.56	116.73	122.16	124.68	124.23
March	135.66	139.89	140.98	138.88	133.63
April	167.44	166.97	162.85	155.22	144.29
May	199.80	194.31	184.16	169.84	152.10
June	210.89	203.00	190.38	173.49	153.96
July	220.87	213.53	201.32	184.42	164.37
August	201.00	199.23	192.68	181.57	166.44
September	176.65	181.84	182.58	178.86	170.78
October	126.03	134.15	139.05	140.57	138.66
November	93.60	102.74	109.41	113.40	114.55
December	65.01	71.94	76.95	80.00	81.16
Total, kWh/m ²	1783.05	1809.85	1793.91	1735.99	1640.63
Horizontal, kWh/m ²	1616				
Gains (%)	9.37	10.71	9.92	6.91	1.50

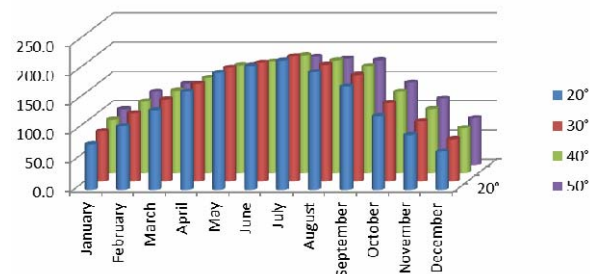


Fig. 7. Monthly solar radiation for south orientated collector (azimuth 180°) for different tilt angle

The results in Table 3 provide quantitative overview for the solar radiation values for winter and summer months for different tilt angles and constant collector azimuth toward south 180°. In the simulation programme as winter months are considered: January, February, March and April while the rest are summer months. Comparing the results can be seen that: for winter period optimal angles for biggest solar energy are the angles around 50°±5°, where the solar gains would be nearly 3% higher compared if the surface was placed horizontal and for summer months optimal angle would be 2–3% higher compared with horizontal orientation. Angles in summer period which

are bigger than 40° would result in smaller gains compared to horizontal position of the collector even 20% lower if the collector is placed with tilt of 60°.

Table 3

Solar radiations for winter and summer months for different collector tilt angle and constant azimuth of 180°

Collector slope, °	Solar gain, kWh/m ²					
	20	30	40	50	60	Horizontal
Winter	606.40	650.98	679.95	692.60	688.68	606.91
Summer	1009.21	991.91	951.11	888.18	807.65	980.01
Gain/W(%)	-0.08	6.77	10.74	12.37	11.87	
Gains (%)	2.8	1.20	-3.04	-10.34	-21.34	

c/ Available solar radiation on the collector plane with two axis tracking system

Azimuth-elevation and tilt-roll tracking mechanisms are among the most commonly used sun-tracking methods for aiming the solar collector towards the sun at all times.

The simulation program developed for simulation and calculation of the available solar radiation on the collector plane with two axis tracking mechanism tracking azimuth and tilt-roll uses all of the previously described blocks as it is shown on Figure 8.

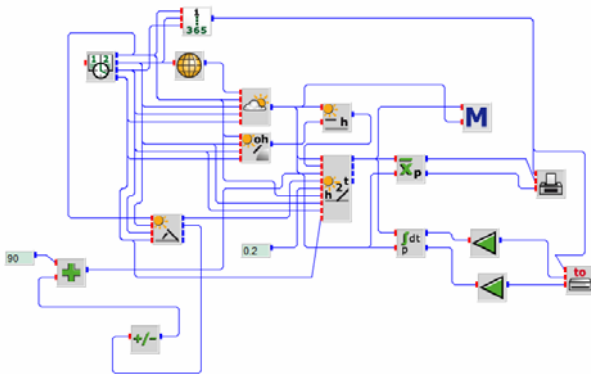


Fig. 8. Monthly solar radiation for south orientated collector in regard of the tilt angle

The azimuth and tilt angle tracking is performed with the SUNAE block in which one of the outputs is the azimuth. The tilt angle which is required in the GH2GT block is given with a sub-program which converts the output of the SUNAE block-angle of the current Sun elevation which then is multiplied with minus sign and subtracted

from 90 thus obtaining the value for the tilt angle which is complementary to the sun elevation angle. The results from the simulation are presented in Table 4.

Solar collector systems with two axis tracking, i.e. continuously tracking the sun position and thus minimizing the incidence angle are obtaining maximal solar radiation gain on the collector plane. With the two-axis tracking system is possible to achieve increase in more than 30% of available solar energy compared with the values if the collector were installed horizontal, i.e. the collector tilt angle $\beta = 0^\circ$.

Table 4

Solar radiation gains for two-axis tracking collector

	Solar gain , kWh/m ²		
	Tracking	Horizontal	Gain, %
January	105.88	56.63	47
February	144.45	85.07	41
March	172.26	118.48	31
April	209.82	157.87	25
May	266.08	199.19	25
June	278.37	214.54	23
July	296.93	221.42	25
August	266.92	191.06	28
September	231.13	153.80	33
October	166.72	101.28	39
November	129.10	69.18	46
December	86.42	47.15	45
Total	2354.08	1615.67	31

In Fig. 9 graphically is presented the difference between the two axis tracking system and horizontal available radiation.

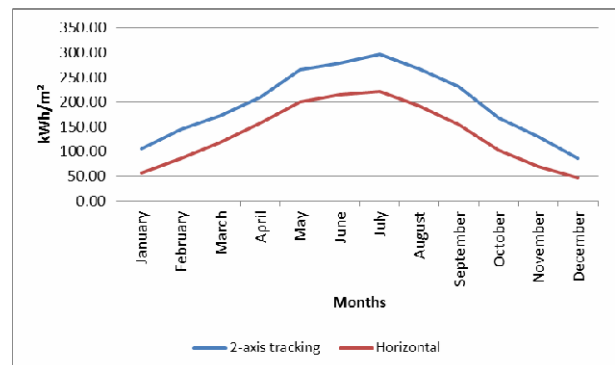


Fig. 9. Available solar radiation on collector plane for two axis solar tracking and horizontal position

It is conducted comparative analysis between all four previously analyzed cases in regard of the maximal annual solar radiation gains providing better overview for the efficiency. In this analysis for all of the considered cases are taken only monthly values for solar radiation for those variants which total end – annual sum is the biggest. i.e. only the values for optimal tilt such as for collectors with constant azimuth. In Table 5 is given the overview for monthly solar radiation values for the four cases where the first is solar collector completely tracking the sun by two axis mechanism, the second is placed in constant position toward south- azimuth 180° and at the optimal tilt angle of 30, third is collector which has one axis mechanism for the azimuth installed under the optimal tilt angle of 50° and the last case are the values for the horizontal position, i.e. values for horizontal sun radiation.

Table 5

Solar radiation gains for different cases in the optimal variant

	Solar radiation, kWh/m ²			
	Two-axis tracking	Optimal tilt angle; Constant azimuth, 30°	One axis tracking azimuth; Tilt angle constant, 50°	Horizontal solar radiation
January	105.9	85.5	105.6	56.6
February	144.4	116.7	145.2	85.1
March	172.3	139.9	173.6	118.5
April	209.8	167.0	208.6	157.9
May	266.1	194.3	259.5	199.2
June	278.4	203.0	270.0	214.5
July	296.9	213.5	289.0	221.4
August	266.9	199.2	263.2	191.1
September	231.1	181.8	231.1	153.8
October	166.7	134.2	167.8	101.3
November	129.1	102.7	128.6	69.2
December	86.4	71.9	87.0	47.1
Total	2354.1	1809.9	2329.4	1615.7
Gains (%)	92.87	90.73	92.80	

Graphical presentation of the simulated result for all four cases with the solar radiation gains per month are given on Figure 10.

The total yearly solar radiation gains for each of the previously considered systems presented in Table 5 are given in the diagram on Fig. 11.

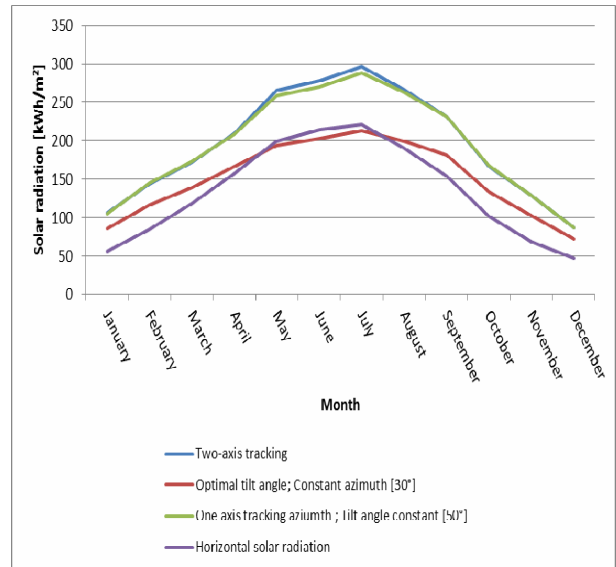


Fig. 10. Monthly solar radiation gains for the considered cases

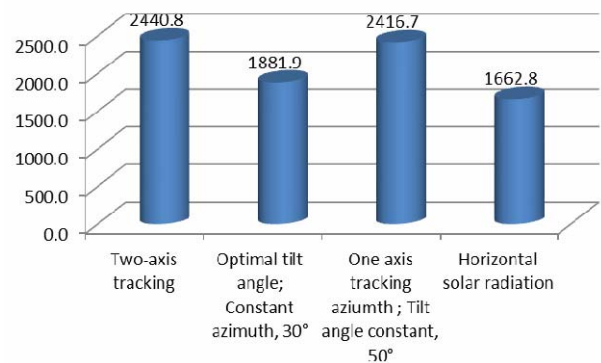


Fig. 11. Total solar radiation gain per year

CONCLUSION

The main aim of this paper was to determine the optimum solar collector angles, i.e. tilt and surface azimuth angles in order to obtain the maximum solar energy gain on annual basis for location in Ohrid, Macedonia. First, in order to reach this point that using solar trackers are helpful or not, the daily, monthly, seasonally and yearly optimum angles are calculated and the gain of solar energy is determined.

There were examined four cases of solar collectors with tracking and non-tracking devices for which optimization processes were developed simulation software's using data programming language.

Solar collectors with constant azimuth angle of 180°, i.e. oriented toward south should be installed on optimal tilt angle in the range of 30°±5°

which would provide 10% more solar gains of solar radiation compared if installed horizontal. If the optimization is performed on seasonal basis, i.e. for winter and summer periods results for winter months with optimal collector tilt angle of 50° and for summer months it's 20° . Variations in the collector tilt angle in the limits of $\pm 5^\circ$ doesn't affect much on the end amount of solar radiation gain, i.e. not more than 1%.

Optimization was done for the solar collectors which track the azimuth of the sun. In this case the optimal tilt angle is 50° allowing 2330 kWh/m^2 available solar radiation on the collector plane instead of the 1616 kWh/m^2 solar horizontal radiation, i.e. in total 31% increase.

The last complete comparison of all of the previously optimized cases showed that with two axis tracking system will be gained the most solar radiation compared with the rest three cases. But should be noted that two axis tracking system gains not more than 1% from the one axis tracking system with the optimal tilt which opens field for further techno-economic analysis.

REFERENCES

- [1] International Energy Agency: *Key World Energy Statistics*, IEA (2012).
- [2] Kok-Keong Chong, Chee-Woon Wong: *Solar Collectors and Panels, Theory and Applications*, Sciyo (2010).
- [3] Elsayed, M. M.; Optimum orientation of absorber plates, *Solar Energy*, **42**, 89–102 (1989).
- [4] Benford, F, J. E. Bock: A Time Analysis of Sunshine, *Trans. of American Illumination Engineering Soc.*, vol. 34 (1939).
- [5] Braun, J. E, J. C. Mitchell: Solar Geometry for Fixed and Tracking Surfaces, *Solar Energy*, vol. 31 (1983).
- [6] Klein, S. A.: Calculation of Monthly Average Insolation on Tilted Surfaces, *Solar Energy*, vol. 19 (1977).
- [7] Hottel, H. C, B. B. Woertz: *Performance of Flat-Plate Solar Heat Collectors*.
- [8] Klein, S. A., J. C. Theilacker: An Algorithm for Calculating Monthly-Average Radiation on Inclined Surfaces, *Trans. ASME. Solar Energy Engr.*, vol. **29** (1981).
- [9] D. Yogi Goswami, F. Kreith, Ja F. Kreider: *Principles of solar engineering* (1999).
- [10] Holland P.G , Mayer I.: On Calculating the position of the Sun, *International Journal of Ambient Energy*, vol. **9** (1) (1988).
- [11] Schumacher. J.: INSEL 8 Tutorial Simulation of Renewable Energy Systems (2012).

GREENHOUSE PRODUCTION IN MACEDONIA – CHALLENGES AND OPPORTUNITIES

Gordana Popsimonova¹, Biljana Ristovska¹, Dame Dimitrovski², Goce Georgievski³

¹Institute of Agriculture, "SS. Cyril and Methodius" University in Skopje, Republic of Macedonia

²Faculty of Mechanical Engineering, "SS. Cyril and Methodius" University in Skopje,

P.O. Box 464, MK-1001 Skopje, Republic of Macedonia

³Agrostratus, MK-1000 Skopje, Republic of Macedonia

gpopSimonova@yahoo.com

Abstract: Greenhouse tomato makes the largest share of vegetable production in the World. The developments of biological sciences and high technology in the protected crops sector have enabled drastic increase in the yield and contributed to improvement of the fruit quality. Main indicators for the fruit quality still remain to be evaluated by appearance (shape, color, size) whereas the sensor traits (taste and aroma) are somehow neglected. Among the consumers there is general impression that tomatoes grown on substrates are artificial, plastic, tasteless products, compared to the "genuine" tomato raised on soil. On the other hand, Macedonian vegetables have a very good reputation in the region with their fresh recognizable taste and aroma. It will be a challenge in the future to preserve it. Limiting factors for profitable glasshouse production in the Republic of Macedonia are the extreme temperatures in winter and in summer time. For that reason, not only that the glasshouse capacities are underutilized, but the expensive tomato hybrids that are intended for at least 10 months cropping period cannot return the profit within the short cropping period of 3-4 months. The institutional and educational systems in Macedonia do not keep the pace with latest developments in the greenhouse industry. Some of the Macedonian operators have made large investments in greenhouse production to be able to follow the market demands. In the newly erected greenhouses in Macedonia on total area of 7 ha in two locations (Kocani and Gevgelija) tomato is grown on substrates and the production is completely atomized in regards to fertirrigation, environment control etc. This technology gives room for larger plants density and consequently, higher yields per unit of area. However, the substrate cultivation is not entirely adopted by the operators and they are completely dependent on the services provided by the supplier. It is of crucial importance to support them in this initial period of new production in identifying the bottlenecks and providing eventually intervention for optimal usage of the new technology.

Key words: vegetable production; greenhouse; energy

СТАКЛАРНИЧКО ПРОИЗВОДСТВО ВО МАКЕДОНИЈА – ПРЕДИЗВИЦИ И МОЖНОСТИ

Апстракт: Најголем дел од извозот на раноградинраски производи од стакларничко производство го сочинуваат доматиите. Развојот на биолошките науки и високата технологија која се применува во заштитените простори овозможуваат драстично зголемување на производството и подобрување на квалитетот. Главните индикатори за оцена на плодот и понатаму се негов изглед (форма, боја и големина), додека осетните критериуми (вкус и арома) се запоставени. Кај крајните корисници постои убедување дека доматиите кои растат со супстрати се вештачки, пластични, бесвкусни производи во споредба со „оригиналниот“ домат кој расте на земја. Од друга страна, македонските домати имаат извонредна репутација во регионот, ќе биде предизвик таа да се зачува. Ограничувања за профитабилно оранжериско производство се екстремните температури зиме и лете. Од оваа причина голем број од стакларниците во Македонија не се доволно искористени, а затоа скапите хибридни домати, кои се наменети за 10-месечна интензивна берба, не можат да создадат профит поради кратката берба од 3 до 4 месеци. Институционалниот и образовниот систем во Република Македонија не се во чекор со развојот на технологијата кај оранжериското производство. Некои од македонските инвеститори вложуваат огромни средства за да ги следат потребите на пазарот. Најновите стакларници работат со целосно автоматизирани процеси. Оваа технологија овозможува поголема густина на

растенија и поголема берба на истата површина. Сепак, технологијата не е целосно усвоена од операторите и тие сèуште се зависни од набавувачот. Клучно е операторите, во оваа рана фаза да бидат поддржани.

Клучни зборови: раноградинарско производство; стакларник; енергија

1. INTRODUCTION

The greenhouse sector in the Republic of Macedonia is one of the largest employment generators, both permanent as well as seasonal. Since the establishment of the first PE tunnels and later on with erection of the glasshouses, by the end of 70 s, the sector has undergone severe crises, but the production and the revenues have remained relatively stable. The challenge of the sector in general is in diversifying export market, which is possible only if the product responds better to export market requirements in terms of crop diversity, applied technologies, quality, grading and packaging.

Macedonian vegetables have a very good reputation in the region with their fresh recognizable taste and aroma. It will be a challenge in the future to preserve this reputation due to the lack of investment in modern technologies that will reduce the cost of production. Limiting factors for profitable glasshouse production in the Republic of Macedonia are the extreme temperatures in winter and in summer time. For that reason, not only that the glasshouse capacities are underutilized, but the expensive tomato hybrids that are intended for at least 10 months cropping period cannot return the profit within the short cropping period of 3 to 4 months. The seasonal production and avoidance of the extreme winter conditions due to the high costs for heating also evokes problems with a very low marketing price because the harvest is set to a specific period which overlaps with the harvest period in the plastic tunnels at the same time.

2. MATERIAL AND METHODS

The analysis was prepared in the period from January to April 2013. At this period the greenhouses are heated and in the means of gaining real-time data, there have been several meetings and field visits with the representatives of several greenhouse companies. The conducted surveys included the following greenhouses producing of vegetables in different types of protected areas:

- Kanet Agro, Negorci
- Badzo PT, Bogdanci

- Eko oaza Samandov, Štip
- Vegefresh, Kukliš
- IGN Magro, Čucher-Sandevo.

In addition, the study conclusions and recommendations have been discussed on one hand with group of individual agricultural households producing in plastic tunnel producers through focus group discussion and on the other hand with some of the members of the Association of glasshouse producers through the Economic Chamber of Macedonia.

The end results provide comparison analysis of the heating systems for greenhouses and glasshouses. In addition, it provides recommendations for the value chain participants for the most cost efficient systems and opportunities for energy savings through the implementation of environmentally friendly technology. The term “greenhouse” used in the study is referring to all protected areas (glasshouse and plastic tunnels) with installed heating systems which are considered within the scope of the study.

3. CURRENT SITUATION

Macedonia has approximately 260 ha of agricultural cultivable area under glasshouses, but the exploitation of these capacities ranges between 70–75%. Most of the greenhouse complexes are blocks of 6–24 ha units in extent. In addition the area of vegetables cultivated under plastic tunnels is not precisely known, however it is estimated to be between 4.000 and 6.000 ha used mainly for cultivation of tomatoes, cucumbers and peppers.

Analyzing the large producers, the heating system used is generally made of fuel supply system, fuel burner, heat exchanger, heat distribution system and a control unit. System used in Macedonia in large greenhouses are central systems, where the boilers is located in separate house outside the greenhouse and the heat (medium is warm water) is distributed to the greenhouses by a distribution system (steel pipes) (Fig. 1).

The hot water is delivered to the greenhouses by a main supply and return systems of pipes that are insulated from the surrounding to minimize heat loss. Secondary net of pipes is installed inside

the greenhouse, and is delivering heat to the crop by convection and radiation (Figs. 2 and 3).



Fig. 1. Distribution heating system used in a glasshouse in Macedonia



Fig. 2. Heating pipes. Material. Black steel. Purpose: The heating pipes are also used for movement of the harvesting carts



Fig. 3. High position of heating pipes

Warm water boilers are generally used in order to ensure continuous optimized thermostat regime. Heavy fuel and petrol are the main energy sources (Figs. 4, 5, 6), while geothermal water is being used in smaller level. The clear price advan-

tage against heavy oil heating should stimulate greenhouse operators to investigate the assumptions indicating existence of over 200 geothermal wells in Macedonia (Fig. 7).

The small producers use external boilers, typically on wood. The system is connected to main steel pipes and secondary plastic thermo pipes. Measurements of temperature and humidity are manual, and interventions in the systems are temporary.



Fig. 4. Heavy oil boiler. Installed in 1973; heating capacity: 6 ha; place of origin: The Netherlands



Fig. 5. Boiler chamber with chimneys



Fig. 6. Propane-butane tanks.
Usage: Installed but not in function

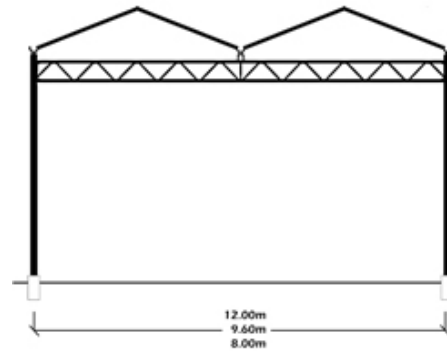


Fig. 7: Hot water reservoir.
Capacity: 50 t. temperature: 65°C

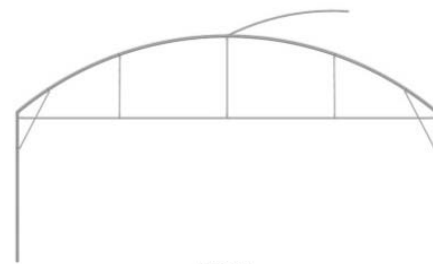
Construction

The first line of defense in efficient heating of a greenhouse is the structure itself. Losses vary depending on the greenhouse covering and the age of the structure. In general, newer structures will have better seals around the coverings and openings than older houses. The most commonly present types of greenhouses used in Macedonia is Venlo type including a heating system where the total investment consists solely of the purchase of the entire greenhouse with existing construction, heating system and glass cover. This requires investments in renewal of durable equipment, which is however limited to the minimum [1, 2, 3]. The glasshouses in Macedonia are generally multi-span, single wall and are mainly imported from dealers from Holland, Bulgaria or Israel. There have been build 250 ha multi-span glasshouses and only 20 ha single-span. The construction of Dutch 'Venlo' 3.20 m, mixed with Bulgarian type prevail. In plastic covered greenhouses the old domestic type construction are being followed by Israeli or Greek type.

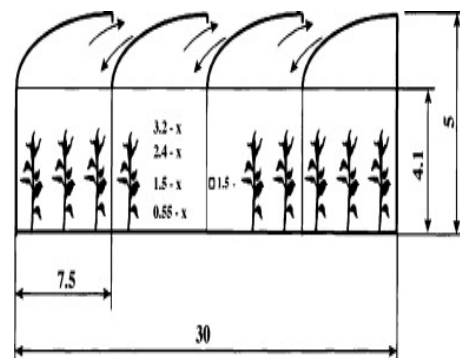
The tunnels are covered mainly with PE UV stabilized, with CO extruded 3 layer film and also PVC is used. The plastic materials have a thickness of 18–20 μ . PE is used mainly for mulching and also straw for cucumber growing. The plastic film for tunnels is used for three years. Aluminum and galvanized steel are used along with wood for plastic greenhouses, while for glasshouses galvanized steel and steel + aluminum are more used. Some of the producers use double layer of plastic covering but it is not sealed cover and it is only used not to allow the heat to go fast to the sealing of the greenhouse.



Dutch Venlo type



GEOM
Greek type



Israeli type

Production

In the 260 ha of agricultural cultivable area under glasshouses (blocks of 6–24 ha per unit) 70–75% of the capacities are used. Although the production of peppers is very favorable in the south-east part of Macedonia, the greenhouse producers are generally not interested in production of peppers for fresh market and are drastically reduced [4]. Yields per unit are quite variable depending on the year, producer, variety, cultivation technology, etc. It is noted that the vegetables produced with hydroponics have bigger yields than the production on soil. This production technology is mostly implemented for production of tomatoes. The difference between the yields of tomatoes produced on soil and with hydroponics is very high. The yields

of traditional production on soil vary from 150 t/ha to 200 t/ha, and with hydroponics the average yield varies from 450 to 600 t/ha depending of the variety [5, 6, 7]. Cucumbers have average yield of 220 t/ha. The average yield of peppers is 35–36 t/ha for some varieties that are meant for the processing industry. Although a number of other crops are cultivated under protected cover, such as early potatoes, watermelons under small tunnels and strawberries under plastic soil cover, the largest area is planted by tomato, cucumber and hot pepper. Most of the tomato varieties grown in green-

houses are: Belle, Balet, Magnus, Yena, Alandra, Bonito and Geronda. There are short cucumber varieties (Adrain, Pontia, Jazer), long type cucumbers (Navada, Kalunga, Palmera) as well as gherkins (Motiva, Componist, Parker, Levina) [8, 9]. The quantities of peppers grown in protected area are insignificant compared to the aforementioned crops. Predominant pepper varieties are: Fortesa and Struma (hot peppers) and Pinokio (sweet peppers). The production of Macedonian greenhouse sector is shown in Table 1.

Table 1.

Production and area under glasshouses in the period 2005–2010 [10]

Crop	2005		2006		2007		2008		2009		2010	
	ha	t	ha	t	ha	t	ha	t	ha	t	ha	t
Tomatoes	117.2	9554	120	12580	121	14960	140.6	14952	154.2	18275	147.0	18285
Cucumbers	45.5	7350	42.5	7100	50.4	8860	54.0	9812	55.8	7845	62.0	9700
Pepper	39.0	212	1.5	75	2.0	65	3.8	147	5.0	80	3.0	105
Cabbage	2.5	100			17.0	850	15.0	700	18.8	587	17.0	650

The start of cultivation depends on the possibility of heating the greenhouses. The few glasshouse operations that have the financial means to purchase sufficient crude oil and start nurseries (first tomato, later the more cold-sensitive cucumber) already in November, transplant the seedlings in December and harvest the crop in February and March when very high prices can be obtained. Most glasshouse operators, who cannot afford the heating expenses (up to 0,39 Euro/kg.), start later to save on fuel consumption but fetch lower prices for the crop.

Next, production in the plastic tunnels starts in February/March with harvest in May/June, depending on whether or not, the tunnels are heated. In case of heating this is done subsoil by passing hot water through plastic tubes that are laid below the ground [11]. Most foil tunnels, however, are not heated and thus come later into production. Then the open field season starts in April, often using seedlings grown in protected nurseries and continues until September. In the hot summer months, protected cultivation cannot compete with open field cultivation [12]. The protected cultivation starts again in September for a second crop (only tomato and cucumber – often gherkins) as practiced by an increasing number of growers, where heating is available.

Technology

Modern technologies offered by importing companies from Holland and Israel are used in glasshouses. Strong links with these companies supply glasshouses with appropriate seeds, fertilizers, predators for biological control, etc. Soil-less technology is applied only in some private glasshouses where rock wool, perlite and peat are used as substrate.

Heating is used in all glasshouses and also in some plastic covered greenhouses. Warm water boilers are generally used in order to ensure continuous optimized thermostat regime. Heavy fuel and petrol are the main energy sources, while geothermal water is being used in smaller level, in about 40 ha, mainly in glasshouses, in Kočani. Cooling is mainly static of mist and fog type and ventilation is achieved through ridge ventilation and also through combined type (with gable and side wall). Drip irrigation and fertigation are the most used, but furrow irrigation is applied too, even to some glasshouses. In glasshouses fertigation is generally used with dosing pump and also with diluters. The greenhouses are disinfected using steam (mainly in glasshouses) and other

chemicals treatments. Biological and integrated pest control has been applied successfully in some glasshouse blocks under the direction of Vegetable Crop Institute, as the unique control. Biological products have been as well produced, but this kind of production needs further stimulation, i.e. relative to controls, labeling and price mechanism.

Research, education and institutional framework

The institutional and educational systems in Macedonia do not keep the pace with latest developments in the greenhouse industry. In absence of the know-how the greenhouse operators are directed to search for consultancy, technology and equipment from foreign suppliers and providers. The research where respective vegetable departments of agriculture faculties are included must be supported to increase their activities relative to the technical level of farmers and also prepare and distribute projects dealing with the most suitable constructions for protected cultivation in different areas; the most suitable areas for future expansion of plastic covered greenhouses, supporting the objectives of the national strategy.

The competencies for the greenhouse sector in the Republic of Macedonia are located in several institutions including:

- Ministry of Economy
- Ministry of Agriculture, Forestry and Water Economy
- Ministry of Environment and Physical Planning
- Ministry of Transport and Communications
- Energy Regulatory Commission
- Local Self-Government

The key documents setting out the Government policies for Macedonia's development of agriculture and rural development include:

- (i) the Government's Pre-Accession Economic Programme;
- (ii) the National Agricultural and Rural Development Strategy for 2007-2013 with the National Plan (IPARD Programme) and in coherence with the national strategic objectives for EU Integration;
- (iii) the Industrial Policy for 2009–2020;
- (iv) the Strategy on Food Safety;
- (v) the Fourth Program for Stimulating Investments for 2011–2014;
- (vi) the Public Investment Program.

The Agency for financial support of agriculture and rural development is a part of the operating structure for implementing the funds from the fifth component of the Instrument for Pre-Accession assistance from the European Union (IPARD).

Current issues

The delayed privatization process has restrained glasshouse operators from making necessary expenses for maintenance and re-equipment. For many glasshouse operations, there is an acute lack of working capital to pay for heating, which means that these greenhouses have no competitive advantage over plastic tunnels production with regards to the time of harvesting. In the last 15 years and so there have been no significant investments in the glasshouse sector, which has lowered the output and substantially raised the cost of production. Only recently some modifications have been made in the sense of technology modernization and computerization.

Part of the greenhouse companies are organized in the Association of Greenhouse Producers that operates within the Economic Chamber of Macedonia. The other part of the companies operates with the Agro Business Chamber which is part of the Macedonian Chambers of Commerce. Even though these companies are one of the largest job generators in this sector, there is a serious lack of communication and understanding between the Associations and the government bodies; therefore there is no National Strategy for greenhouse production developed yet.

Due to the situation with infection with *Escherichia coli* in the consumption of fresh vegetables, there was a drastic reduction in sales of vegetables, especially exports, lower prices, and cancellation of purchases by foreign buyers. In this situation, a large part of the production of cucumbers and tomatoes produced in greenhouses is sold in the domestic instead on the foreign markets. Reduced sales and prices adversely affect the income of greenhouse producers. In addition of the problems with the foreign markets, the greenhouse companies suffer negative revenue impact and higher production costs due to the increased investment in seed and fertilizers which are with higher prices compared with previous years. Also, the price of the heavy oil drastically increased by 269% compared to the price in 2009.

In 2011, the Association of Greenhouse Producers within the Economic Chamber of Macedonia held a meeting in the Ministry of Agriculture on which were presented the current situation and problems of greenhouse production and sales, with suggestions and requests directed to a partial compensation of suffered damage and assistance with specific measures to increase direct payments for greenhouse production of 500,000 MKD/ha, compensation for the increased cost of heavy oil amounting to 50% of the value of spent heavy oil, enabling the use of favorable working capital loans (with interest rates no higher than 4%) and higher repayment period (5 years with 1 year grace period) by means of ACDF, Compensation Fund, earmarked loans for primary agricultural production and other sources, such as loans earmarked for repayment of loans to commercial banks, increasing the maximum loan of 100,000 € to 700,000 €, and additional compensation from funds collected from European funds for suffered damage for the vegetable producers as a result of disruption in the market due to the emergence of *Escherichia coli*.

The greenhouse constructions in the current legislation are defined as “temporary construction”, and this causes issues in the terms of tax obligations to the companies. The companies are complaining that they cannot gain full ownership of the land and construction due to this issue, and they demand that the land on which the greenhouses are built to be transformed into construction land. It is pointed out that in the latest version of the national Law on Agricultural Land, the fee amount for legalization of the objects is foreseen and too high (10 MKD/m²) and should be revised. Other anomalies regarding greenhouse production are located in several legislatives that are directly or indirectly regulating the greenhouse production. These laws mostly refer to the regulation of heating sources, irrigation and energy use. The greenhouse companies pointed out several articles in the Law on waters that should be revised and modified according to their suggestions in order to comply with more efficiency in their functioning.

More than 40 ha of greenhouses in Macedonia are heated with geothermal water. The geothermal energy source is currently the most cost-effective energy source for heating compared with the use of heavy oil or natural gas because of the price. But, as of 17 January 2012, by the decision of the Government of Republic of Macedonia, the price of geothermal water is increased by 588% from the initial price per m³ of geothermal water.

At the same time, the greenhouse companies that are interested to invest in new geothermal wells are pointing out that the activities for new welling are very expensive (circa 700.000 € per well) and there is no guarantee that the wells will result with the water temperature that is needed for use of heating, nor that the water flow per second will be sufficient to be used in geothermal pumps. That additionally increases the risk and is drawing attention even more to the fact that there have not been any geological researches performed in this field for their assurance of the investments. Thus, the investments can grow up to few million Euros for innovative geothermal technology that can be consistent for the needs of the producer.

4. CONCLUSIONS

The greenhouse sector in the Republic of Macedonia is one of the largest employment generators, both permanent as well as seasonal. As the price of energy is permanently increasing, heating costs negatively influence the productivity and overall competitiveness of fresh vegetable producers and it is necessary to introduce “alternative” energy in the agriculture. Increased fuel costs and winters colder than normal make heating costs a significant burden on many greenhouse operations. For many glasshouse operations, there is an acute lack of working capital to pay for heating, which means that these greenhouses have no advantage over tunnels with regard to the time of harvesting.

The greenhouse constructions in the current legislation are defined as “temporary construction”, and this causes issues in the terms of tax obligations to the companies. The general conclusion is that the government should make efforts to support the greenhouse sector by several measures that can increase the regional competitiveness. The measures should be by means of direct support and intervention in the current legislative, competent for the greenhouse sector. The main problem of vegetable production from protected cultivation is their marketing. Macedonia lacks big auction centers, which decreases the real value of production.

Macedonia is well-positioned to be the low-cost greenhouse producer for the European market thanks to:

- good winter sunlight in comparison to most of Europe;
- low cost land and geothermal water;
- low cost labor;

- rapid refrigerated truck transport to major European markets in 30 to 60 hours;
- low electricity costs;
- direct subsidies for new greenhouse construction and for introduction of new technologies as e.g. soil-less cultivation, drip irrigation and fertigation, etc.

Relative to present situation of protected cultivation and their development in the future in Macedonia the main constraints met by greenhouse vegetable production sector are as follows:

- relatively low average yield because of prevailing of low tunnels;
- lack of coordination in production, which influences in price;
- there is no tax alleviation for inputs that will be used in greenhouses or for greenhouse construction;
- market competition coming from countries out of the area that possess high level of marketing preparation of product;
- the lack of needed marketing information;
- in conditions of fragmented small farms the associations of vegetable growers are yet not very strong to defend and help the produce

There is not a particular national strategy for vegetable development including greenhouse crop production and vegetable marketing, which is economically and socially very important for the country. In order to maintain and further extend the export markets towards Western Europe some measures would be needed to be applied to pass

from extensive to a more intense phase of protected cultivation, i.e. improving the technology for greenhouse production diversification in time, species and cultivars.

REFERENCES

- [1] C. J. Molyneux: *A Practical Guide on NFT*, Nutriculture Ltd, 153 pages.
- [2] Maynard, Donald N., Hochmuth, George J.: *Knott's Handbook for Vegetable Growers*, Wiley Interscience Publications, New York, p. 640 (1988).
- [3] Dennis R.: *Decoteau Vegetable Crops*, Prentice Hall, p. 464 (1999).
- [4] EPI CENTAR: *Profile of the Macedonian Fresh Vegetable Value Chain*, study developed for the USAID AgBiz Programme in Macedonia (2008).
- [5] Joe J. Hanan: *Greenhouses: Advanced Technology for Protected Horticulture*, CRC; p. 720 (1997).
- [6] John Mason: *Commercial Hydroponics*, Simon & Schuster Australia, p. 172 (2000).
- [7] Ian G. Walls, *The complete Book of Greenhouse*, Ward Lock, p. 305 (1993).
- [8] Macedonian Consulting Group: *Floriculture and Horticulture Sectors in the Republic of Macedonia*, Prepared for the Embassy of the Kingdom of the Netherlands, Skopje, Macedonia, Final Report (2008).
- [9] MAFWE: *National Agricultural and Rural Development Strategy (Nards) for the Period 2007–2013*, Skopje, June 2007.
- [10] MAFWE: *Information on Vegetable Production*, Department of Field Crops, May 2011.
- [11] Paul V. Nelson: *Greenhouse Operation and Management*, Prentice Hall, p. 704 (2002).
- [12] Pierce Lincoln C., *Vegetables: characteristics, production and marketing*, John Wiley and Sons, p. 429 (1987).

FRANCHISING AS A FORM FOR STARTING A SMALL BUSINESS – PRESENCE AND OPPORTUNITIES FOR DEVELOPMENT IN REPUBLIC OF MACEDONIA

Vase Jordanoska, Radmil Polenaković

Faculty of Mechanical Engineering, "SS. Cyril and Methodius" University in Skopje,
Karpoš II b.b., P.O. Box 464, 1000 Skopje, Republic of Macedonia
radmil.polenakovikj@mf.edu.mk

Abstract: The aim of this study was to introduce better franchised businesses, to evaluate the opportunities for the Macedonian entrepreneurs to start such businesses and to analyze what are the conditions of the Macedonian market for franchised businesses. For this purpose survey was conducted, and also interviews with 21 enterprises took place. The results showed that the owners of franchises are generally entrepreneurs who already had some kind of business experience and also in most of the cases one businessman has more than one franchised business. Hence, the Macedonian market needs regulation and introduction of standards in certain segments of franchising. As for the financial aspects there should be special loan or credit programs for franchise and there should be more domestic specialized consultants that will support entrepreneurs in the process of acquiring new franchises

Key words: franchise; franchisor; franchisee; franchise fees; franchise opportunities

ФРАНШИЗАТА КАКО ОБЛИК ЗА ЗАПОЧНУВАЊЕ МАЛ БИЗНИС – ЗАСТАПЕНОСТ И МОЖНОСТИ ЗА РАЗВОЈ ВО РЕПУБЛИКА МАКЕДОНИЈА

Апстракт: Целта на оваа студија беше да се запознае подобро бизнисот со франшиза, да се оценат можностите за македонските претприемачи да започнат таков бизнис и да се анализира какви се условите на пазарот во Македонија за бизниси со франшиза. За оваа намена беше спроведено истражување во кои учествуваа 21 претпријатие. Резултатите покажуваат дека сопствениците на франшизи се главно претприемачи кои веќе имале некој вид бизнис и, исто така, во повеќето случаи еден претприемач е корисник на повеќе од една франшиза. Анализите покажаа дека на македонскиот пазар потребно е регулирање и воведување стандарди во одредени сегменти за структурирање на франшизингот. Особено значајно е дека од финансиски аспект треба да се има посебни заеми или кредитни програми за франшиза, а и да се зголеми бројот на специјализираните консултанти кои ќе посредуваат во добивањето и работењето на франшизата.

Клучни зборови: франшиза; франшизор; франшизант; франшизни надоместоци; можности за франшиза

1, INTRODUCTION

Franchising is practice of using successful business model from another enterprise. For the franchisor, the franchise is an alternative way of building chain of sale points for distributing goods and at the same time to avoid investing and total responsibility of the sale chain. Franchisor success is actually franchisees success. Generally, the franchise has specified duration, divided into shorter periods that request renewal and it serves defined

territory or region around its location. According to International Franchise Association [1], a franchise is the agreement or license between two legally independent parties which gives:

- a person or group of people (franchisee) the right to market a product or service using the trademark or trade name of another business (franchisor);
- the franchisee the right to market a product or service using the operating methods of the franchisor;

- the franchisee the obligation to pay the franchisor fees for these rights;
- the franchisor the obligation to provide rights and support to franchisees.

Both franchise parties, franchisor and franchisee, have several interests to protect. The franchisor is mostly involved in providing protection of its trademark, controlling the business concept and securing its know-how. Hence, the franchisee is requested to perform the work due to which the trademark became widely known or eminent. In franchises there is great deal of proposed standardization. The service place or the store should carry the franchisor sign, logo and trademark on prominent location. The franchisee personnel uniforms should be with determined shade and colour. The service should be in accordance with the model followed by the franchisor in its successful operation. Thus, the franchisor has no complete control over the franchisees business, as it would be in retailing [2].

Mainly three factors do business suitable for franchising [6]:

- business is based on a proven system for serving the end users,
- system could be reduced to sum of operational rules that could be transferred to others in written form,
- there are enough potential concept buyers to make it worth the investment costs, for establishment of franchised system.

Figure 1 shows the franchise distribution by industries, for the period 2001–2005 [3]. Although we do not have figure for nowadays it is not much changed, fast food franchises continue to dominate with 19%, followed by retailing with 11% and service businesses with the same 11%.

Examples of using franchise existed since the middleages, in Europe in the 20th century in taverns in Germany, but it is considered that the franchising actually started in USA [4]. In 1851 Isaac Singer became the first American franchisor with a product name, when he began to sell rights to independent travel retailers to sell its machines to end users. Although the company Singer for sewing machines was the earliest American name of franchised product, very quickly it was exceeded by a more important franchised name: Coca Cola. At the beginning of 1890s Coca Cola chose to give franchise rights for bottling its drink to many independent businessmen, who got exclusive territory for drink distribution. In return, they paid and undertook the risk of product distribution. Franchis-

ing as a business form really took off in the 1950s and 1960s, when many of the current big franchise chains were established, names such: Taster-Freez[®], KFC[®], McDonald's and Burger King[®].

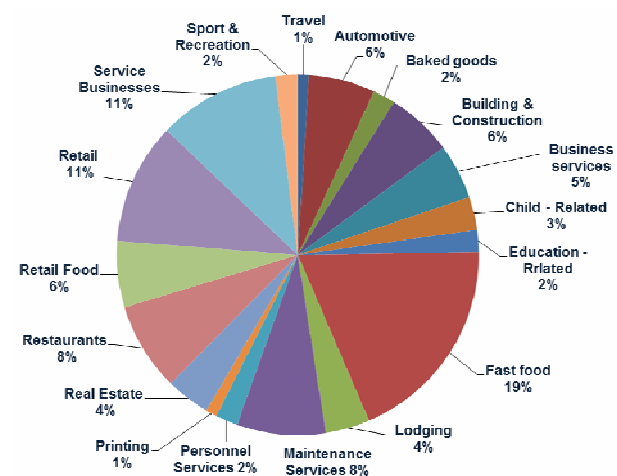


Fig. 1. Franchise businesses by sectors
Source: Half Hollow Hills Community Library, Quarterly Newsletter – Winter 2008, Focus on Franchising

It is estimated that more than 800 companies are international franchises and additional 100 are starting its own expansion internationally every year. This is a real chance to seek opportunities among the worldwide well known franchisors [9].

ON-SITE RESEARCH

Around 90% of Macedonian companies are registered as small enterprises, in which work around 55% from the employees in private sector. According to the main business activity registered, the majority of businesses are in the commercial sector of wholesale and retail (47%), production sector (13.1%) and transport, storage and communications sector (approximately 10%) [5].

Statistics says enough about the importance of small businesses for the economy of Republic of Macedonia. The commercial sector of wholesale and retail (47%) is the share where franchised businesses belong [8].

To evaluate the overall state of franchise businesses in Macedonia, research was conducted through a survey of a number of companies that are using franchise or work as sales representatives. The goal was to discover the purpose of starting business with franchise, from which sectors are the most Macedonian franchise units, the financial and legal condition they had to face, im-

plementation process, relations with franchisors and attractiveness and prospects of starting business by buying franchise. In survey 21 enterprises (Setimiano – 7 CAMICIE, AvtoKuća – Opel, Chevrolet and Dunlop, Makedonijaturist – HOLIDAY INN Hotels & Resorts and BEST WESTERN Hotels, Eurostandardbanka – MASTER CARD EUROPE, FuksMak – FUCHS PETROLUB AG and others) took place with their brands (in most cases one enterprise works with more than one brand). Managers from surveyed enterprises were interviewed, in which they gave detailed answers from their viewpoints about the franchise opportunities and market environment in Macedonia.

During the creation of survey the well-known pros and cons of buying franchise were taken into account [2]. The common advantages of buying a franchise are:

- proven blueprint,
- established trademark,
- possible cost saving,
- industry experience might not be necessary,
- monitoring and peer support.

As general disadvantages can be stated:

- set-up costs,
- franchise fees,
- operational constraints, and
- structural weaknesses.

Also, the survey is related to the Macedonian buyers of franchises, because as the market research showed there are not known Macedonian products or services that are sold as franchise in or out of the country borders.

RESULTS

By the number of employees, small enterprises are those with a number of employees from 6 to 50, where belong most of the Macedonian businesses with franchise, as given on Figure 2.

As for the presence, 54.5% of franchises have only one operational unit in the country, mostly due to the small market, where one unit is sufficient to serve the territory, but this is also dependent by the type of business.

Analysis of the franchise ownership in terms of gender shows that owners to these businesses in Macedonia are generally men. 51.5% of the owners are in the age group 25 to 40 years, 35% in the age group of 41 to 55 years and the rest are over 55 years old. The ownership by gender is given on Figure 3.

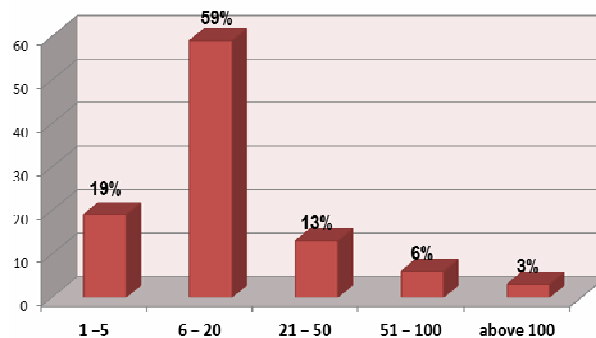


Fig. 2. Number of employees in franchise businesses

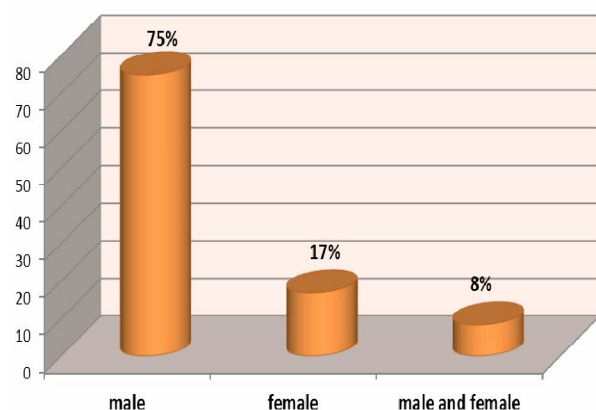


Fig. 3. Franchise ownership by gender in Macedonia

The reasons for starting a franchise business are given in Figure 4.

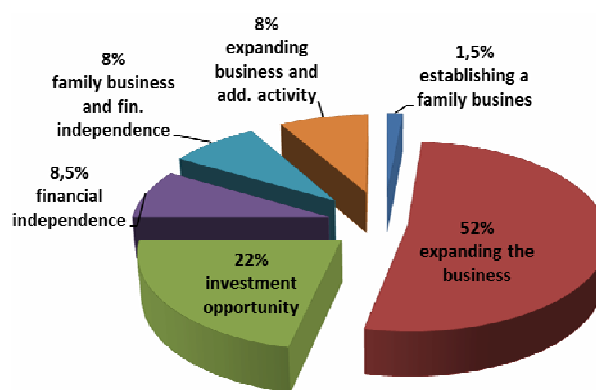


Fig. 4. Reasons for starting-up a franchise business

50% of the franchisees consider the franchise fees as high and another 40% consider them as reasonable.

The majority of the franchisees have done it by themselves the market / competition analysis in the region they work in; the percentages are shown in Figure 5.

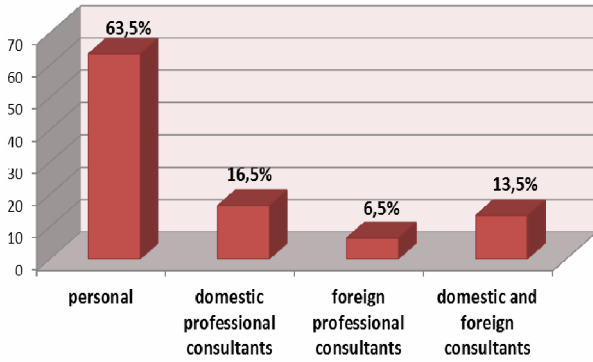


Fig. 5. Market / competition analysis

Financial sources that were used by Macedonian franchisees are given in Figure 6.

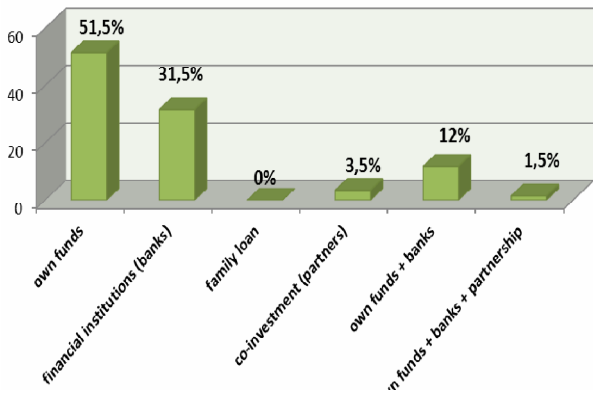


Fig. 6. Financial sources when starting-up the business

Figure 7 gives the franchisee content from the communication with its franchisor.

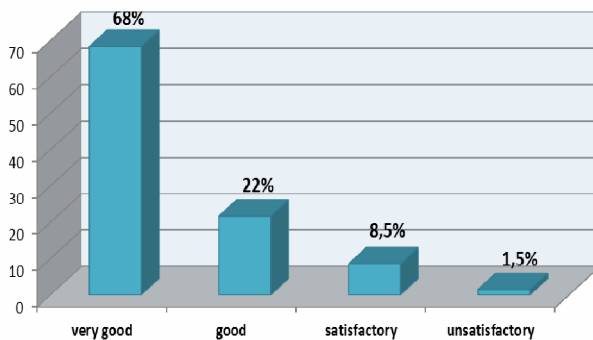


Fig. 7. Franchisee communication content

Difficulties franchisees encountered in establishing the business in Macedonia are given on Figure 8.

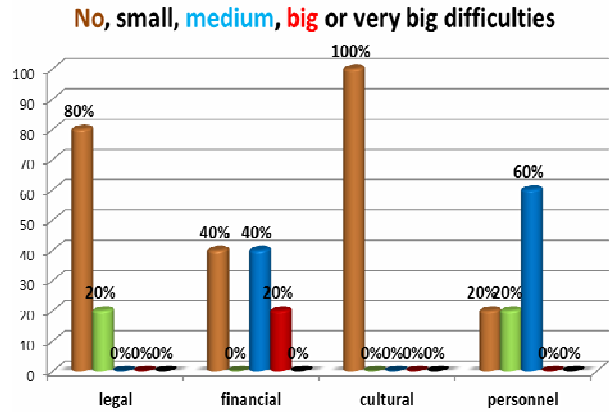


Fig. 8. Legal / financial / cultural / personnel difficulties

In terms of the opportunity to develop their business 62% responded positively, and the remaining 38% negative, but neither of them did not think to leave franchise work.

As for the views about attractiveness and prospects of franchises, they are more than positive, current users believe that franchising is an attractive business model that has excellent prospects in the next decade.

The personal views of the respondents about the main advantages and disadvantages are saying that they generally see the advantage in working with worldwide famous brand, working practice that somewhere already succeeded. Macedonian franchisees found personal satisfaction and clear financial performance and records in this work.

Most complain was focused to high stakes, high costs and standards, and a small profit. Due to the unpredictable economic situation in Macedonia it appears powerless to calculate the actual loss.

RECOMMENDATIONS AND CONCLUSIONS

The recommendation of the Macedonian franchisees is to identify the right brand that would succeed in Macedonian market, and to be patient because the effects of working with franchise are not coming right away. It takes time, investment capital, private education and most importantly, investing in staff [7].

Nevertheless, it is advantage to work with well-known trademarks regardless of whether it is a product or service. Choosing to start a business with a franchise reduces the risk of failure, because everything that should be known for the business is given by the franchisor. Therefore business format

franchising is the most widespread. In business format franchise, the franchisor gives the franchisee licenses of his/her business format, operating system and trademark. So, the business format franchise does not use just the product, service and trademark of the franchisor, but also the complete method for conducting the business, such as marketing plans and operating instructions. That is why specific prior knowledge of the field it is not necessary to start a franchise business. However, should not be forgotten that the initial costs of starting a franchise business are very higher than in other small businesses. So, the new franchisees should make a good calculation and have backup plan due to the unpredictable market in Macedonia.

As summary [4] can be stated that franchises nowadays are more often used as business models in Macedonia, the younger population often recognizes the franchise as good way for starting up a business. One of the biggest problems is finding adequate personnel and there are some market non-regulated segments, and also Macedonian market is considered a market with a very unstable and unpredictable economic situation.

Recommendation and areas in which there are opportunities for further research:

- increasing the number of professional consultants and organizations that work on market research,
- banks to create special, more favorable loan program for future franchisees,
- franchising legislative introduction in Republic of Macedonia,

- regulation of certain market segments and introduce standards,
- creation of Macedonian franchise products or services.

REFERENCES

- [1] IFA. *What is a Franchise?*. Вчитано на 27 декември 2011 од http://www.franchise.org/franchisees_econdary.aspx?id=52625.
- [2] Illetschko, Kurt: *Franchising*. London: Hodder Education (2006).
- [3] „Focus on Franchising“, Quarterly Newsletter, Winter 2008, Half Hollow Hills Community Library.
- [4] Јорданоска, Васе: *Франшизајта и ирејисјавнишијвојто како облик за зайочнување мал бизнис, иредносјти и недосјтајтоци на исјитије и нивнајта засјтајеносјт во Република Македонија*, магистерски труд. Машински факултет – Скопје (2011).
- [5] <http://www.investinmacedonia.com/Default.aspx?item=menu&themeid=296&itemid=719>
- [6] Бошковска, Вера: *Франшизајта – начин на зайочнување со мал бизнис*. Магистерски труд. Економски факултет – Скопје (2009).
- [7] Поленаковиќ, Радмил (прир.): *Како до сојсјвен бизнис*. Скопје: Центар за развој на нови бизниси при УКИМ (2007).
- [8] Тасевски, А.: *Франшизајта како ајтракјивен начин за йочнување бизнис* (2010, ноември 8). Вчитано 27 декември 2011 од <http://money.mnogoo.mk/mk/articles/Biznis/fransizata-kako-atraktiven-nacin-za-zapocnuvanje-biznis>
- [9] IFA. *About Franchising – Help with Buying a Franchise*. Вчитано 27 декември 2011 од <http://www.franchise.org/aboutfranchising.aspx>

A REVIEW OF SOME RECENT RESULTS ABOUT LAPLACE TRANSFORM AND CONVOLUTION OF ULTRADISTRIBUTIONS

Bojan Prangoski

Faculty of Mechanical Engineering, "SS. Cyril and Methodius" University in Skopje,
Karpoš II b.b., P.O. Box 464, 1000 Skopje, Republic of Macedonia
bojan.prangoski@mf.edu.mk

Abstract: We give some recent results in the theory of Laplace transform and convolution in ultradistribution spaces.

Key words: ultradistributions; Laplace transform; convolution

ПРЕГЛЕД НА НЕКОИ НЕОДАМНЕШНИ РЕЗУЛТАТИ ЗА ЛАПЛАСОВАТА ТРАНСФОРМАЦИЈА И КОНВОЛУЦИЈА НА УЛТРАДИСТРИБУЦИИ

Апстракт: Дадени се неколку неодамнешни резултати од теоријата на Лапласовата трансформација и конволуција во просторите на ултрадистрибуции.

Клучни зборови: ултрадистрибуции; Лапласова трансформација; конволуција

1. INTRODUCTION

This article is a review of some recent developments in the theory of Laplace transform and convolution of ultradistributions. All the results that we give here are already stated and proven in recent papers. They are stated here without proof and always there is an explicit reference to the paper where they appear.

The Laplace transform is a widely used tool in mathematical analysis. Its close relationship with a number of other transforms, like the Mellin, Borel and Z-transform, makes it very interesting from theoretical point of view. Also, it finds its own use for solving of differential and integral equations. Besides its theoretical importance, the Laplace transform is widely used in physics for analysis of linear time-invariant systems (like harmonic oscillators).

To motivate the study of convolution one doesn't need to look further than the simplest ex-

amples. For if $P(D) = \sum_{|\alpha| \leq n} c_\alpha D^\alpha$ is an ordinary partial differential operator then $P(D)u$ can be rewritten as $P(\delta) * u$, where $P(\delta)$ is the (ultra)distribution $\sum_{|\alpha| \leq n} c_\alpha D^\alpha \delta$. In ultradistributional setting one can consider infinite such sums with appropriate conditions on the coefficients c_α .

2. PRELIMINARIES

The sets of natural, integer, positive integer, real and complex numbers are denoted by N , Z , Z_+ , R , C . We use the symbols for $x \in R^d$:

$$\langle x \rangle = \left(1 + |x|^2\right)^{1/2}, \quad D^\alpha = D^{\alpha_1} \cdots D^{\alpha_d},$$

$$D^{\alpha_j}_j = i^{-1} \partial^{\alpha_j} / \partial x_j, \quad \alpha = (\alpha_1, \dots, \alpha_d) \in N^d.$$

If $z \in C^d$, by z^2 we will denote $z_1^2 + \dots + z_d^2$. Note that, if $x \in R^d$, $x^2 = |x|^2$.

Following [8], we denote by M_p a sequence of positive numbers such that $M_0 = 1$ and:

$$M_p^2 \leq M_{p-1}M_{p+1} \tag{M.1}$$

for $p \in Z_+$;

$$M_p \leq c_0 H^p \min_{0 \leq q \leq p} \{M_{p-q}M_q\}, \tag{M.2}$$

$p, q \in N$, for some $c_0, H \geq 1$;

$$\sum_{p=q+1}^{\infty} \frac{M_{p-1}}{M_p} \leq c_0 q \frac{M_q}{M_{q+1}}, \quad q \in Z_+, \tag{M.3}$$

although in some assertions we could assume the weaker one (M.3)' (see [8]). Note that the Gevrey sequence $M_p = p!^s$, $s > 1$, satisfies all of this conditions.

For a multi-index $\alpha \in N^d$, $M_\alpha = M_{|\alpha|}$,

$$|\alpha| = \alpha_1 + \dots + \alpha_d.$$

Recall, $m_p = M_p / M_{p-1}$, $p \in Z_+$ and the associated function for the sequence M_p is defined by

$$M(\rho) = \sup_{p \in N} \log_+ \frac{\rho^p}{M_p}, \quad \rho > 0.$$

It is non-negative, continuous, monotonically increasing function, which vanishes for sufficiently small $\rho > 0$ and increases more rapidly than $\ln \rho^p$ when ρ tends to infinity, for any $p \in N$.

Let $U \subseteq R^d$ be an open set and $K \subset\subset U$ (we will use always this notation for a compact subset of an open set). Then $E^{\{M_p\},h}(K)$ is the space of all

$\varphi \in C^\infty(R^d)$ which satisfy $\sup_{\alpha \in N^d} \sup_{x \in K} \frac{|D^\alpha \varphi(x)|}{h^{|\alpha|} M_\alpha} < \infty$

and $D_K^{\{M_p\},h}$ is the space of all $\varphi \in C^\infty(R^d)$ with

supports in K , which satisfy $\sup_{\alpha \in N^d} \sup_{x \in K} \frac{|D^\alpha \varphi(x)|}{h^{|\alpha|} M_\alpha} < \infty$.

As in [8], we define:

$$E^{\{M_p\}}(U) = \lim_{K \subset\subset U} \text{proj} \lim_{h \rightarrow 0} \text{proj} E^{\{M_p\},h}(K),$$

$$E_K^{\{M_p\}}(U) = \lim_{K \subset\subset U} \text{proj} \lim_{h \rightarrow \infty} \text{ind} E^{\{M_p\},h}(K),$$

$$D^{\{M_p\}}(U) = \lim_{K \subset\subset U} \text{ind} \lim_{h \rightarrow \infty} \text{proj} D_K^{\{M_p\},h},$$

$$D_K^{\{M_p\}}(U) = \lim_{K \subset\subset U} \text{ind} \lim_{h \rightarrow \infty} \text{ind} D_K^{\{M_p\},h}.$$

The spaces of ultradistributions and ultradistributions with compact support of Beurling and Roumieu type are defined as the strong duals of $D^{\{M_p\}}(U)$ and $E^{\{M_p\}}(U)$, resp. $D_K^{\{M_p\}}(U)$ and $E_K^{\{M_p\}}(U)$. For the properties of these spaces, we refer to [8], [9] and [10]. In the future we will not emphasise the set U when $U = R^d$. Also, the common notation for the symbols (M_p) and $\{M_p\}$ will be $*$.

For $f \in L^1$, its Fourier transform is defined by $\int_{R^d} e^{-ix\xi} f(x) dx, \xi \in R^d$.

By \mathfrak{R} is denoted a set of positive sequences which monotonically increases to infinity. For $(r_p) \in \mathfrak{R}$, consider the sequence $N_0 = 1$,

$$N_p = \prod_{j=1}^p r_j, \quad p \in Z_+.$$

One easily sees that this sequence satisfies (M.1) and (M.3)' and its associated function will be denoted by $N_{r_p}(\rho)$, i.e.

$$N_{r_p}(\rho) = \sup_{p \in N} \log_+ \frac{\rho^p}{M_p \prod_{j=1}^p r_j}, \quad \rho > 0.$$

Note, for given (r_p) and every $k > 0$ there is $\rho_0 > 0$ such that $N_{r_p}(\rho) \leq M(k\rho)$, for $\rho > \rho_0$. In [21] the following lemma is proven.

Lemma 2.1. [21] Let $(k_p) \in \mathfrak{R}$. There exists $(k'_p) \in \mathfrak{R}$ such that $k'_p \leq k_p$ and

$$\prod_{j=1}^{p+q} k'_j \leq 2^{p+q} \prod_{j=1}^p k'_j \prod_{j=1}^q k'_j, \quad \text{for all } p, q \in Z_+.$$

Hence, for every $(k_p) \in \mathfrak{R}$, we can find $(k'_p) \in \mathfrak{R}$, as in lemma 1.1, such that $N_{k_p}(\rho) \leq N_{k'_p}(\rho)$,

$\rho > 0$ and the sequence $N_0 = 1, N_p = \prod_{j=1}^p k'_j, p \in Z_+$, satisfies (M.2) if M_p does.

From now on, we always assume that M_p satisfies (M.1), (M.2) and (M.3). It is said that $P(\xi) = \sum_{\alpha \in \mathbb{N}^d} c_\alpha \xi^\alpha$, $\xi \in \mathbb{R}^d$, is an ultrapolynomial of the class (M_p) , resp. $\{M_p\}$, whenever the coefficients c_α satisfy the estimate $|c_\alpha| \leq CL^{|\alpha|} / M_\alpha$, $\alpha \in \mathbb{N}^d$ for some $L > 0$ and $C > 0$, resp. for every $L > 0$ and some $C_L > 0$. The corresponding operator $P(D) = \sum_{\alpha \in \mathbb{N}^d} c_\alpha D^\alpha$ is an ultradifferential operator of the class (M_p) , resp. $\{M_p\}$ and they act continuously on $E^{(M_p)}(U)$ $D^{(M_p)}(U)$, resp. $E^{\{M_p\}}(U)$ and $D^{\{M_p\}}(U)$ and the corresponding spaces of ultradistributions.

We denote by $S_2^{M_p, m}(\mathbb{R}^d)$, $m > 0$, the space of all smooth functions φ which satisfy

$$\sigma_{m,2}(\varphi) = \left(\sum_{\alpha, \beta \in \mathbb{N}^d} \int_{\mathbb{R}^d} \left| \frac{m^{|\alpha|+|\beta|} \langle x \rangle^{|\alpha|} D^\beta \varphi(x)}{M_\alpha M_\beta} \right|^2 dx \right)^{1/2} < \infty$$

supplied with the topology induced by the norm $\sigma_{m,2}$. The spaces $S^{(M_p)}$ and $S^{\{M_p\}}$ of tempered ultradistributions of Beurling and Roumieu type respectively, are defined as the strong duals of the spaces

$$S^{(M_p)} = \lim_{m \rightarrow \infty} \text{proj } S_2^{M_p, m}(\mathbb{R}^d)$$

and

$$S^{\{M_p\}} = \lim_{m \rightarrow 0} \text{ind } S_2^{M_p, m}(\mathbb{R}^d),$$

respectively. In [2] (see also [17]) it is proved that the sequence of norms $\sigma_{m,2}$, $m > 0$, is equivalent with the sequences of norms $\|\cdot\|_m$, $m > 0$, where

$$\|\varphi\|_m = \sup_{\alpha \in \mathbb{N}^d} \frac{m^{|\alpha|} \|D^\alpha \varphi(\cdot) e^{M(m|\cdot|)}\|_{L^\infty}}{M_\alpha}.$$

If we denote by $S_\infty^{M_p, m}(\mathbb{R}^d)$ the space of all infinitely differentiable functions on \mathbb{R}^d for which the norm $\|\cdot\|_m$ is finite (obviously it is a Banach space), then

$$S^{(M_p)} = \lim_{m \rightarrow \infty} \text{proj } S_\infty^{M_p, m}(\mathbb{R}^d)$$

and

$$S^{\{M_p\}} = \lim_{m \rightarrow 0} \text{ind } S_\infty^{M_p, m}(\mathbb{R}^d).$$

Also, for $m_2 > m_1$, the inclusion

$$S_\infty^{M_p, m_2}(\mathbb{R}^d) \rightarrow S_\infty^{M_p, m_1}(\mathbb{R}^d)$$

is a compact mapping. So, S^* is a (FS)-space in (M_p) case, resp. a (DFS)-space in the $\{M_p\}$ case. Moreover, they are nuclear spaces. In [2] (see also [19]) it is proved that

$$S^{\{M_p\}} = \lim_{(r_j), (s_j)} \text{proj } S_{(r_p), (s_q)}^{M_p},$$

where

$$S_{(r_p), (s_q)}^{M_p} = \left\{ \varphi \in C^\infty(\mathbb{R}^d) \mid \|\varphi\|_{(r_p), (s_q)} < \infty \right\}$$

and

$$\|\varphi\|_{(r_p), (s_q)} = \sup_{\alpha \in \mathbb{N}^d} \frac{\|D^\alpha \varphi(x) e^{N_{s_p}(|x|)}\|_{L^\infty}}{M_\alpha \prod_{p=1}^{|\alpha|} r_p}.$$

Also, the Fourier transform is a topological automorphism of S^* and of S^{*^*} .

As in [19], we define $D_{L^\infty}^*(\mathbb{R}^d)$ by

$$D_{L^\infty}^{(M_p)}(\mathbb{R}^d) = \lim_{h \rightarrow \infty} \text{proj } D_{L^\infty, h}^{M_p}(\mathbb{R}^d), \text{ resp.}$$

$$D_{L^\infty}^{\{M_p\}}(\mathbb{R}^d) = \lim_{h \rightarrow 0} \text{ind } D_{L^\infty, h}^{M_p}(\mathbb{R}^d),$$

where $D_{L^\infty, h}^{M_p}(\mathbb{R}^d)$ is the (B)-space of all $\varphi \in C^\infty(\mathbb{R}^d)$ for which the norm $\sup_{\alpha \in \mathbb{N}^d} \frac{h^{|\alpha|} \|D^\alpha \varphi\|_{L^\infty}}{M_\alpha}$

is finite. $D_{L^\infty}^{(M_p)}$ is a (F)-space. Also, define $\tilde{D}_{L^\infty}^{\{M_p\}}(\mathbb{R}^d)$ as the space of all $C^\infty(\mathbb{R}^d)$ functions such that, for every $(t_j) \in \mathfrak{R}$, the norm

$$\|\varphi\|_{(t_j)} = \sup_{\alpha \in \mathbb{N}^d} \frac{\|D^\alpha \varphi(x)\|_{L^\infty}}{T_\alpha M_\alpha}$$

is finite, where we denote $\prod_{j=1}^{|\alpha|} t_j$ by T_α . The space $\tilde{D}_{L^\infty}^{\{M_p\}}(\mathbb{R}^d)$ is complete

i.e.s. because $\tilde{D}_{L^\infty}^{\{M_p\}}(\mathbb{R}^d) = \lim_{(t_j)} \text{proj } \tilde{D}_{L^\infty, (t_j)}^{M_p}(\mathbb{R}^d)$,

where $\tilde{D}_{L^\infty, (t_j)}^{M_p}(\mathbb{R}^d)$ is the (B)-space of all $\varphi \in C^\infty(\mathbb{R}^d)$ for which the norm $\|\varphi\|_{(t_j)}$ is finite. In

[19] it is proved that $D_{L^\infty}^{\{M_p\}}(R^d) = \tilde{D}_{L^\infty}^{\{M_p\}}(R^d)$ as sets and the former has a stronger topology than the latter. Denote by $\dot{B}^{\{M_p\}}$, resp. $\tilde{B}^{\{M_p\}}$ the completion of $D^{(M_p)}$, resp. $D^{\{M_p\}}$, in $D_{L^\infty}^{(M_p)}$ resp. $\tilde{D}_{L^\infty}^{\{M_p\}}$. Then, $\dot{B}^{\{M_p\}}$ is a (F) -space. Also $S^{(M_p)}$, resp. $S^{\{M_p\}}$, is continuously injected into $\dot{B}^{\{M_p\}}$, resp. $\tilde{B}^{\{M_p\}}$. The strong dual of $\dot{B}^{\{M_p\}}$, resp. $\tilde{B}^{\{M_p\}}$, will be denoted by $D_{L^1}^{(M_p)}$, resp. $\tilde{D}_{L^1}^{\{M_p\}}$. They are continuously injected into $S^{(M_p)}$, resp. $S^{\{M_p\}}$, and hence into $D^{(M_p)}$, resp. $D^{\{M_p\}}$. Ultradifferential operators of class (M_p) , resp. $\{M_p\}$, act continuously on $\dot{B}^{\{M_p\}}$, resp. $\tilde{B}^{\{M_p\}}$, and on $D_{L^1}^{(M_p)}$, resp. $\tilde{D}_{L^1}^{\{M_p\}}$. For the further properties of these spaces we refer to [19].

3. LAPLACE TRANSFORM IN SPACES OF ULTRADISTRIBUTIONS

The Laplace transform of distributions was defined and studied by Schwartz [23]. Later, Carmichael and Pilipovic in [1] (see also [2]), considered the Laplace transform in Σ'_α of Beurling-Gevrey tempered ultradistributions and obtained some results concerning the so-called tempered convolution. In particular, they gave a characterization of the space of Laplace transforms of elements from Σ'_α supported by an acute closed cone in R^d . Komatsu has given a great contribution to the investigations of the Laplace transform in ultradistribution and hyperfunction spaces considering them over appropriate domains, see [11] and references therein (see also [27]). Michalik in [13] and Lee and Kim in [12] have adapted the space of ultradistribution and Fourier hyperfunctions to the definition of the Laplace transform, following ideas of Komatsu.

Here we give the two main theorems of [21] concerning the Laplace transform of ultradistributions. There, the theory is developed within the space of already constructed ultradistributions of Beurling and Roumieu type. The ideas in the proofs of these theorems (theorem 2.1 and theorem 2.2) are similar to those in [26] in the case of Schwartz distributions. These theorems character-

ize ultradistributions defined on the whole R^d through the estimates of their Laplace transforms.

For a set $B \subseteq R^d$ denote by $ch B$ the convex hull of B .

Theorem 3.1. [21] *Let B be a connected open set in R_ξ^d and $T \in D^*(R_\xi^d)$ be such that, for all $\xi \in B$, $e^{-x\xi}T(x) \in S^{**}(R_x^d)$. Then the Fourier transform $F_{x \rightarrow \eta}(e^{-x\xi}T(x))$ is an analytic function of $\zeta = \xi + i\eta$ for $\xi \in ch B$, $\eta \in R^d$. Furthermore, it satisfies the following estimates: for every $K \subset\subset ch B$ there exist $k > 0$ and $C > 0$, resp. for every $k > 0$ there exists $C > 0$, such that $|F_{x \rightarrow \eta}(e^{-x\xi}T(x))(\xi + i\eta)| \leq Ce^{M(k|\eta)}$, $\forall \xi \in K$, $\forall \eta \in R^d$.*

If, for $S \in D^*(R_\xi^d)$, the conditions of the theorem are fulfilled, we call $F_{x \rightarrow \eta}(e^{-x\xi}S(x))$ the Laplace transform of S and denote it by $L(S)$.

Theorem 3.2. [21] *Let B be a connected open set in R_ξ^d and f an analytic function on $B + iR_\eta^d$. Let f satisfies the condition:*

For every compact subset K of B there exist $C > 0$ and $k > 0$, resp. for every $k > 0$ there exists $C > 0$, such that $|f(\xi + i\eta)| \leq Ce^{M(k|\eta)}$, $\forall \xi \in K$, $\forall \eta \in R^d$.

Then, there exists $S \in D^(R_\xi^d)$ such that $e^{-x\xi}S(x) \in S^{**}(R_x^d)$, for all $\xi \in ch B$ and*

$$L(f)(\xi + i\eta) = F_{x \rightarrow \eta}(e^{-x\xi}T(x))(\xi + i\eta) = f(\xi + i\eta),$$

$\xi \in B$, $\eta \in R^d$.

4. CONVOLUTION OF ULTRADISTRIBUTIONS

The existence of convolution of distributions was considered by Schwartz [22], [23] and later by many authors in various directions (see also [4], [5], [6] and [15]). In [22], it is proved that if $S, T \in D'(R^d)$ are two distributions such that $(S \otimes T)\varphi^\Delta \in D'_{L^1}(R^{2d})$ for every $\varphi \in D(R^d)$

(where $\varphi^\Delta(x, y) = \varphi(x + y)$) then the convolutions $S * T$ can always be defined as an element of $D'(R^d)$. Later on, Shiraishi in [24] proved that this condition is equivalent to the condition that for every $\varphi \in D(R^d)$, $(\varphi * \tilde{S})T \in D'_{L^1}(R^d)$. Many authors gave alternative definitions of convolution of two distributions and were proved that are equivalent to the Schwartz's definition (see, for example, [3]–[6], [14]–[16], [24], [25]). These results are more than forty years old and fairly well-known facts. Here we will give a review to the theory for existence of convolution of ultradistributions, which was rather recently developed.

The Beurling case was considered by Pilipovic [18] and Kaminski, Kovacevic and Pilipovic in [7] (see also [2]). The key component in the Beurling case is the fact that $B^{(M_p)}$ is a (F) -space. In fact, it is proved that the bidual of $B^{(M_p)}$ is isomorphic to $D_{L^\infty}^{(M_p)}$, i.e. $(D_{L^1}^{(M_p)})_b$ and $D_{L^\infty}^{(M_p)}$ are isomorphic l.c.s. Equip $D_{L^\infty}^{(M_p)}$ with the topology of compact convergence (from the duality $\langle D_{L^1}^{(M_p)}, D_{L^\infty}^{(M_p)} \rangle$) and denote it by $D_{L^\infty, c}^{(M_p)}$. One actually proves that $B^{(M_p)}$ is complete distinguished (F) -space and hence $D_{L^1}^{(M_p)}$ is barrelled and bornological. The topology of compact convergence on $D_{L^\infty}^{(M_p)}$ is the same as the topology of compact convex circled convergence (from the duality $\langle D_{L^1}^{(M_p)}, D_{L^\infty}^{(M_p)} \rangle$). That is the reason for the index c . The inclusions $D_{L^\infty, c}^{(M_p)} \rightarrow E^{(M_p)}$ and $D_{L^\infty}^{(M_p)} \rightarrow D_{L^\infty, c}^{(M_p)}$ are continuous. One proves that the bounded sets of $D_{L^\infty}^{(M_p)}$ and of $D_{L^\infty, c}^{(M_p)}$ are the same. Moreover, the induced topology by $D_{L^\infty, c}^{(M_p)}$ on a bounded subset of $D_{L^\infty}^{(M_p)}$ is the same as the induced one by $E^{(M_p)}$. Also, $D_{L^1}^{(M_p)}$ is dense in $D_{L^\infty, c}^{(M_p)}$ and the dual of $D_{L^\infty, c}^{(M_p)}$ is algebraically isomorphic to $D_{L^1}^{(M_p)}$. Because of this, if $S, T \in D_{L^1}^{(M_p)}$ are such that, for every $\varphi \in D^{(M_p)}(R^d)$, $(S \otimes T)\varphi^\Delta \in D_{L^1}^{(M_p)}(R^{2d})$, then the convolution of S and T can be defined by

$$\langle S * T, \varphi \rangle =_{D_{L^1}^{(M_p)}} \langle (S \otimes T)\varphi^\Delta \rangle_{D_{L^\infty, c}^{(M_p)}},$$

where 1 is the constant function which is always equal to 1. Moreover, one actually proves that the mapping $\varphi \mapsto (S \otimes T)\varphi^\Delta$,

$$D^{(M_p)}(R^d) \rightarrow D_{L^1}^{(M_p)}(R^{2d}),$$

is continuous and hence, $S * T$ is well defined ultradistribution. In [7], the following important theorem which gives the equivalence between this definition and the analogous form of the Shiraishi's definition, is proven (for its proof, we refer to [7]).

Theorem 4.1. [7] *Let $S, T \in D^{(M_p)}$. The following statements are equivalent:*

- i) *the convolution of S and T exists;*
- ii) *for all*

$$\varphi \in D^{(M_p)}(R^d), (\varphi * \tilde{S})T \in D_{L^1}^{(M_p)}(R^d)$$

and the convolution of S and T is given by

$$\langle S * T, \varphi \rangle = \langle (\varphi * \tilde{S})T, 1 \rangle;$$

- iii) *for all*

$$\varphi \in D^{(M_p)}(R^d), (\varphi * \tilde{T})S \in D_{L^1}^{(M_p)}(R^d)$$

and the convolution of S and T is given by

$$\langle S * T, \varphi \rangle = \langle (\varphi * \tilde{T})S, 1 \rangle;$$

- iv) *for all*

$$\varphi, \psi \in D^{(M_p)}(R^d), (\varphi * \tilde{S})(\psi * T) \in L^1(R^d).$$

The Roumieu case was considered by S. Pilipovic and B. Prangoski in [20]. Here we give a brief survey of the results obtained there, for the complete treatment of the problem (and the proofs of the results presented here) we refer to [20].

To begin, we define an alternative l.c. topology on $\tilde{D}_{L^\infty}^{(M_p)}$ such that its dual is algebraically isomorphic to $\tilde{D}_{L^1}^{(M_p)}$ (c.f. [16] for the case of Schwartz distributions). Let $g \in C_0(R^d)$ (the space of all continuous functions that vanish at infinity) and $(t_j) \in \mathfrak{R}$. The seminorms

$$p_{g, (t_j)}(\varphi) = \sup_{\alpha \in N^d} \sup_{x \in R^d} \frac{|g(x) D^\alpha \varphi(x)|}{T_\alpha M_\alpha}, \quad \varphi \in \tilde{D}_{L^\infty}^{(M_p)}$$

generate l.c. topology on $\tilde{D}_{L^\infty}^{\{M_p\}}$ and this space with this topology is denoted by $\tilde{\tilde{D}}_{L^\infty}^{\{M_p\}}$. Note that the inclusions $\tilde{D}_{L^\infty}^{\{M_p\}} \rightarrow \tilde{\tilde{D}}_{L^\infty}^{\{M_p\}}$ and

$$D^{\{M_p\}} \rightarrow \tilde{\tilde{D}}_{L^\infty}^{\{M_p\}} \rightarrow E^{\{M_p\}}$$

are continuous. Denote by $\left(\tilde{\tilde{D}}_{L^\infty}^{\{M_p\}}\right)'$ the strong dual of $\tilde{\tilde{D}}_{L^\infty}^{\{M_p\}}$.

Proposition 4.1. [20] The sets $\tilde{D}_{L^1}^{\{M_p\}}$ and $\left(\tilde{\tilde{D}}_{L^\infty}^{\{M_p\}}\right)'$ are equal and the inclusion

$$\left(\tilde{\tilde{D}}_{L^\infty}^{\{M_p\}}\right)' \rightarrow \tilde{D}_{L^1}^{\{M_p\}}$$

is continuous.

Lemma 4.1. ([20]) Let $S, T \in D^{\{M_p\}}(R^d)$ are such that, for every

$$\varphi \in D^{\{M_p\}}(R^d), (S \otimes T)\varphi^\Delta \in \tilde{D}_{L^1}^{\{M_p\}}(R^{2d}).$$

Then $F : D^{\{M_p\}}(R^d) \rightarrow \left(\tilde{\tilde{D}}_{L^\infty}^{\{M_p\}}\right)'(R^{2d})$ defined by $F(\varphi) = (S \otimes T)\varphi^\Delta$ is linear and continuous.

Definition 4.1. Let $S, T \in D^{\{M_p\}}(R^d)$ be such that for every

$$\varphi \in D^{\{M_p\}}(R^d), (S \otimes T)\varphi^\Delta \in \tilde{D}_{L^1}^{\{M_p\}}(R^{2d}).$$

Define the convolution of S and T ,

$$S * T \in D^{\{M_p\}}(R^d),$$

by

$$\langle S * T, \varphi \rangle = \left\langle \left(\tilde{\tilde{D}}_{L^\infty}^{\{M_p\}}\right)', \left\langle (S \otimes T)\varphi^\Delta, 1 \right\rangle_{\tilde{\tilde{D}}_{L^\infty}^{\{M_p\}}} \right\rangle; \\ \left(1 \in \tilde{\tilde{D}}_{L^\infty}^{\{M_p\}}\right).$$

One proves that $S * T \in D^{\{M_p\}}(R^d)$ is well defined element of $D^{\{M_p\}}$.

For every $a > 0$, define the space $\dot{B}_a^{\{M_p\}} = \left\{ \varphi \in \dot{\tilde{B}}^{\{M_p\}}(R^{2d}) \mid \text{supp } \varphi \subseteq \Delta_a \right\}$, where $\Delta_a = \left\{ (x, y) \in R^{2d} \mid |x + y| \leq a \right\}$. With the seminorms $\|\varphi\|_{(t_j)}$ (now over R^{2d}), $\dot{B}_a^{\{M_p\}}$ becomes a

l.c.s. Define the space $\dot{B}_\Delta^{\{M_p\}} = \lim_{a \rightarrow \infty} \text{ind } \dot{B}_a^{\{M_p\}}$,

where the inductive limit is strict; $\dot{B}_\Delta^{\{M_p\}}$ is a l.c.s. because we have a continuous inclusion $\dot{B}_\Delta^{\{M_p\}} \rightarrow E^{\{M_p\}}$. One verifies that the inclusion $\left(\dot{B}_\Delta^{\{M_p\}}\right)' \rightarrow D^{\{M_p\}}(R^{2d})$ is continuous ($\left(\dot{B}_\Delta^{\{M_p\}}\right)'$ is the strong dual of $\dot{B}_\Delta^{\{M_p\}}$). Now, we can give the theorem which proofs the equivalence between the analogous forms of Schwartz' and Shiraishi's definitions of convolution.

Theorem 4.2. [20] Let $S, T \in D^{\{M_p\}}(R^d)$. The following statements are equivalent:

i) the convolution of S and T exists;

ii) $S \otimes T \in \left(\dot{B}_\Delta^{\{M_p\}}\right)'$;

iii) for all $\varphi \in D^{\{M_p\}}(R^d)$,

$$(\varphi * \tilde{S})T \in \tilde{D}_{L^1}^{\{M_p\}}(R^d)$$

and for every compact subset K of R^d ,

$$(\varphi, \chi) \mapsto \left\langle (\varphi * \tilde{S})T, \chi \right\rangle,$$

$$D_K^{\{M_p\}} \times \dot{\tilde{B}}^{\{M_p\}}(R^d) \rightarrow C,$$

is a continuous bilinear mapping;

iv) for all

$$\varphi \in D^{\{M_p\}}(R^d), (\varphi * \tilde{T})S \in \tilde{D}_{L^1}^{\{M_p\}}(R^d)$$

and for every compact subset K of R^d ,

$$(\varphi, \chi) \mapsto \left\langle (\varphi * \tilde{T})S, \chi \right\rangle,$$

$$D_K^{\{M_p\}} \times \dot{\tilde{B}}^{\{M_p\}}(R^d) \rightarrow C,$$

is a continuous bilinear mapping;

v) for all

$$\varphi, \psi \in D^{\{M_p\}}(R^d), (\varphi * \tilde{S})(\psi * T) \in L^1(R^d).$$

The proof heavily relies on the topological properties of the ε tensor product

$$\dot{\tilde{B}}^{\{M_p\}}(R^d) \varepsilon \dot{\tilde{B}}^{\{M_p\}}(R^d).$$

In fact, in order to prove the theorem, the authors studied the properties and the relation between the ε tensor product of $\dot{\tilde{B}}^{\{M_p\}}(R^d)$ with a complete l.c.s. E and the space of vector valued ultradifferentiable functions $\dot{\tilde{B}}^{\{M_p\}}(R^d; E)$.

REFERENCES

- [1] R. Carmichael, S. Pilipovic: On the convolution and the Laplace transformation in the space of Beurling-Gevrey tempered ultradistributions, *Math. Nachr.* **158**, 119–131 (1992).
- [2] R. Carmichael, A. Kaminski, S. Pilipovic: *Boundary Values and Convolution in Ultradistribution Spaces*, World Scientific Publishing Co. Pte. Ltd., 2007.
- [3] P. Dierolf, S. Dierolf: Topological Properties of the Dual Pair $(\dot{B}(\Omega)', \dot{B}(\Omega)'')$, *Pacific J. Math.* **108**, 51–82 (1983).
- [4] P. Dierolf, J. Voigt: Convolution and \mathcal{S}' -convolution of distributions, *Collectanea Math.* **29**, 185–196 (1978).
- [5] J. Horvath: Sur la convolution des distributions, *Bull. Sci. Math.*, **98**, 2, 183–192 (1974).
- [6] A. Kaminski: Convolution, product and Fourier transform of distributions, *Studia Math.*, **74**, 83–96 (1982).
- [7] A. Kaminski, D. Kovacevic, S. Pilipovic: The equivalence of various definitions of the convolution of ultradistributions, *Trudy Mat. Inst. Steklov.* **203**, 307–322 (1994).
- [8] H. Komatsu: Ultradistributions, I: Structure theorems and a characterization, *J. Fac. Sci. Univ. Tokyo, Sect. IA Math.*, **20**, 1, 25–105 (1973).
- [9] H. Komatsu: Ultradistributions, II: The kernel theorem and ultradistributions with support in submanifold, *J. Fac. Sci. Univ. Tokyo, Sect. IA Math.*, **24**, 3, 607–628 (1977).
- [10] H. Komatsu: Ultradistributions, III: Vector valued ultradistributions and the theory of kernels, *J. Fac. Sci. Univ. Tokyo, Sect. IA Math.*, **29**, 3, 653–717 (1982).
- [11] H. Komatsu: Laplace transforms of hyperfunctions and their applications, International Conference in Applied Analysis (Hanoi, 1993). *Southeast Asian Bull. Math.* **19**, 37–50 (1995).
- [12] E. Lee, D. Kim: Laplace hyperfunctions, *Integral Transforms Spec. Funct.* **19**, 5–6, 399–407 (2008).
- [13] S. Michalik: Laplace ultradistributions supported by a cone, Linear and non-linear theory of generalized functions and its applications, *Banach Center Publ., Polish Acad. Sci. Inst. Math., Warsaw*, **88**, 229–241 (2010).
- [14] N. Ortner: On convolvability conditions for distributions. *Monatsh. Math.* **160**, 313–335 (2010).
- [15] N. Ortner, P. Wagner: Applications of weighted D'_{L^p} -spaces to the convolution of distributions, *Bull. Polish Acad. Sci. Math.*, **37**, 579–595 (1990).
- [16] N. Ortner, P. Wagner: *Distribution-Valued Analytic Functions – Theory and Applications*, Max-Planck-Institut für Mathematik in den Naturwissenschaften, Leipzig, 2008.
- [17] S. Pilipovic: Tempered ultradistributions, *Boll. Un. Mat. Ital. B*, **2**, 7, no. 2, 235–251 (1988).
- [18] S. Pilipovic: On the convolution in the space of Beurling ultradistributions, *Comment. Math. Univ. St. Paul.*, **40**, 15–27 (1991).
- [19] S. Pilipovic: Characterizations of bounded sets in spaces of ultradistributions, *Proceedings of the American Mathematical Society*, **120**, 4, 1191–1206 (1994).
- [20] S. Pilipovic, B. Prangoski: On the convolution of Roumieu ultradistributions through the \mathcal{E} tensor product, to appear in *Monatshefte für Mathematik*.
- [21] B. Prangoski: Laplace transform in spaces of ultradistributions, *FILOMAT*, **27**, 5, 747–760 (2013).
- [22] L. Schwartz: Theorie des distributions a valeurs vectorielles. I, *Ann. Inst. Fourier*, **7**, 1–141 (1957).
- [23] L. Schwartz: Theorie des distributions. I, II, 2nd ed., Hermann, Paris, 1966.
- [24] R. Shiraishi: On the definition of convolution for distributions, *J. Sci. Hiroshima Univ. Ser. A*, **23**, 19–32 (1959).
- [25] R. Shiraishi, M. Itano: On the multiplicative product of distributions, *J. Sci. Hiroshima Univ., A-I Math.*, **28**, 223–235 (1964).
- [26] V. S. Vladimirov: *Methods of the Theory of Functions of Many Complex Variables*, (Russian version), M, Nauka, 1964.
- [27] V. V. Zharinov: Fourier-ultrahyperfunctions (Russian), *Izv. Akad. Nauk SSSR Ser. Mat.* **44**, 533–570 (1980).

VIBRATION BASED FAULT DETECTION TECHNIQUES FOR MECHANICAL STRUCTURES

Marjan Djidrov, Viktor Gavriloski, Jovana Jovanova

*Institute of Mechanics, Mechanization and Vehicle, Faculty of Mechanical Engineering,
"SS. Cyril and Methodius" University in Skopje,
P.O. Box 464, MK-1001 Skopje, Republic of Macedonia
marjan.djidrov@mf.edu.mk*

Abstract: Fault detection techniques for mechanical structures and their application are becoming more important in recent years in the field of structure health monitoring. The intention of this paper is to present available state of the art methods that could be implemented in mechanical structures. Global based methods that contribute on detection, isolation and analysis of fault from changes in vibration characteristics of the structure are presented. Techniques are based on the idea that modal frequencies, mode shapes and modal damping as model properties of the structure can be determine as function of physical properties. In addition, if a fault appears in mechanical structure, this can be recognized as changes in the physical properties, which leads to cause changes in the modal properties of the structure.

Key words: fault detection; vibration analysis; vibration-based damage detection

ТЕХНИКИ НА ДЕТЕКЦИЈАТА НА ГРЕШКИ ВО МЕХАНИЧКИТЕ СТРУКТУРИ БАЗИРАНИ НА АНАЛИЗА НА ВИБРАЦИИТЕ

Апстракт: Техниките на детекцијата на грешки во механички структури и нивна примена во последните години стануваат сè поважни во областа на мониторингот на состојбата на конструкциите. Намерата на овој труд е да се презентираат современи методи кои можат да се применат кај механичките структури. Во трудот се прикажани методите базирани на глобалното однесување кои придонесуваат за детекција, изолација и анализа на грешки поради промена на вибро-динамичките карактеристики на структурите. Овие техники се базираат на идејата дека својствата на моделот како што се фреквенција, модот на осцилации и пригшување на структурата можат да бидат детерминирани како функција од физичките својства. Дополнително, доколку настане грешка во механичката структура, таа мода се препознае како промени во физичките својства кои предизвикуваат промени во карактеристиките на моделот на истата таа структурата.

Клучни збораови: детекција на грешка; анализа на вибрации; детекција на дефект преку вибрации

1. INTRODUCTION

Detection, diagnostic and identification of faults in mechanical systems and structures are significant and unavoidable in today modern technology. Permanent needs of excellent efficiency and better quality of products or integration of automatic control systems in more and more sophisticated and high costs processes, during the last decades makes faults detection and identification

(FDI) to be very popular theoretical and experimental research area [1]. A lot of methods and approaches were proposed by researchers and the purpose of this paper will be to cover commonly-practiced methods as inevitable part with significant impact in this research field.

Modern and advance technologies, processes or systems cannot be vulnerable to faults and to guaranty fault free operations. Therefore monitoring systems are develop and used to detect, locate

faults and determinate their size. Subsequently to FDI methods presentation, it is important to define, introduce basics notions and terms. A *fault* in a dynamical system is deviation of the system structure or the system parameters from the nominal situation [2] or as an unpermitted deviation of at least one characteristic property or parameter of the system from the acceptable, usual or standard condition [3]. A fault is to be understood as an unexpected change of system function, although it may not represent physical failure or breakdown [5]. Faults may lead to degraded performance, malfunctions or failures. Different from fault the consequences of a *failure* are usually more serious, such as a permanent interruption of a system's ability to perform a required function under specified operating conditions, or *malfunctions* as intermittent irregularity in the fulfillment of a system's desired function [1, 3]. When comes to sources of faults, structure can be disturbed from the environment and change its parameters. In mechatronic system and smart structures, faults can also appear from failures in equipment, sensors and actuators or from controller malfunctions (Fig. 1) [7].

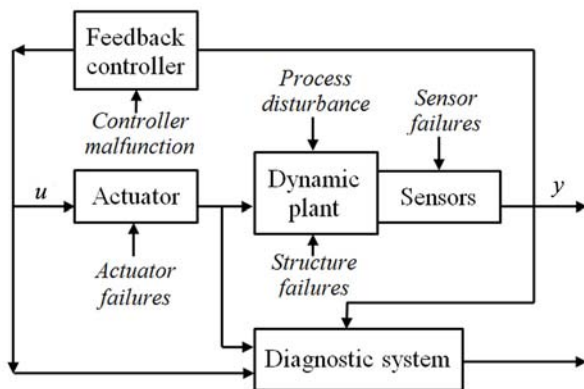


Fig 1. A general diagnostic framework

Undamaged and damaged components at the beginnings were investigated by measuring their properties and used correlating numerical models. In 70's and 80's the oil industry was attractive for researcher to examine the detection of faults because of adverse operating environments and offshore platforms problems. Investigation were about failing of drilling equipment, oil pumps and impact of wave motion or increasing on board marines. FDI methods are different and are based on the type of exploit measured data, and/or the technique used to identify the damage from the measured data. Applications for analysis of damage were

through frequencies changes approach; inspect changes in resonant frequencies or monitoring of ambient vibration response by accelerometers; usage of finite element analysis (FEA) to examine the effects of different parameters or implementation of statistical methods. In coming years focus for theoretical work and experimental techniques of FDI methods was about beams, plates, frames, bridges and other mechanical, civil and aerospace structures and structures made from different materials, including the composites. All of this are investigated by methods based on natural frequencies, frequency response functions (FRFs), mode shapes, mode shape and FRF curvatures, auto-regressive moving average (ARMA) family models, dynamic flexibility, modal strain energy, time-frequency analysis, principal component analysis (PCA) and singular value decomposition (SVD), neural networks and others. This paper is limited to global based methods that are used to infer damage from changes in vibration characteristics of the structure and some of the most prominent works are described in more details.

2. BASIC CONCEPT OF FAULT DETECTION TECHNIQUES

The framework for detection and diagnostic faults in mechanical systems and structures is consists of few steps. First one is *fault detection* as binary decision, to determinate that everything is o.k, or something has gone wrong. The second tasks is determination of the fault location know as *fault isolation* step follow by *fault identification* step which aims for estimation of the size, type and nature of the fault [3, 4, 5 and 6]. All these steps as tasks are implemented in monitoring fault diagnosis system and depending on its performance can be called: for *fault detection* – FD system, for *fault detection and isolation* – FDI system or for *fault detection, isolation and analysis* – FDIA system [4].

The field of FDI is very broad and this paper covers just FDI techniques and methods that are related for faults form changes in vibration characteristics of the mechanical structure. Model properties of the structure as modal frequencies, mode shapes and modal damping can be determine as function of physical properties (material, geometry characteristics). In addition, if a fault appears in mechanical structure, this can be recognized as changes in the physical properties, which

leads to cause changes in the modal properties of the structure. For example, reduction in stiffness induced by crack or disconnection will cause evident changes in these modal properties. In case where this relation can be model by linear equation, effects of faults on a structure can be classified as linear otherwise as non-linear. For example, opening and closing on crack situated on a beam and depending on the manifestation and position of the applied force, bending moment will induce non-linearity case of FDI [11, 19]. This paper will not cover FDI methods and techniques in non-linear conditions.

Two major classification groups of fault detection and identification approaches are: local and global methods. When structure is under certain applied excitation, structural response measurements in case of using local methods are obtained from small localized area of the structure. Ultrasonic waves, eddy currents, thermal field and acoustic emission are examples that contribute in local FDI. The methods that are most often used for the design of FDI systems are guided waves, those based on FBG sensors (strain, temperature measurements and ultrasound sensing), vibrothermography and electromechanical impedance [8]. All of this methods have limitation because of the localization i.e. can detect fault on or close to the surface of the structure, hence these limitations are overcome by global based methods which can be used on more complex structures by considering the global effects of fault. However, global-based approaches are only sensitive to significant structural damage, and it can be argued that damage is a localized process that takes place at structural components. As a result, local-based damage detection techniques seek to identify component-level structural damage (e.g. cracks in welded connections and corrosion) before it adversely affects the overall structural performance [9].

Global-based methods can be differentiated as signal or model based methods. After excitation on the mechanical structures, relationship between measured responses and potential faults are subject of signal based methods. General used methods are Fourier analysis, wavelet analysis, Wigner-Ville analysis and diagnostic parameter analysis. They are commonly applied in rotating and reciprocating machinery diagnostics for fault detection, but for localization and damage assessment need additional information [8]. Model based fault detection techniques opposite to signal based, allow better and deeper understanding of the structure behav-

iors. Parameters or outputs of undamaged and damaged structure models are compared and if there is a difference (*residues*), this can be related to given faults. Hence, the fundamentals of modal based FDI relies on redundancy which means, acquired signals are compared and advance evaluation can identify, locate an existing faults in component, structure or a system [10]. Figure 2 depicts the general structure of model-based approaches [3].

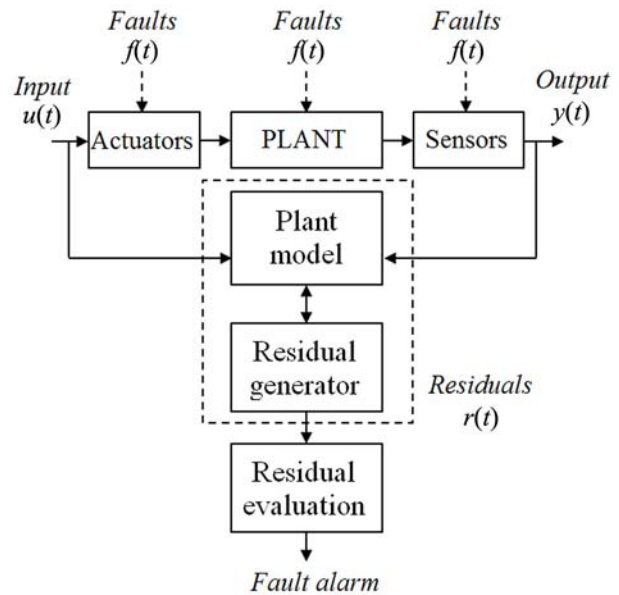


Fig. 2. Model-based fault detection

In general, a model based FDI system consists of two modules: residual generator and residual evaluator, as shown in Figure 2. The residual generator uses system measurements as input to generate residuals as fault symptoms. Then, these residuals are sent to the residual evaluator to make diagnosis decisions. Residuals for better and effective FDI system should be designed robust to disturbances, noise and other uncertainties, while remaining sensitive to faults. Therefore, an ideal residual should follow:

$$r(t) = 0 \quad \text{as} \quad f(t) = 0$$

and

$$r(t) \neq 0 \quad \text{as} \quad f(t) \neq 0 \quad (1)$$

where, $f(t)$ represents a fault and $r(t)$ represents the residual designed for the detection of that fault. Equation (1) indicates that $r(t)$ should be zero when the fault $f(t)$ does not occur, and be nonzero otherwise. In model-based approach, focus is residual generation and techniques that have been proposed in literature for this residual generation

are: parity space, observer-based and parameter estimation approach. The most intuitive fault detection method is parity relations through directly check of the consistency between the model and measured system outputs. Computational efforts are relatively small, simple in implementation and consideration of *a priori* model parameters. The basic idea behind the observer or filter based techniques is to estimate the outputs of the system from the measurements by using either Luenberger observers in a deterministic setting or Kalman filters in a noisy environment [3, 5]. Errors between estimated and measured outputs are used as residual. Parameter estimation techniques are based on idea for repeatedly online estimation of actual model parameters and analyzing the changes from the parameters of the reference model. In this case can be assumed that faults affect the outputs through the system parameters and any discrepancy can indicate that a fault may have occurred [3, 5]. Accurate model of the system is necessity for parity relations and the observer-based methods. Parameters of a structure, system model for some reason may continuously vary in certain ranges or they are not known exactly enough and in this situation above two methods cannot handle this problem and parameter estimation is mandatory.

3. FAULT DETECTION METHODS

3.1. Frequency changes

Change in natural frequencies is a classic method in FDI because of the easy determinations, high accuracy and sensibility to all kind of faults in structures [11]. When a fault happens in a mechanical structure, natural frequencies of the system are consequently decreasing because of stiffness reduction. A quite huge number of researchers used this method via practicing classical vibrational measurement techniques through experimental methods to determinate the resonant frequencies. The first significant effort in this area was conducted on off-shore oil platforms in the late 70s but analytical models failed in simple practical implementations. Reasons were environmental limitation and difficulties in distinguishing of changes in vibration caused by induced damage or shifts in the dynamics due to marine growth.

Determination of fault which is present in the structure as *forward problem* of this issue is consists of define the natural frequency changes of a given structure based on fault location and sever-

ity, usually through mathematically modelling of the fault. Silva and Gomes [12] proposed a method which uses the knowledge of the changes in the values of the experimental natural frequencies in order to predict the location and depth of an ‘unknown’ crack on beam. The technique involves an analytical model for the frequency shifts as a function of crack length and position. At least, the use of more than two natural frequencies led to more accurate results by minimizing the value

$$R = \sqrt{\frac{1}{n} \sum_{i=1}^{i=n} \left[\frac{(\omega_{fi})_e - (\omega_{fi})_p}{(\omega_{fi})_e} \right]^2}, \quad (2)$$

where R is auxiliary variable, n number of modes of vibration, ω_i natural frequency (mode i) of an untracked beam, ω_{fi} natural frequency (mode i) of a cracked beam, $(\omega_{fi})_e$ expected value of ω_{fi} , $(\omega_{fi})_p$ predicted value of ω_{fi} .

The *inverse problem* of FDI methods by using frequency changes and natural frequency measurements is concerns to determination of fault location and/or size of a given structure. Method which estimates the ratio of frequency shifts for various vibration modes was proposed by Hearn and Testa [13]. By assumption that the damage does not change the mass matrix $[M]$ and neglecting second-order terms in the formulation they showed that the change in the i^{th} natural frequency can be approximated by

$$\Delta\omega_i^2 = \frac{(\varepsilon_N(\varphi_i))^T \Delta k_n (\varepsilon_N(\varphi_i))}{\varphi_i^T M \varphi_i}, \quad (3)$$

where φ_i defines the i^{th} mode shape vector, $\varepsilon_N(\varphi_i)$ the element deformation vector computed from the mode shapes and Δk_n is the change in the matrix stiffness due to the presence of damage. Hearn and Testa also established that the ratio of the changes in two natural frequencies $\Delta\omega_i^2/\Delta\omega_j^2$ for two modes i and j is independent on the damage severity and so a function of the crack position only.

3.2. Mode shape changes

To provide information about fault location, as a result of damage sensitivity mode shape can be used especially when are considered higher ones. Modal Assurance Criterion (MAC) is the earliest analysis using mode shape to compare measured or damaged modes, with undamaged or numerical ones. Fault in mechanical structure can affect as changes in the mode shapes which con-

tingent on both the severity and the location of the damage. The spatial description of the amplitude of each resonance may be used as a fault indicator and magnitude change seen from spatial description with respect to each mode may vary from one to another as a result of the fault (crack) location. The MAC as the most common way of demonstrate a correlation between experimental and analytical models [14], is defined:

$$MAC(i, j) = \frac{(\{\varphi^A\}_i^T \{\varphi^B\}_j)^2}{(\{\varphi^A\}_i^T \{\varphi^A\}_i) (\{\varphi^B\}_j^T \{\varphi^B\}_j)}, \quad (4)$$

where $\{\varphi^A\}_i$ is the modal vector of the intact structure's i^{th} mode, $\{\varphi^B\}_j$ is the j^{th} modal vector of the structure after damage. MAC is a scale quantity ranging from 0 to 1, representing that the degree of correlation between two sets of modal vectors is uncorrelated at all or perfectly correlated respectively. Thus, the reduction of a MAC value may be an indication of damage. The method is based on the assumption that changes in modal vectors at the degrees of freedom near the damage are relatively larger than others located far from the damage. Modal Assurance Criterion uses only one pair of modes for fault localisation, hence as an extension of MAC is the coordinate modal assurance criterion (COMAC) which attempts to identify which measurement degrees-of-freedom contribute negatively to a low value of MAC [14].

$$COMAC(i) = \frac{\left(\sum_{r=1}^m \varphi_{Ar}^i \varphi_{Br}^i \right)^2}{\left(\sum_{r=1}^m \varphi_{Ar}^i \varphi_{Ar}^i \right) \left(\sum_{r=1}^m \varphi_{Br}^i \varphi_{Br}^i \right)}, \quad (5)$$

where φ_{Ar}^i and φ_{Br}^i are modal component of the r^{th} mode shape at location i for the two paired mode shapes respectively and m is the number of the measured modes. The location where a COMAC value is close to zero is the possible damage location. Another form of the MAC is the partial MAC (PMAC), which correlates parts of modal vectors and allows easy comparison of the selected parts. Ko *et al.* [15] proposed a combination of MAC and COMAC and sensitivity analysis to detect damage in steel framed structures.

3.3. Mode shape curvature

Direct relationship between curvature and bending strain can be used in order to obtain in-

formation about sources of vibration changes, therefore as alternative of mode shapes is using mode shape derivatives, such as curvature. Flexural rigidity of beam cross-sections is related to curvature mode shapes, and at a point curvature is given by:

$$n = M / EJ, \quad (6)$$

where, M is the bending moment at a section, E is the Young's modulus (modulus of elasticity) and J is the second moment of the cross-sectional area.

If fault is introduced in a structure, magnitude of curvature is increases by reduction in the value of flexural rigidity (defined as EI) at the cracked section or in the damaged region. Typically, the changes in the curvature are local and therefore can be used to detect and locate a crack or damage in the structure. Among the first who proposed the curvature mode shape as method for FDI was Pandey *et al.* [16, 17].

3.4. Methods using dynamic flexibility

FDI methods can use the dynamically measured flexibility matrix for estimation of changes in the static behaviour of the structure. The flexibility matrix is defined as the inverse of the stiffness matrix and, therefore, relates the applied static force to the resulting structural displacement:

$$\{u\} = [G] \{F\}, \quad (7)$$

where, $\{u\}$ represents static displacement vector, $[G]$ is flexibility matrix and $\{F\}$ is static force loading vector. Each column of the flexibility matrix represents the displacement pattern associated with a unit force applied at the associated degrees of freedom.

The expression of the flexibility matrix can be approximating by only keeping the first few modes of the structure [18]:

$$[G] = [\varphi] [\Lambda]^{-1} [\varphi]^T, \quad (8)$$

where $[\Lambda]$ and $[\varphi]$ represent the measured eigenvalue and mass-normalized eigenvector matrices, respectively. FDI approaches based on usage of dynamic flexibility identified faults in mechanical structures by comparison of the flexibility matrices of the structure in the undamaged (which may be obtained using a finite element model) and damaged states. Due to the inverse relation to the square of the modal frequencies, the dynamic flexibility matrix is very sensitive to changes in the

lower order modes, while the stiffness matrix is more sensitive to higher order modes.

4. CONCLUSION

Referred works and authors in this paper presents only a small segment of the published works available on the topic. Other works are excluded because of different approaches that were not covered in this paper. For example, methods based on the modification of structural model matrices such as mass, stiffness and damping; neural network approaches; statistical methods; methods covering nonlinearity and other hybrid methods and applications. Today, a lot of techniques stand for detection and identification of faults, but there is no general procedure that can be recognized as resolution of all kinds of problems in all kinds of structures. Regard of the techniques variety and their particular advantages and disadvantages, all of them tends to have fault related sensitivities. Faults can be detected, recognized only above a certain size, i.e. techniques with less sensitive may lead to fault negative or very sensitive techniques may produce fault positive.

Methods and techniques for fast estimation for not very small faults in mechanical structures are initially based on linear approaches. Change in frequency for detection faults appears to be more practical in engineering applications, but it should be noted that frequency shifts have practical limitations. Low sensitivity of change in frequency from faults requires very accurate measurements usually in controlled environment, otherwise is case of large levels of structural damage. As damage indicators, using methods based on mode shapes, modal assurance criterion have disadvantage related to capability of estimation a detailed mode shape. This implies that number of measurements at each of the points of the structures and the duration of each measurement is vital in demand of detailed mode shape, including the uncertainties at the boundaries conditions that may drastically affect the methods.

Broad majority of the literature are based on laboratory tests and mathematical modeling which are useful in terms of testing proposed fault detection techniques but cannot replicate the environmental effects to which real mechanical structures are exposed to. Environmental effects as issue for filtering from measured data used in FDI techniques have not yet been tackled comprehensively

in the literature. Beside this, remaining lifetime estimation and quantification of damage belong to issues that are particularly important and most difficult to deal with. This can be specified as challenge for research community to face the fault consequences as the last step in FDI methodology, by obtaining knowledge about the actual safety of the structure at certain fault stage.

REFERENCES

- [1] R. Isermann: *Fault-Diagnosis Systems: An Introduction from Fault Detection to Fault Tolerance*, Springer-Verlag, Berlin Heidelberg, 2005.
- [2] M. Blanke, M. Kinnaert, J. Lunze, Marcel Staroswiecki: *Diagnosis and Fault-Tolerant Control*, 2nd Edition, Springer-Verlag, Berlin Heidelberg, 2006.
- [3] S. Simani, C. Fantuzzi, R. J. Patton: Model-based fault diagnosis in dynamic systems using identification techniques, *Advances in Industrial Control*, Springer-Verlag, Berlin Heidelberg, 2002.
- [4] S. X. Ding: *Model-based Fault Diagnosis Techniques Design Schemes, Algorithms, and Tools*, Spring-Verlag, Berlin Heidelberg, 2008.
- [5] J. Chen, R. J. Patton: *Robust Model-Based Fault Diagnosis for Dynamic Systems*, The International Series on Asian Studies in Computer and Information Science, Kluwer Academic Publishers, 1999.
- [6] J. J. Gertler: *Fault Detection and Diagnosis in Engineering Systems* (Electrical Engineering & Electronics), Marcel and Dekker, New York, 1998.
- [7] V. Venkat, R. Rengaswamy, K. Yin, S. N. Kavuri: A review of process fault detection and diagnosis: Part I: Quantitative model-based methods, *Computers & Chemical Engineering*, **27**, 3, 15, pp. 293–311, March 2003, ISSN 0098-1354.
- [8] T. Stepinski, T. Uhl, W. Staszewski: *Advanced Structural Damage Detection from Theory to Engineering Applications*, John Wiley & Sons, 2013.
- [9] K. Jan-Hwang Loh: *Development of Multifunctional Carbon Nanotube Nanocomposite Sensors for Structural Health Monitoring*, ProQuest, UMI Dissertation Publishing, 2011.
- [10] R. Kothamasu, S. H. Huang, W. H. VerDuin: System health monitoring and prognostics – A review of current paradigms and practices, *The International Journal of Advanced Manufacturing Technology*, **28**, 9–10, pp. 1012–1024, ISSN 1433-3015, 2006.
- [11] A. Rytter: *Vibration Based Inspection of Civil Engineering Structures*, Ph. D. Dissertation, Department of Building Technology and Structural Engineering, Aalborg University, Denmark, 1993.
- [12] J. M. M. Silva, A. J. M. A. Gomes: Crack Identification of Simple Structural Elements Through the use of Natural Frequency Variations: The Inverse Problem, *Proc. of the 12th International Modal Analysis Conference*, pp. 1728–1735 (1994).
- [13] R. Testa: Characteristics and detection of damage and fatigue cracks. A. Morassi, F. Vestroni (Editors), *Dy-*

- namic Methods for Damage Detection in Structures*, CISM Courses and Lectures, Springer Verlag, Wien-New York, pp. 183–195, 2008.
- [14] R. J. Allemang: The modal assurance criterion (MAC): twenty years of use and abuse, *Sound and Vibration*, **37**, 8, pp. 14–23 (2003).
- [15] J. M. Ko, C. W. Wong, H. F. Lam: Damage Detection in Steel Framed Structures by Vibration Measurement Approach, In: *Proc. of 12th International Modal Analysis Conference*, pp. 280–286, 1994.
- [16] M. Mehdizadeh: *Curvature Mode Shape Analyses of Damage in Structures*, M.Sc. Dissertation, School of Aerospace, Mechanical & Manufacturing Engineering, College of Science, Engineering and Technology, RMIT University, Australia, 2009.
- [17] V. B. Dawari, G. R. Vesmawala: Structural Damage Identification Using Modal Curvature Differences, *IOSR Journal of Mechanical and Civil Engineering (IOSR-JMCE)*, ISSN: 2278–1684, pp: 33–38 (2009).
- [18] N. A. Robinson, L. D. Peterson, G. H. James, S. W. Doebling: Damage Detection in Aircraft Structures Using Dynamically Measured Static Flexibility Matrices, *Proc. of the 14th International Modal Analysis Conference*, pp. 857–865 (1996).
- [19] T. L. Luo, James S. S. Wu, J. P. Hung: A study of non-linear vibrational behavior of cracked structures by the finite element method, *Journal of Marine Science and Technology*, Vol. **13**, No. 3, pp. 176–183 (2005).

FINITE ELEMENT ANALYSIS OF AN ACCIDENT SEVERITY ACCORDING TO THE EUROPEAN STANDARD EN1317

Nikola Avramov, Petar Simonovski

Faculty of Mechanical Engineering, "SS. Cyril and Methodius" University in Skopje,
P.O. Box 464, MK-1001 Skopje, Republic of Macedonia
petar.simonovski@mf.edu.mk

Abstract: The increase in traffic safety and the design of safer roads includes installation of restraint systems on separate road segments as part of the highway infrastructure for withholding the vehicle back on the road. The existing European normative EN1317 is the framework for the guardrail design. The regulative is determining for example both the maximum deceleration in the passenger compartment considering the vehicle and the maximum guardrail deflection for specific type of impact, given in the test matrix. If all of the parameters are within the prescribed range and if other obligations are fulfilled the guardrail can be safe for use. In other words the guardrails are designed to absorb the energy coming from the vehicle motion safely lowering the velocity through desired vehicle path. The aim of this paper is with numerical simulation to find the crashworthiness of a vehicle to guardrail impact.

Key words: accident severity; test dummy; guardrail; acceleration parameters

АНАЛИЗА НА ГОЛЕМИНАТА НА СООБРАЌАЈНА НЕСРЕЌА, СПОРЕД СТАНДАРДОТ EN1317 СО ПОМОШ НА МЕТОДОТ НА КОНЕЧНИ ЕЛЕМЕНТИ

Апстракт: Зголемувањето на безбедноста во сообраќајот вклучува побезбедни патишта и поставување на системи за заштита од излетување на возилата на одделни делови од патот. Постојната европска норма EN1317 ја содржи рамката за конструкција на патните одбојници. Оваа регулативата во тест матрица ги наведува максималното забавување внатре во возилото и максималната деформација на одбојникот во случај на удар. Ако сите параметри се во пропишаните граници и ако другите обврски се исполнети, одбојникот е безбеден за употреба. Со други зборови, одбојникот е конструиран да ја прифати енергијата којашто доаѓа со движењето на возилото, безбедно намалувајќи ја неговата брзина преку посакувана траекторија. Целта на овој труд е преку нумерички симулации да се определи сериозноста на несреќата при удар на возило во одбојник за заштита од излетување.

Клучни зборови: големина на несреќа; кукла за испитување; одбојник; параметри за одредување на несреќата

1. INTRODUCTION

1. Accident severity parameters

The accident crashworthiness or the passenger injury severity level is determined by the below stated parameters. Any of these parameter higher value means more serious injuries or fatal in the worst case.

Acceleration Severity Index (ASI)

This parameter measures the severity of the vehicle motion over a person seated in the proximity of a chosen point during an impact. When calculated the ASI values should be in a prescribed boundaries [1].

$$ASI(t) = \sqrt{\left[\left(\frac{ax}{ax}\right)^2 + \left(\frac{ay}{ay}\right)^2 + \left(\frac{az}{az}\right)^2\right]}$$

where \widehat{ax} , \widehat{ay} , \widehat{az} are the threshold values of a human body accelerations and \overline{ax} , \overline{ay} , \overline{az} are the accelerations of a vehicle selected point, averaged over a time interval of 50 ms. The generally used limit accelerations for passengers using safety belts are $ax = 12 g$, $ay = 9 g$, $az = 10 g$ [2].

Theoretical Head Impact Velocity (THIV)

This factor shows the impact velocity of a freely moving object impacting the vehicle interior surface. It is calculated with the ground and the vehicle reference averaged over time of the impact duration. After the impact both the vehicle and the theoretical head are considered to stay in contact for the rest of the period.

$$THIV = \sqrt{V_x^2(T) + V_y^2(T)}$$

Post Impact Head Deceleration (PHD)

This is the maximum value of an averaged longitudinal and transversal component accelerations of a vehicle centre of gravity computed over 10ms.

$$PHD = \max \sqrt{\left(x_c''\right)^2 + \left(y_c''\right)^2}$$

2. FEM MODELS

2.1. Vehicle FEM model

For FEM vehicle model the Ford Taurus (model year 2001) is chosen because its closeness to the European mid-sized vehicle fleet. The model was developed for general purposes so it needed some modifications to address certain deficiencies in the vehicle to barrier simulations. The model had to undergo modifications for lowering the simulation time and bringing the response closer to the realistic [3]:

- Removing parts of less importance for the vehicle behaviour.

- Adding element mass adequate to the removed parts mass. The element mass was added at the B-pillars because of the position of the centre of gravity at the mid plane between the B-pillars.

- Fixing the free turning of the wheel with the first contact to the guardrail and consequently the change of the load path. During the research phase it was seen from the crash test videos that the wheel experience slight inclination after the engagement during the oblique collision.

- Mass was added to the accelerometers to damp the oscillation amplitude of high frequency noise and getting more stable results.

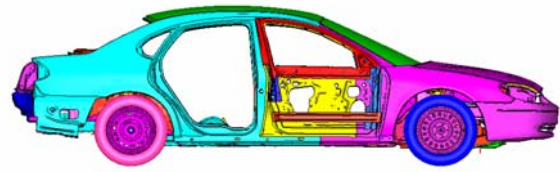


Fig. 1. Simplified vehicle geometry model

2.2. Guardrail FEM model

The guardrail consists of twelve segments or rails and thirteen support posts pressed in the ground. For the rails connection eight pairs of fastener sets are used, and for the rail to post connection one pair of fastener is used. For a more accurate representation the guardrail model had to undertake some adjustments like:

- The bolt to nut connection is modeled by using bar connections, specifying the bar stiffness, cross-section area and the mass density. This type of connection gives us the possibility of defining the pre-load force and is used as more direct approach instead of already known methods of temperature difference or initial strain method. The joining components, bolt and nut are modelled with their standard dimensions except modelling the threads which was found in the literature as non-essential factor affecting the results. They are tied together between connecting nodes, first as the centre node of spider rigid body elements around the circumference at the end of the bolt head and the second one as the centre node of spider rigid body elements around the hole at the beginning of the nut [4].

- The soil is modelled as a solid cylinder meshed with hexagonal elements, with a centre hole trimmed with the projection nodes of the post.

- The friction on separate segments is defined through the static and dynamic coefficient of friction, one between the guardrails segments, other between the post and the ground and the last between the vehicle and the guardrail elements.

- Guardrail end elements are connected by dampers to rigid constrains. Dampers are used because they have the possibility to absorb energy, corresponding to the deformation of the adjacent rails.

- Local weakening around the fastener holes. From the examination of the real crash can be concluded that the bolt head is pulled out of the guardrail segment. These local deformation can be achieved in the model by weaken elements around the holes that will enable the fastener unbuckle, shown as light elements on Fig. 2 [5].

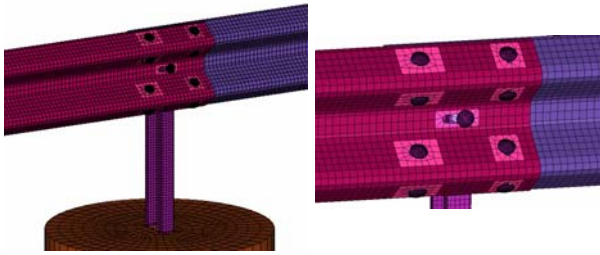


Fig. 2. Guardrail FEM model and segment to segment connection

2.3. Crash test dummy FEM model

The crash test dummy corresponds to the 50th percentile Hybrid III male dummy, 175 cm tall and 77 kg weight. All body parts are ellipsoidal, modeled with hexagonal 3D solid elements required for the used material definition. For connecting the body parts constrained node sets between adjacent parts were used. They are tied together between connecting nodes, first as the centre node of spider rigid body elements around the circumference at the end of the connecting part and the second one as the centre node of the connected part, Fig. 3. The two connecting nodes are constrained in all the direction, both translation and rotational, except the corresponding rotations around the common axis. That simulates the ankle joints between the parts. At the head and the chest centre of gravity and at the proximity of the seating point P three tri-axial accelerometers were used. The most general method for accelerometer use is the solid body rigid cube. It is positioned at the centre of gravity and rigidly connected to the related part. The body displacement information can be taken from the local coordinate system consisting of the accelerometer edge nodes or in the global coordinate system. The head acceleration is measured for determining the THIV (acc. 1 shown on Fig. 3) and the *P* acceleration of a seating person which is the centre of gravity of the driver's pelvis is used for calculating the ASI value (acc. 3 shown on Fig. 3). For representation only and not for the purpose of this study one accelerometer is placed at the chest centre of gravity (acc. 2 shown on Fig. 3). For the body parts material, low density foam was used with defined density, modulus of elasticity and load curve for determining the material nominal stress versus strain relationship. This material was chosen because it is closest to the human body characteristics as compressible low density material. This dummy model is simplified and not all parts of the human body anatomy are modelled. Their damping is considered in the compression factor of the foam material instead. It is also good to note that all the parts

were modelled as individual parts because their individual freedom in the part behaviour.

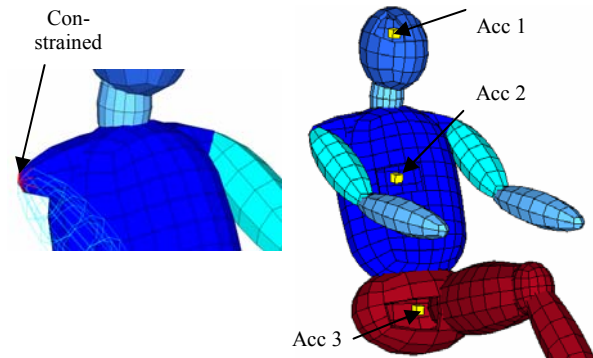


Fig. 3. Crash test dummy constrained nodes and accelerometers location

3. RESULTS AND DISCUSSION

3.1. Acceleration diagram (vehicle centre of gravity and dummy head acceleration)

The vehicle impact characteristics were defined according to the test matrix given in the standard EN1317. The testing vehicle is a passenger vehicle with total mass of 1500 kg, closing speed of 110 km/h and an angle of impact to the restraint system of 20 degrees, as the highest containment level for this vehicle category. [2]

On the Fig. 4 presented above can be seen the vehicle CoG and the dummy head acceleration curve. The first milliseconds of the curve were cropped because of initiating a head acceleration peak from the sudden vehicle increase of velocity at the start of the simulation. The acceleration calculations start after the vehicle to driver bonding and the driver motion together with the vehicle. In the following some of the simulations tracing points are described.

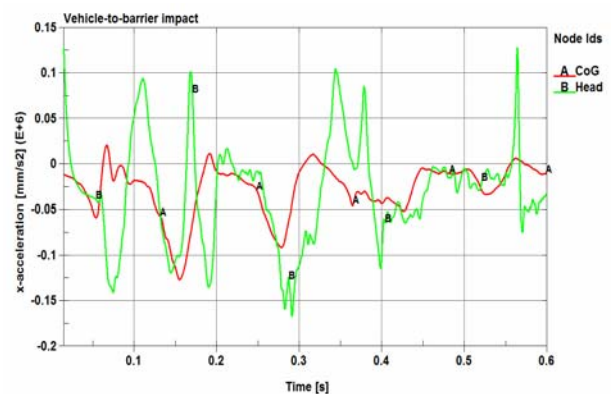


Fig. 4. Vehicle centre of gravity and crash test dummy head accelerations

The first contact of the vehicle to guardrail starts at 0.01s. At 0.05 s the vehicle wheel comes into contact with the guardrail post but no wheel snagging occurs because the wheel slides outside the post. The second vehicle to post interaction occurs at 0.15 s when the direct impact separates the post from the guardrail. At time of 0.27 s the most severe accident severity happens and this is time when the highest accelerations start. At this time the guardrail deforms so that it gets the vehicle front shape and together with the coming post holds back the vehicle (Fig. 5). For the rest of the time duration the guardrail segments separate and the accelerations are decreasing.

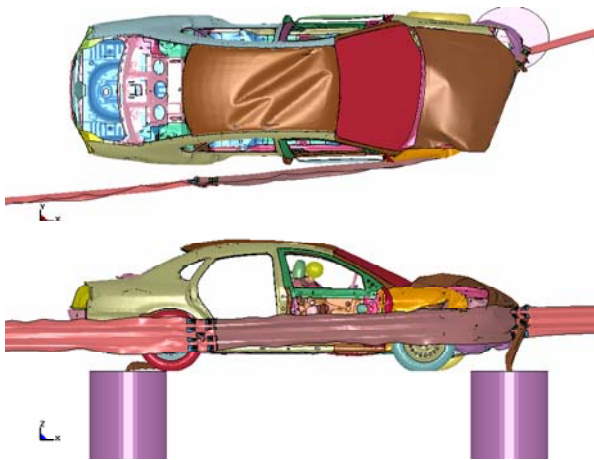


Fig. 5. Vehicle deformation mode at time 0.27 s

3.2. Acceleration severity calculation (*ASI*, *THIV*, *PHD*)

The *ASI* value is calculated using the driver seating *P*-point or the pelvis acceleration curve for all components of the vehicle velocity vector. After finding the maximum values of the acceleration component vectors or the acceleration component peak value, 250 samples before and after this values were taken. The standard states 50 ms or in our case for the sample time of 0.0001 samples/sec gives total 500 samples for 50 ms. For the *ASI* and *PHD* calculation numerical software MATLAB was used. It is good to note that according to EN1317 the impact severity level is graded with level A, B or C.

$$ASI = 7.6 [/] \quad \text{out of grading level}$$

For calculating the *THIV* the vehicle has been considered as the reference moving object. Local coordinate system was placed at the vehicle centre of gravity in the direction of the vehicle velocity vector and was taken as a point where no deformation can reach. *THIV* has been calculated as the theoretical head motion relative to vehicle or the

average of the head velocity in longitudinal and transversal direction relative to the vehicle reference.

$$THIV = 8.87 \text{ km/h} < 33 \text{ km/h.}$$

PHD is calculated as the component acceleration of the vehicle centre of gravity averaged over 10 ms interval, same as the *ASI* calculation with the difference that for 10ms average, 100 samples were needed, 50 before and after the peak value as stated in the standard EN1317. Also is assumed that the head remains in contact with the vehicle after the impact for the rest of the time period.

$$PHD = 13.07 \text{ g} < 20 \text{ g.}$$

4. CONCLUSIONS

The background for choosing this research was recognizing the advantages of the numerical simulations beside the real crash tests. Properly modelled and verified model can be adequate replacement of the actual tests. The models have to be adapted for the required tests. Two main conclusions regarding this paper can be underlined. The vehicle to guardrail FE model used can be appropriate representative considering the above stated modifications, and can be recommended for future research.

For this guardrail installation can be said that regarding the standard EN1317, the *ASI* parameter is out of the grading level or is above the thresholds values defined, meaning that the accelerations in the passenger compartment are above the permitted leading to possible higher injury factors. The *THIV* and the *PHD* are in the permissible interval values. If this was verified model by series of crash tests and complete test matrix varying the parameters and lowering the uncertainty contributors the drawbacks would be that the examined guardrail is not safe for use for all highway sections and has to address certain modifications.

REFERENCES

- [1] EN 1317-1: *Road restrain systems. Part 1: Terminology and general criteria for test methods*, 1998.
- [2] EN 1317-2: *Road restrain systems. Part 2: Performance classes, impact test acceptance criteria and test methods for safety barriers*, 1998.
- [3] NCAC (National Crash Analysis Centre) models URL: <http://www.ncac.gwu.edu/vml/models.html>
- [4] Montgomery J.: *Methods for modelling bolts in the bolted joints. ANSYS User's Conference* (2002).
- [5] Rogers A. Colin; Hancock J. Gregory: *Failure Modes of Bolted Sheet Steel Connections Loaded in Shear* (1998).

INSTRUCTIONS FOR AUTHORS

Mechanical Engineering – Scientific Journal is published twice yearly. The journal publishes **original scientific papers, short communications, reviews** and **professional papers** from all fields of mechanical engineering.

The journal also publishes (continuously or occasionally) the bibliographies of the members of the Faculty, book reviews, reports on meetings, news of future meetings, important events and dates, and various rubrics, which contribute to the development of the corresponding scientific field.

Original scientific papers should contain hitherto unpublished results of completed original scientific research. The number of pages (including tables and figures) should not exceed 15.

Short communications should also contain completed but briefly presented results of original scientific research. The number of pages should not exceed 5 (including tables and figures).

Reviews are submitted at the invitation of the Editorial Board. They should be surveys of the investigations and knowledge of several authors in a given research area. The competency of the authors should be assured by their own published results.

Professional papers report on useful practical results that are not original but help the results of the original scientific research to be adopted into scientific and production use. The number of pages (including tables and figures) should not exceed 10.

Acceptance for publication in the Journal obliges the authors not to publish the same results elsewhere.

1. SUBMISSION

Manuscript should be submitted **in triplicate**, typed (1½ spaced) on A4 paper with margins of 2.5 cm on each side at the following address:

Faculty of Mechanical Engineering
(Mechanical Engineering – Scientific Journal)

Editor in Chief
P.O. Box 464
MK-1001 Skopje
Republic of Macedonia

The papers and appendices should be numbered. It is strongly recommended that the MS Word 2003 and/or PDF files of the manuscript be sent on the disc or by e-mail on mesj@mf.edu.mk.

A letter must accompany all submissions, clearly indicating the following: title, author(s), corresponding author's name, address and e-mail address, suggested category of the manuscript and a suggestion of five referees (their names, e-mail and affiliation).

2. THE REVIEW PROCESS

Papers received by the Editorial Board are sent to two referees (one in the case of professional papers). The suggestions of the referees and Editorial Board are sent to the author(s) for further action. The corrected text should be returned to the Editorial Board as soon as possible but in not more than 30 days.

3. PREPARATION OF MANUSCRIPT

The papers should be written in the shortest possible way and without unnecessary repetition.

The original scientific papers, short communications and reviews should be written in English, while the professional papers may be submitted also in Macedonian.

Only SI (Système Internationale d'Unités) quantities and units are to be used.

Double subscripts and superscripts should be avoided whenever possible. Thus it is better to write $v_3(\text{PO}_4)$ than $v_{3\text{PO}_4}$ or $\exp(-E/RT)$ than $e^{-E/RT}$.

Strokes (/) should not be used instead of parentheses.

Figures (photographs, diagrams and sketches) and **mathematical formulae** should each be given on a separate sheet. Figures should also be inserted in the correct place in the manuscript, being horizontally reduced to 8 or 16 cm. The size of the symbols for the physical quantities and units as well as the size of the numbers and letters used in the reduced figures should be comparable with the size of the letters in the main text of the paper. Diagrams and structural formulae should be drawn in such a way (e.g. black Indian ink on white or tracing paper) as to permit high quality reproduction. The use of photographs should be avoided. The tables and the figures should be numbered in Arabic numerals (e.g. Table 1, Fig. 1). Tables and figures should be self-contained, i.e. should have captions making them legible without resort to the main text. The presentation of the same results in the form of tables and figures (diagrams) is not permitted.

Footnotes are also not permitted.

When a large number of compounds have been analyzed, the results should be given in tabular form.

Manuscript should contain: title, author(s) full-name(s), surname(s), address and e-mail, short abstract, key words, introduction, experimental or theoretical back-ground, results and discussion, acknowledgment (if desired), references and summary.

The **title** should correspond to the contents of the manuscript. It should be brief and informative and include the majority of the key words.

Each paper should contain an **abstract** that should not exceed 150 words. The abstract should include the aim of the research, the most important results and conclusions.

In the **introduction** only the most important previous results related to the problem in hand should be briefly reviewed and the aim and importance of the research should be stated.

The **experimental** section should be written as a separate section and should contain a description of the materials used and methods employed – in form which makes the results reproducible, but without detailed description of already known methods.

Manuscripts that are related to **theoretical studies**, instead of experimental material, should contain a sub-heading and the **theoretical background** where the necessary details for verifying the results obtained should be stated.

The **results and discussion** should be given in the same section. The discussion should contain an analysis of the results and the conclusions that can be drawn.

The **reference** should be given in a separate section in the order in which they appear in the text. The surname of one or two authors may be given in the text, whereas in the case of more than two authors they should be quoted as, for example, Kuzinovski and collaborators [1] or Vrtanoski *et al.* [1].

Papers from scientific journals should be cited as follows:

[1] G. Vrtanoski, V. Dukovski, K. Yamaguchi: Use of polymer concrete for construction materials, *Proc. Fac. Mech. Eng. – Skopje*, **21**, 1, 43–48 (2002).

Books should be cited as follows:

a) books without editor:

[2] V. Georgievski: *Lake metalne konstrukcije. Prostorni rešetkasti sistemi*, Građevinska knjiga, Beograd, 1990, pp. 134–157.

b) books with editor:

[3] M. Golay, in *Gas Chromatography*, D. Desty, ed. Butterworths, London, 1958, p. 36.

Manuscripts should also contain a **summary** in Macedonian at the end of the paper. The summary in Macedonian for foreign authors will be prepared by the Editorial Board. The summary should contain: **title, author(s) full-name(s), surname(s) and address, key words and abstract.**

The **category** of the paper is proposed by the author(s) but the Editorial Board reserves for itself the right, on the basis of the referees' opinion, to make the final choice.

Proofs are sent to the author(s) to correct printers' errors. Except for this, alterations to the text are not permitted. The proofs should be returned to the Editorial Board in 2 days.

The author(s) will receive, free of charge, 20 reprints of every paper published in the Journal.